2-1-2015

Low complexity blind and data-aided IQ imbalance compensation methods for low-IF receivers

Mohamed Hussein Eissa

Follow this and additional works at: https://fount.aucegypt.edu/etds

Recommended Citation

APA Citation
Eissa, M. (2015).*Low complexity blind and data-aided IQ imbalance compensation methods for low-IF receivers* [Master's Thesis, the American University in Cairo]. AUC Knowledge Fountain.
https://fount.aucegypt.edu/etds/1244
MLA Citation
Eissa, Mohamed Hussein. *Low complexity blind and data-aided IQ imbalance compensation methods for low-IF receivers*. 2015. American University in Cairo, Master's Thesis. *AUC Knowledge Fountain*.
https://fount.aucegypt.edu/etds/1244

The American University in Cairo

School of Sciences and Engineering

Low Complexity Blind and Data-Aided IQ Imbalance Compensation Methods For Low-IF Receivers

A Thesis Submitted to

Electronics and Communications Engineering Department

In partial fulfillment of the requirements for
the degree of Master of Science

by Mohamed Hussein Mohamed Eissa

Supervisor: Dr. Ayman Elezabi
Co-Supervisor: Dr. Ahmad Gomaa
June 2014

ACKNOWLEDGEMENTS

First of all, I thank Allah the almighty for providing me persistence and patience to complete this work. I would also like to express a special word of thanks to the following people who supported me till the completion of this work:

To Dr.Ayman Elezabi & Dr.Ahmad Gomaa my thesis supervisors for their valuable supervision, guidance, idea's and advise all through my study period.

To "Hittite Microwave Egypt" for supporting me financially during my study period.

To my work colleagues: Mohamed El-Shennawy, Hossam Aly, Dr.Mohamed Abdalla, Ahmed Naguib & Amr El-Sherief and the rest of them, for their support and advice.

To My lovely wife for believing in me at all times.

To my little girl giving me the spirit to work harder.

To my parents for their continuous dedication and support for me through my life.

To my only brother and real friend for his continuous advise and encouragement.

To my mother and father in law, brothers and sisters in law, for their support and encouragement.

ABSTRACT

The American University in Cairo

Low Complexity Blind and Data-Aided IQ Imbalance Compensation Methods for Low IF Receivers

Student name: Mohamed Hussein Eissa

Thesis supervisor: Dr. Ayman Elezabi

Thesis co-supervisor: Dr. Ahmad Gomaa

Low-IF and Zero-IF (direct conversion) down converters showed a great potential in implementing multi standard single chip solutions, eliminating the need to use off chip components and so reduce the area and the cost of the wireless receivers. One of the main performance limitations in the low-IF & Zero-IF down-converters is the components mismatch between the in-phase path and the quadrature-path named the IQ Imbalance (IQI) which limits the achievable image rejection ratio (IRR) of the down converters. Many techniques had been proposed to enhance the achievable IRR either by using calibration methods, e.g. using lab calibration, or by doing online compensation during signal reception. In this work those techniques are reviewed, proposing three new methods for blind IQI compensation techniques, the first proposed method targets the low input signal to interference ratio (low SIR_{in}) while the second and third methods targets the moderate and high SIR_{in}, showing that the proposed methods reach better performance and/or lower complexity than the methods already introduced in the literature. Also two techniques to perform data aided IQI compensation are introduced exploiting pilot symbols within the desired signal with no prior knowledge about the image signal. The first method exploits a preamble sequence assuming slow fading condition while the second approach exploits a sequence of pilots to compensate for the IQI being suitable for fast fading conditions as well. Simulation results showed that the proposed data aided techniques achieved shorter convergence time and higher image rejection ratio compared to the blind methods at high SNR values.

Contents

IV

List of Figures

List of acronyms

IRR: Image Rejection Ratio
IC: Interference Cancellation
BSS: Blind Source Separation
FD mismatch: Frequency Dependent Mismatch
FI mismatch: Frequency Independent Mismatch
SDR: Software Defined Radio
SOC: System on chip
LMS: Least mean square
IF: intermediate frequency
PLL: phase locked loop
WSN: Wireless sensor networks
SFG: signal flow graph
SAD: Symmetric adaptive decorrelation
PPF: positive pass filter
NPF: negative pass filter
PAR: peak to average power ratio
ISR: image to signal ratio
SIR: Signal to interference ratio

1. Introduction

1.1. Background & Motivation

The wireless communication market has grown substantially in the last few decades. In order to fulfill the unlimited demands of the wireless market, more sophisticated communication standards were invented to achieve more enhanced performance, supporting more applications with lower costs and longer battery life. Having a separate design for each standard is a high cost solution, that is why SDR (software defined radio) is becoming more of a demand in order to support multi communication standards by just loading the appropriate software configuration for the transceiver, this implies that the hardware radio front end must be able to support the different standards including different frequency carriers and channel bandwidths instead of using different hardware sets for each standard and switching between them. That is why having flexible transceiver topologies & adaptive design techniques is of a main concern when targeting a multi standard hardware radio front end.

To support SDR transceivers using the same hardware frontend, the off chip components such as image reject filters and RF filtering stages, normally used for Super-heterodyne receivers, must be eliminated. That is why low IF and direct conversion receiver architectures showed a huge potential in achieving a single chip solution that support SDR transceivers[1]. Different approaches have been used to do image rejection such as using image reject mixers, complex filters or complex ADC's. Historically those image reject approaches showed acceptable performance, but recently due to the need to support more sophisticated multi channel communication standards the IRR (Image rejection ratio) specification became more stringent and hard to achieve using the traditional layout techniques used before [2], that is why IQ mismatch calibration & compensation techniques were implemented in the last decade and proved to be efficient in enhancing the IRR. Another advantage for using the IQ mismatch calibration & compensation techniques is the ability to track the changing operating conditions, such as temperature variation, operating RF power variations and drifting without adding extra complexity on the analog front end circuitry, especially that the analog front end circuitry dominates the total power consumptions in typical receivers. In general adaptive design techniques are one the most important approaches used recently to achieve wideband, multi standard designs.

The image reject mixers using secondary quadrature mixing shown in Fig. 1 showed a lot of potential in implementing image reject receivers with high IRR because ideally if no IQ mismatch exists it achieves an infinite image rejection ratio over a wide bandwidth unlike the case for complex filters or image reject mixers using poly-phase filters which are band limited and being in the signal path introduces losses to the signal reducing the receiver sensitivity unless higher power is consumed [3, 4, 5, 6]. A small overhead of two extra real adders are

required to generate the image signal in the secondary quadrature mixing architecture [4, 7], which adds more flexibility in implementing IQ mismatch compensation and calibration techniques that require the image signal to be part of cancellation process [8].
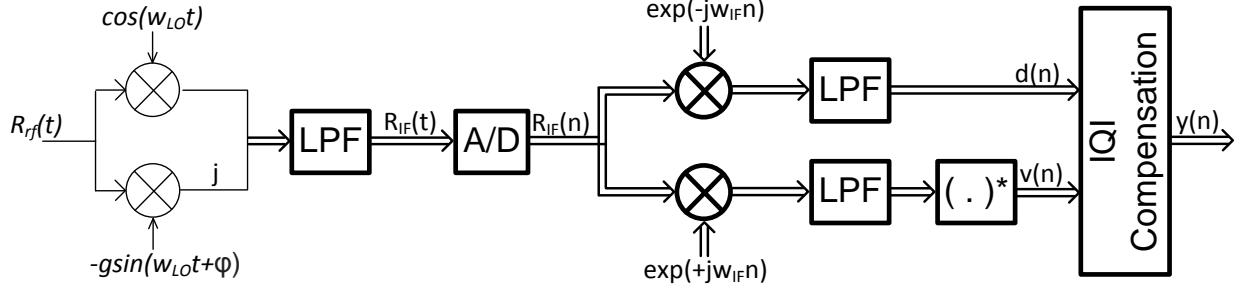
Fig. 1: Secondary Double Quadrature Mixing Image Reject Receiver (Modified Weaver Architecture)

1.2. IQ Mismatch Calibration & Compensation

Secondary quadrature mixing receiver achieves infinite IRR if the I and Q paths are fully symmetric, which is not the case because of the finite manufacturing accuracy, these mismatches between the I & Q paths are called IQ imbalances (IQI) or IQ mismatches or quadrature imbalance, traditionally layout techniques were used to minimize these imbalances. Typical achievable IQI using the layout techniques is a gain mismatch of 1-2% and a phase mismatch of 1-2degrees, this is equivalent to IRR of 35-40dB as shown Fig. 2 and expressed in (1.1) [9]:

$$IRR = \frac{1 + g^2 + 2gcos(\varphi)}{1 + g^2 - 2gcos(\varphi)} \tag{1.1}$$

Where "g" is the gain mismatch between I & Q paths and "φ" is the phase mismatch in the first quadrature mixer, given that the secondary digital mixing stage is ideal and do not add extra IQ imbalances.

This finite IRR will not be suitable for low IF receivers where the IF frequency can be chosen so that the image signal can be an in-band channel with power level 50 dB or more higher than the desired signal as shown in Fig. 3 [10], especially that using such layout techniques adds a new design constrain on the analog frontend which by default compromises other performance parameters.

Digital techniques for IQI estimation and compensation have been proposed achieving much better IRR and so relax the specification on the analog frontends circuitry in terms of IQ mismatches. Some techniques were based on offline lab-calibration using test tones, other techniques were based on online IQI compensation exploiting the signal statistics to compensate for the IQI.
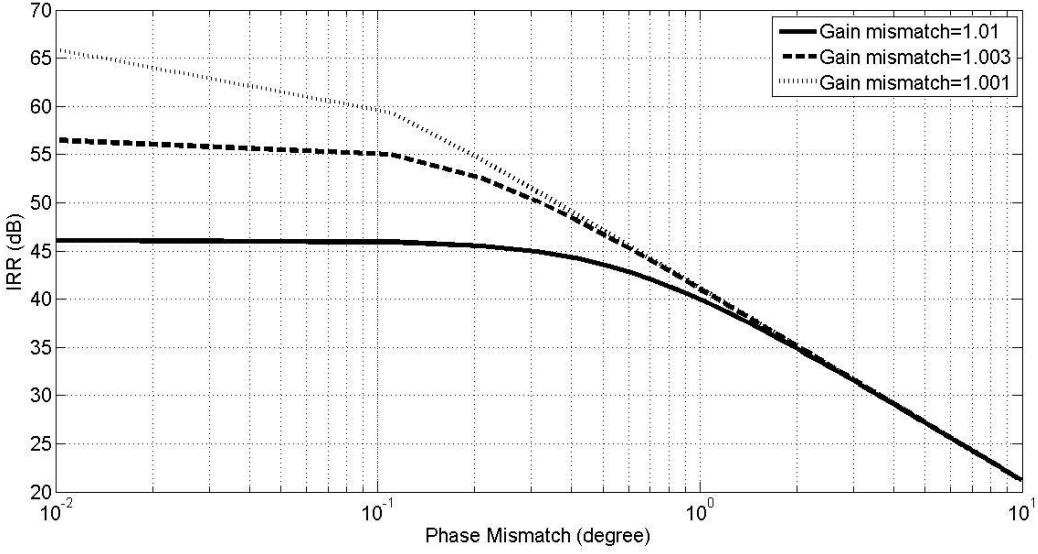
Fig. 2: IRR across Phase Mismatch (ϕ) at different gain mismatches (g)
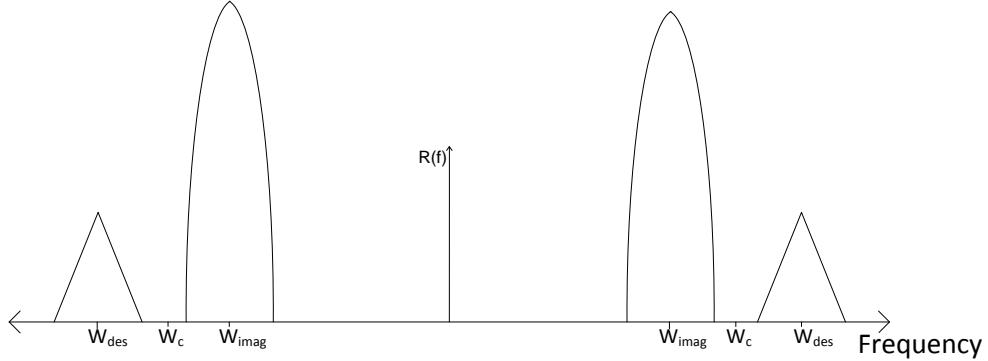
Fig. 3: Multi channel frequency band

1.2.1. IQI Calibration

IQI calibration is the process of adjusting the gain and the phase mismatches to meet certain image rejection requirement. This process can be non-adaptive where the calibration is done once as a factory or a lab calibration, but it is not repeated during normal operation or even at idle modes. In the non adaptive calibration methods a test signal at the image frequency is used as an input to the image-reject down-converter, ideally the image signal will be rejected and so the output will be null, but due to the existence of the IQI some of the image signal will leak to the output, so the output signal is used as an error signal in an iterative (feedback based) algorithm (e.g. LMS,RLS..etc) [11] to update the gain and phase adjustment knobs in the LO amplifiers and the mixers to minimize the IQI. Also it can be adaptive where the calibration can be repeated in the field at the receiver idle modes using an internally generated image signal[8]. IQI calibration is normally a simple approach but it is either not adaptive or requires an extra hardware. Also doing factory calibration is not a preferred solution in mass production due to the extra testing time and cost. That is why IQI compensation methods were proposed.

14

1.2.2. IQI Compensation

In the IQI compensation approaches the gain and phase mismatches are not adjusted instead their effect are cancelled in the digital domain during normal operation and so this approach is an online adaptive approach compensating for the IQI and tracking temperature variations, varying operating conditions or aging [8, 10, 12]. A good example for the varying operating conditions is having a variable gain amplifier (VGA) at the receiver front end and so as the gain of the VGA changes the IQI will change as well which will be a time varying process depending on the received signal power, this is an example that clarify why an adaptive IQI compensation technique would be a must have in many cases. Different methods were proposed to do the IQI compensation; these different methods will be reviewed in chapter 2.

1.3. Research Objectives

The objective of this work is to review the main IQI calibration and compensation techniques introduced in the literature, and to improve upon them for the case of low-IF receivers, focusing on low-complexity techniques. We propose three low complexity and robust methods for blind IQI compensation. In the first method a single tap filter is used to cancel the leaked image from the desired signal similar to the interference cancellation method introduced in the literature, but instead of using iterative LMS algorithm the filter coefficient is estimated using the method of moments, enhancing the steady state output signal to interference ratio (SIR_{out}) and/or the settling time. Furthermore, the output SIR performance analysis was carried out for this method to verify the simulation results. The second method is a variant for the IQI compensation method using a dual-tap filter, in the proposed method the input signal to interference (SIR_{in}) ratio is estimated and used to optimize for the number of symbols required to do the IQI compensation, where again the method of moments is used to estimate the filter coefficient and the estimated SIR_{in}. Then in the third method we propose a simplification for the symmetric adaptive de correlation method introduced before in the literature reaching the same performance with less complexity. Also two data aided IQI compensation method are proposed, exploiting pilot symbols within the desired signal with no prior knowledge about the image signal, the first approach exploit a preamble sequence assuming slow fading conditions while the second approach is suitable for fast fading conditions as well exploiting a sequence of pilot signals to do IQI compensation.

1.4. Thesis Organization

In this work an overview will be given for the different receiver architectures & the image reject receivers focusing on the secondary quadrature mixer receiver in chapter 2. In chapter 3 more insight will be given for the different types of IQI calibration and compensation techniques. The first proposed blind IQI compensation method using a single tap filter will be introduced in chapter 4. Then the two blind IQI compensation methods using dual tap filter will be introduced in chapter 5. In chapter 6 the data aided IQI compensation will be introduced and concluding in chapter 7.

2. Image Reject Receivers & Mixers

2.1. Receiver Architectures

2.1.1. Super-Heterodyne Receiver

Over the last few decades the Superheterodyne receiver architecture was the mostly used architecture for high performance wireless communication standards frontends [13], basically because high image rejection ratios are achieved using off chip image reject filters. As shown in Fig. 4 the line up of the super-heterodyne receiver frontend consists of an antenna that collect the signal for an off-chip RF filter to select the band of interest, then the low noise amplifier is used to amplify the signal adding the minimal possible noise, after that the high image rejection rations (IRR) are achieved using an off chip IR (Image Reject) filter, at this stage a mixer is used to down-convert the band of interest from RF frequency to IF frequency, using another off chip IF filter to do the channel selection before using another mixer to convert the IF signal to baseband signal and using an on chip LPF to remove the higher order harmonics.
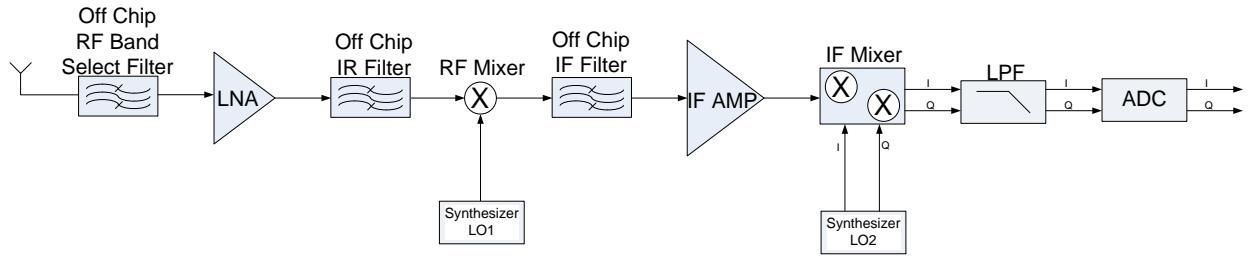
Fig. 4: Superheterodyne Receiver Architecture

In the past few years a lot of effort had been done to integrate the LNA, RF Mixer, IF Filter, IF AMP, IF Mixer, LPF & ADC in a single chip solution, leaving only the RF filter, IR Filter & IF filter as the only off chip components. This was the first step toward having a single chip solution, the second step was to get rid of the off chip filters by using different receiver architectures as will be discussed in the next sections.

An important choice in the Superheterodyne receiver is the value of the IF frequency which depends on the RF frequency and the level of image rejection required from the off chip filters, so to achieve high IRR the IF frequency must be high enough for the IR filter to supply enough rejection [9]. Using off-chip components increases the solution cost and reduce the solution flexibility because for each IF frequency a different IR and IF filters is needed, this means that a bank of filters is needed if multi standards are targeted. This is contradicting with the recent trend to have low cost and multi standard solutions to satisfy the software defined radio (SDR) receivers. That is why a lot of interest had been given to the low IF & direct conversion receivers because of their great potential to achieve a single chip solution reducing the required off-chip components as will be discussed in the next subsections.

2.1.2. Direct Conversion Receiver (homodyne receiver)

In order to avoid the image problem it was proposed to convert the RF signal directly to baseband, which is equivalent to using an IF frequency of zero, that is why it is called a zero-IF or homodyne or direct conversion receiver. In the direct conversion receiver the down conversion occur from the RF frequency to the dc frequency directly using a single mixer as shown in Fig. 5. In direct conversion receivers the channel select filter is a LPF instead of the BPF used in the Superheterodyne receiver. If the modulation scheme produces a symmetric magnitude spectrum, i.e. where the lower and upper sidebands exhibit even symmetry in the magnitude spectrum of the signal, then the image problem is eliminated , but for the non symmetric channels the signal will act as an image for itself, where half of the channel band width act as an image for the other half as shown in Fig. 6 which is called "self imaging", which requires an image reject receiver as well to reject it [13].
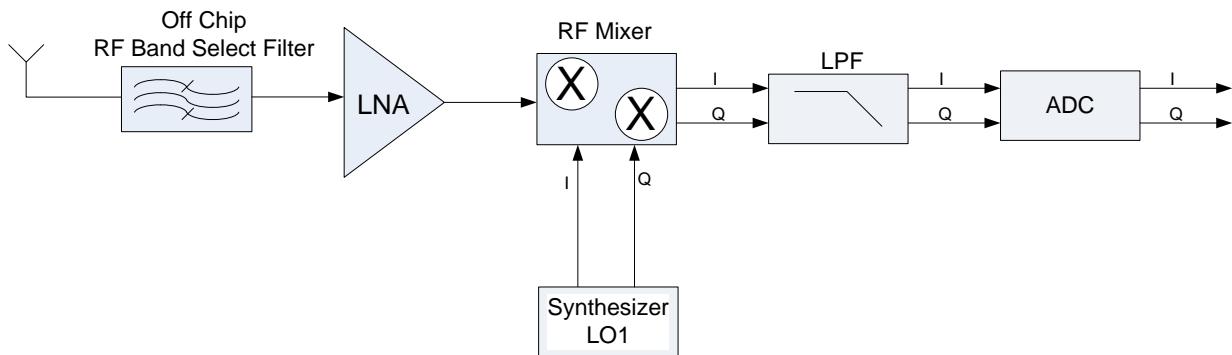
Fig. 5: Direct Conversion Receiver Architecture
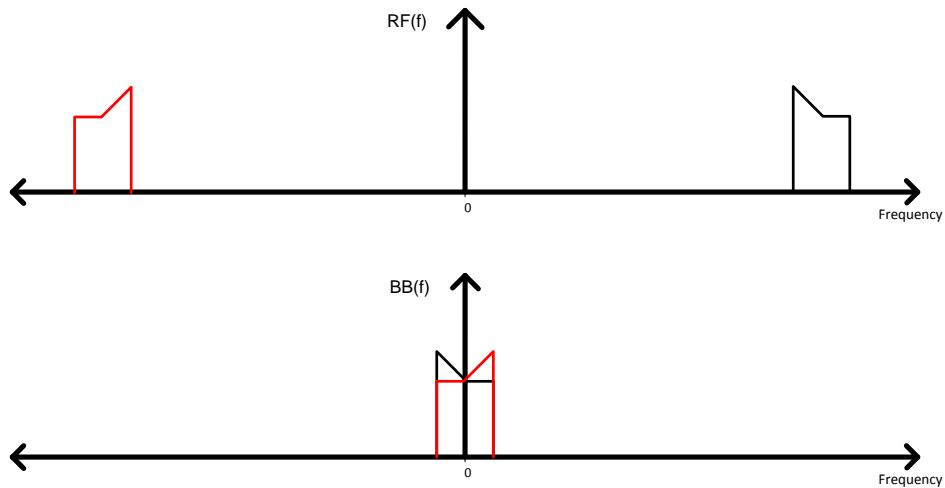
Fig. 6: Self Imaging In Direct Conversion Receiver

Furthermore, the direct conversion receiver suffers from some disadvantage such as the flicker noise [13], i.e. which is the 1/f noise that form a skirt across the DC frequency, because the desired signal now is converted directly to the base band, also the RF frequency is now equal to the LO frequency so LO to RF leakage lead to DC offset which destroys the baseband signal.

IM2 become an issue in direct conversion, these drawbacks complicate the design process adding a lot of constrains on the front end design in order to satisfy the flicker noise and IM2 requirements. DC offset cancellation loops with very narrow cut off frequencies are used to cancel the DC offsets along the receiver chain in order to avoid SNR degradation for the baseband signals, this might cause some limitations because of the need to use off chip capacitors [14].

In order to avoid the drawbacks of the direct conversion receiver and the superheterodyne receivers a compromised solution was proposed which is the Low-IF receiver as discussed next [15].

2.1.3. Low IF Receivers

In order to compromise between the Superheterodyne receiver and the direct conversion receiver the low IF architecture was suggested, in which down conversion is done to a low IF frequency but not a zero IF frequency as shown in Fig. 7, in such case the IF frequency is low enough that having an on-chip IF band pass filter is possible unlike the Superheterodyne receiver. This solved the drawbacks of the direct conversion and benefited from the idea of going to an IF frequency, but the image problem is critical now because the low IF frequency means that the image might be an in band signal, and therefore cannot be attenuated by the RF BPF. Such an image might be stronger than the desired signal by 60-100dB [10, 16]. In some applications the dynamic range might reach 80dB (e.g. GSM and point to point communications). For example if user 1 receives a signal at -90dBm, and user 2 receives a signal at -10dBm, and if user 2 is at the image frequency of user 1 then the input signal to interference ratio for user 1 will be -80dB.

Worth mentioning that the channel selection filter can be implemented in the digital domain as well, but it worth mentioning that as much as the channel select filter is delayed in the chain, the linearity of the front end blocks become harder to be achieved because the whole band will be experienced by the receiver chain, in other words the blocker will be a factor that must be considered through the receiver chain till the channel select filter is reached, so the earliest the better.
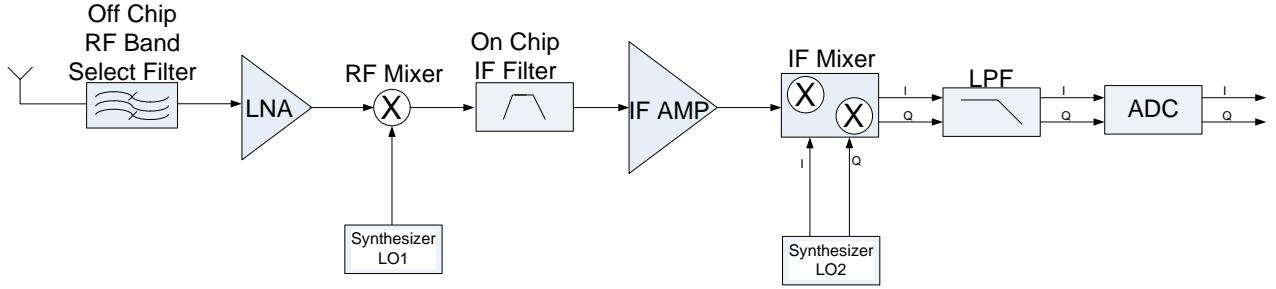
Fig. 7: Low IF Receiver Architecture

The choice of the IF frequency affects the digital sampling rate and so the power consumption, also it affects the image separation from the desired signal and so it is power and how much image rejection is required. Usually the IF frequency is chosen to be equal to or double the channel band width. Generally low IF receivers consumes less power and area compared to direct conversion receivers, because no large on chip or off chip DC decoupling capacitors are required also no need to use large devices to decrease the flicker noise as done in the direct conversion receivers, but the image rejection specifications become more stringent in the low IF receivers because the image signal can be an in band channel that is 50-80 dB stronger than the desired signal. Different solutions to do image rejection in low IF receivers will be discussed in chapter 3 after giving a brief introduction about the complex signaling and the IQ signaling in the next section.

2.2. IQ Signaling & Complex Signaling

2.2.1. Complex Signaling

Complex signaling is used to represent the image reject receiver architectures in a simplified manner, to be easily understood and derived. Instead of using the real signaling representation which is more complicated and not as intuitive as the complex representation.

All physically existing signals are real signals with symmetric frequency responses, and a complex signal is basically two real signals in two separate signal paths, as shown in Fig. 8, the two signals $Y_r(t)$ & $Y_Q(t)$ are mathematically represented as one complex quantity $Y(t)$, where the $Y_r(t)$ represents the real part of $Y(t)$ and $Y_Q(t)$ represents the imaginary part of $Y(t)$. Note that the complex signal on its own is not a physically existing signal so its frequency response might not be symmetric, the basic complex signaling processes will be briefed comparing the real signal flow diagram (RSFD) to the complex signal flow diagram (CSFD) based on the formulations in [4].
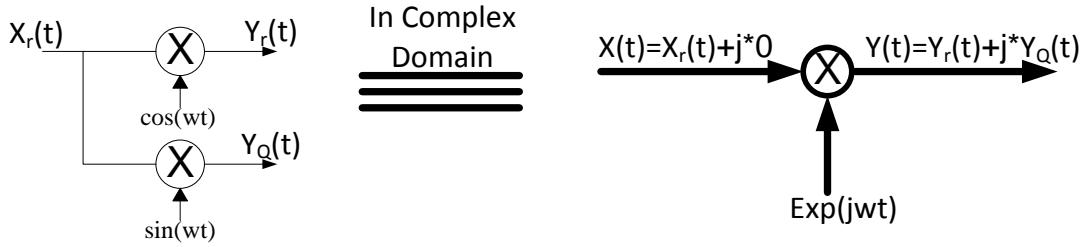
Fig. 8: Quadrature Mixing In Real & Complex Domain

2.2.2. Complex Signal Processing

2.2.2.1. Complex Signal Multiplication

Defining two complex signals X & $(a+jb)$, where the outcome for the signal multiplication of X & $(a+jb)$ is Y in equation(2.3) and shown in Fig. 9 in the real signaling domain and in the complex domain, showing how the complex representation of such multiplication is much easier than the real signaling multiplication.

$$X = X_r + jX_I \tag{2.1}$$
$$Y = Y_r + jY_I \tag{2.2}$$
$$(X_r + jX_I)(a + jb) = (aX_r - bX_I) + j(aX_I + bX_r) \tag{2.3}$$
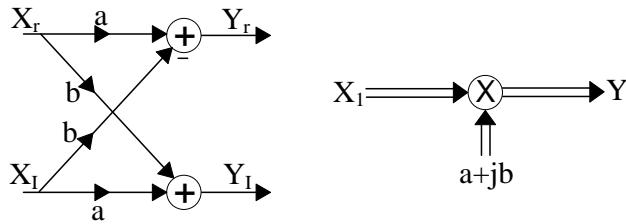
Fig. 9: Real & Complex Signal Multiplication

2.2.2.2. Complex Signal Addition

Defining two complex signals X_1 & X_2 , adding X_1 & X_2 is equivalent to adding the real components and imaginary components together as shown in Fig. 10.

$$X_1 = X_{1r} + jX_{1I} \tag{2.4a}$$
$$X_2 = X_{2r} + jX_{2I} \tag{2.4b}$$
$$Y = (X_{1r} + X_{2r}) + j(X_{1I} + X_{2I)} \tag{2.5}$$
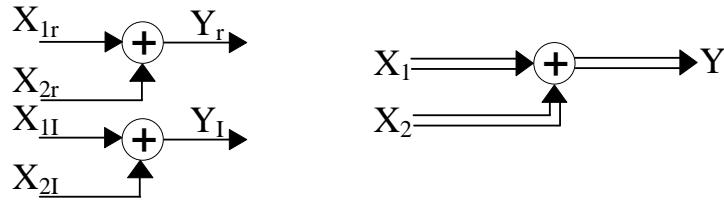
Fig. 10: Complex Signal Addition

2.2.2.3. Complex Signal Conjugation

Taking a conjugate for a complex signal in the time domain is equivalent to mirroring the frequency response across the Y-axis in the frequency, which is not equivalent to multiplying by "j". The real and complex signaling diagrams for conjugation and multiplication by "j" are shown in Fig. 11 & Fig. 12.

Now after reviewing the main complex processes we can review the IQ quadrature signaling and relate it to the complex signaling.
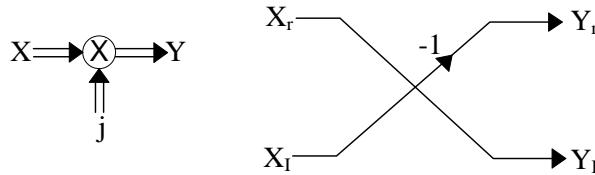
Fig. 11: Complex Signal Multiplication By "j"
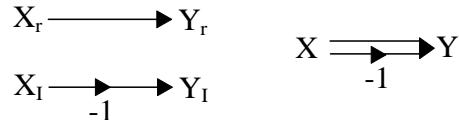
Fig. 12: Complex Signal Conjugation

2.2.3. Quadrature Signaling

Quadrature signaling (IQ signaling) consists of two paths, I path & Q path, having a phase shift of 90 degrees between them, IQ signaling is mainly used for two aspects, the first one is the quadrature modulation schemes to increase the data rate within the same channel band width making advantage of the orthogonal characteristics between the I & Q signals, the second aspect is the image rejection making advantage of the phase shift existing between the down-converted desired and image signals.

The IQ signaling is represented in complex domain (complex signaling) by considering the I signal as the real part and the Q signal as the imaginary part, again this is done to simplify the analysis and representation of the image reject receivers and image reject mixers.

2.3. Image Reject Receivers

Image reject receiver architectures are needed in zero & low IF down converters to do image rejection. In the next section we will review the basic image rejection techniques introduced in the literature, focusing on the secondary down conversion mixer receiver architecture.

2.3.1. Image Reject LNA

In this architecture the image rejection is done using the LNA [18], by having a notch filter after the LNA to null the image frequency as shown in Fig. 13. Using the LNA to cancel the image is a simple approach that can be used for the low IF architecture, that consume low power because no IQ signaling is required, but it's a narrow band solution as shown in Fig. 14 because the filter is tuned at a definite frequency, also if multi carriers are supported this topology will not be adequate because re-tuning such filters will suffer from process limitations and will be limited in the frequency step resolution.
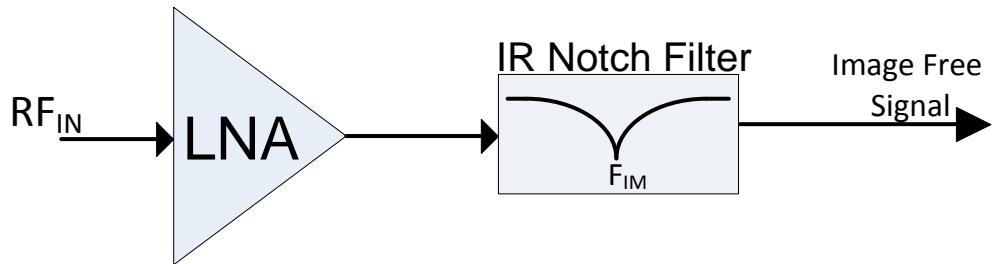
Fig. 13: Image Reject LNA using an image reject notch filter
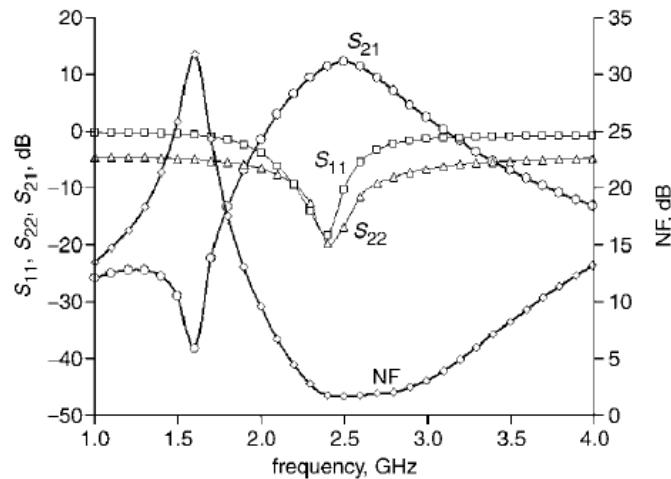
Fig. 14: Frequency Response of the image reject LNA [18]

2.3.2. Image Reject Mixers

In this series of topologies the image is rejected using the phase difference between the image signal and the desired signal when multiplied by the in phase LO signal (cos ($w_{lo}t$)) and the quadrature phase LO signal (sin ($w_{lo}t$)) as shown next.

2.3.2.1.   Hartley Receiver

In Hartley receiver architecture, quadrature mixing is used to convert the RF signal to an IF frequency followed by a 90 degree shift in the I-path, then the I & Q path are added to cancel the image signal as shown in Fig. 15 [13]. In superheterodyne or low IF receivers the addition occurs on chip and the output is a single ended signal, but in direct conversion the output is an I and Q signal and therefore the image rejection can not be performed by summing since this will eliminate the desired signal. Note that, while image rejection is accomplished a single mixer and a low pass filter are needed to bring the signal down to baseband.
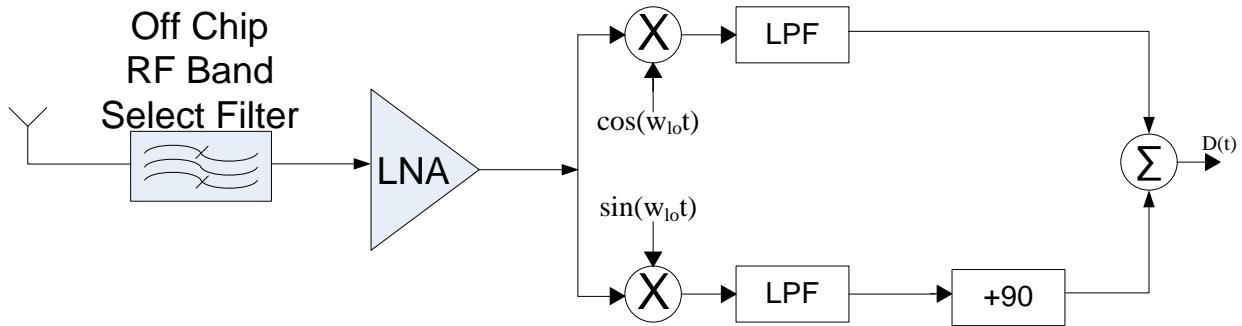
Fig. 15: Hartley Receiver Architecture

Note that in this architecture two 90^0 shifters are required, one in the LO path and the other is in the IF path as shown in Fig. 15. But the same function can be obtained if the 90^0 shifter where in the LO path and in the RF path as shown in Fig. 16, or even in the RF path and the IF path as shown in Fig. 17, but this is not a favorable architecture because the two 90^0 phase shifters are in the signal path and so more insertion loss takes place.
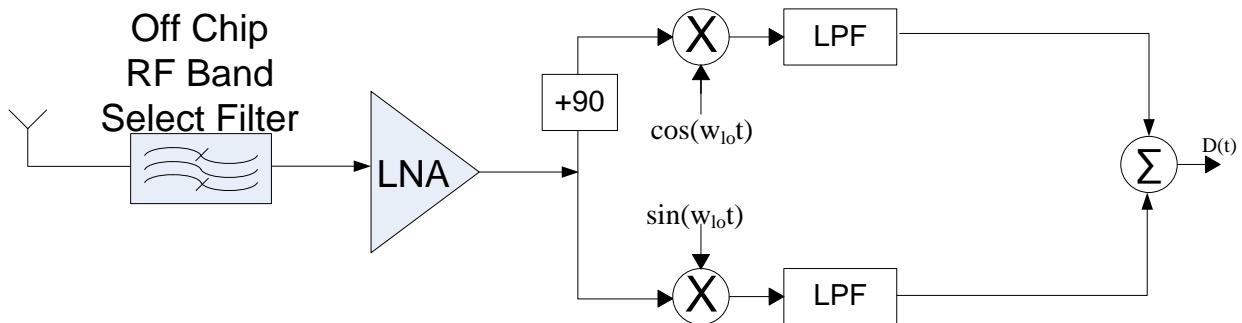
Fig. 16: Hartley Receiver Architecture Using 90^0 Hybrid at the LO & RF Sides
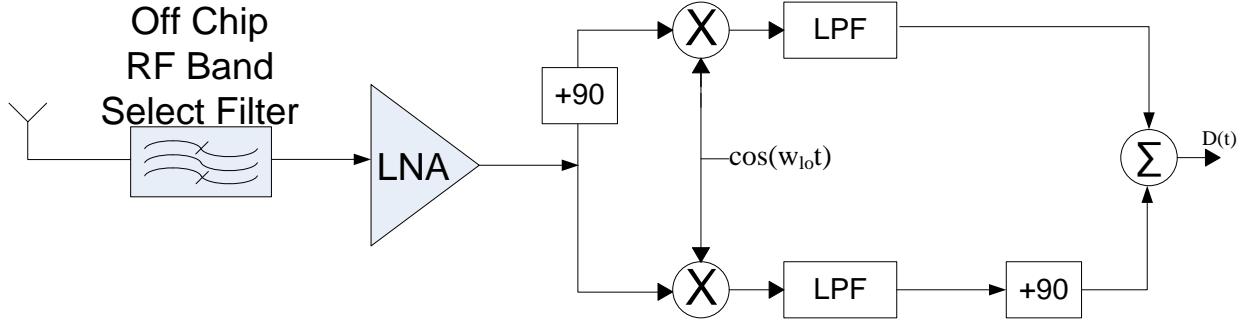
Fig. 17: Hartley Receiver Architecture Using 90^0 Hybrid at the RF & IF Sides

To implement the 90^0 shift, the simplest way is to use two RC filter [13] in the I & Q paths and so the R & C values determine the center frequency of the 90^0 phase shifter, this architecture is simple but suffers from low band width. An alternative is to use the poly-phase filter shown in Fig. 18, being wider in bandwidth than the first solution but it suffers from more components mismatches, which adds complexity to model such mismatches and degrade the overall performance. The poly-phase filter can also be used as an image reject filter and this will be discussed in section 2.3.3.

When the poly-phase filter is used as a 90^0 shift, two of its inputs are grounded, and so it will have 2-inputs and 4-outputs. but when it is used as an image reject filter it will have 4-inputs and 4-outputs.

Another approach used to get the 90 degrees in the LO path is to use a divide by 2 frequency divider that generate the LO quadrature signaling [19] from a signal that is twice the frequency, this approach can only be used in the LO path.
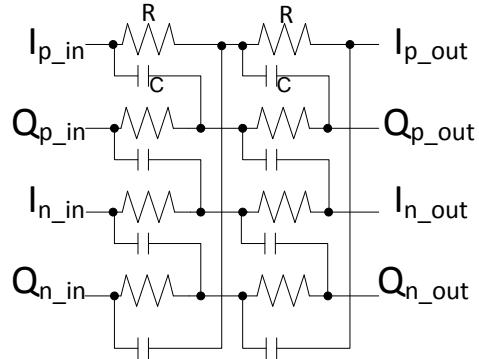
Fig. 18: Poly Phase Filter

2.3.2.2. Weaver Architecture

Quadrature mixing is used in this topology, but it is used twice as shown in Fig. 19. That's why it is sometimes called secondary quadrature mixing. In this architecture, the second quadrature mixing is used to support multi IF frequencies whereas the Hartley architecture is typically fixed to a single IF for a simple 90 degree phase shifter designs.

The Weaver architecture is mostly used in standards where the image rejection specification is tough either due to the standard itself or due to the usage of low IF down converters, which means that the image power can be another adjacent channel with power levels 40-80 dB stronger than the desired signal [10]. Also it is preferred for multi IF and multi standard designs because normally the mixer BW, for our purpose it is the range of the IF frequencies, is wider than the poly phase filter BW [20, 21].
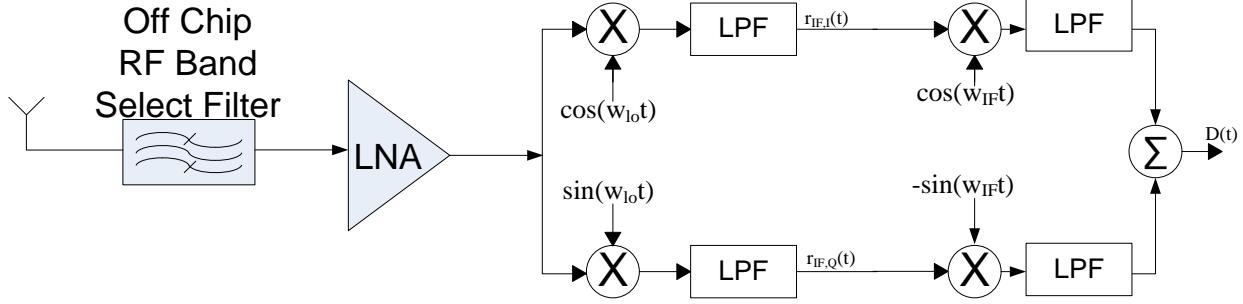
Fig. 19: Weaver Receiver Architecture For Image Reject Mixers (For Low IF Receivers or Direct Conversion Receivers with Symmetric Channel Responses)

Although the fact that implementing two mixers instead of one increase the substrate coupling and increase the power consumption, the quadrature mixing receiver showed a very good potential in multi standard designs because in ideal conditions it allow an infinite IRR over wide band width.

To mathematically explain the image rejection operation that is performed by the weaver architecture, we will assume that a RF signal consists of the summation of the desired signal s(t) and the image signal q(t) as:

$$s(t) = m(t)\cos(w_{des}t) \tag{2.6a}$$
$$q(t) = i(t)\cos(w_{imag}t) \tag{2.6b}$$
$$r(t) = m(t)\cos(w_{des}t) + i(t)\cos(w_{imag}t) \tag{2.6c}$$

And so after the first mixing stage and low pass filtering we get the IF signal as:

$$r_{IF\_I} = r(t).\cos(w_{lo}t)$$
$$= \frac{1}{2}(m(t)\cos(w_{IF}t) + i(t)\cos(w_{IF}t)) \tag{2.7a}$$

$$r_{IF\_Q} = r(t).\sin(w_{lo}t)$$
$$= \frac{1}{2}(-m(t)\sin(w_{IF}t) + i(t)\sin(w_{IF}t)) \tag{2.7b}$$

25

After that the IF signals r_{IF_I} and r_{IF_Q} are multiplied by the secondary mixers the signals at the output of the low pass filters are as follows:

$$r_{IF\_I} \times \cos(w_{IF}t) = \frac{1}{4}(m(t) + i(t)) \tag{2.8a}$$

$$r_{IF\_Q} \times -\sin(w_{IF}t) = \frac{1}{4}(m(t) - i(t)) \tag{2.8b}$$

Then by adding (2.8a) to (2.8b) as shown in Fig. 19, the image signal is cancelled leaving only the desired signal as the output signal. The above analysis shows that infinite image rejection is theoretically achievable, but in practical situations the existence of the gain and phase mismatches only allows a finite IRR as will be discussed in more details in section 2.4.

In Fig. 19 it is assumed that non-quadrature modulation is applied at the transmitter, e.g. amplitude modulation or BPSK, for quadrature modulations the second down conversion must consists of four mixers producing the I-path and the Q-path as shown in Fig. 20. The second mixing stage can be performed either in the analog or digital domain but it is typically performed in the digital domain as shown in Fig. 20. In the literature this architecture is sometimes called "Modified Weaver Architecture " or " Secondary Double Quadrature Receiver" [22].
The modified Weaver architecture showed high flexibility in terms of re generating the image signals as easy as re generating the desired signal, this is a good characteristic that adds flexibility when choosing the IQI compensation technique. Throughout this work, we operate on quadrature modulation signals (QPSK).
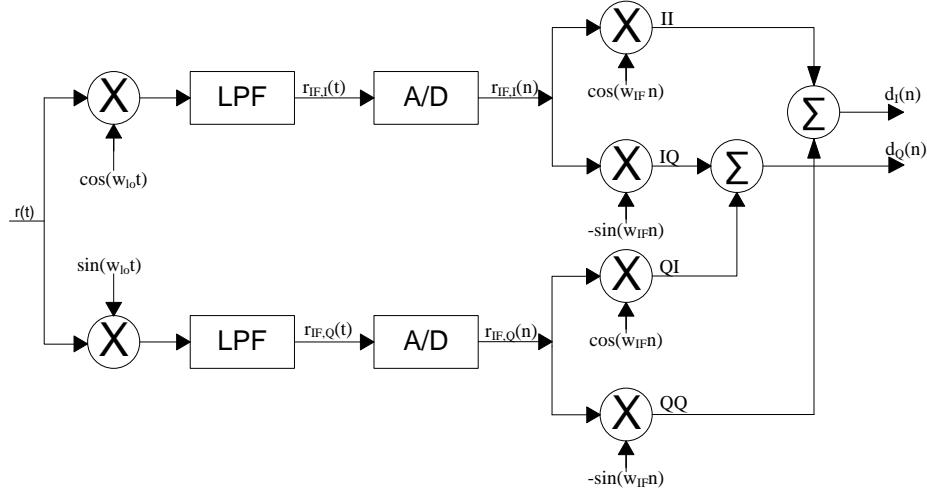
Fig. 20: Modified Weaver Receiver Architecture (Secondary Double Quadrature Receiver)

26

2.3.3. Image Reject Complex Filters

The complex filter, also called positive pass filter(PPF), is a filter that reject the image signal as shown in Fig. 21. The complex filter basically consists of two low pass filters cross coupled in a certain way to reject the image frequency [1, 17]. The mostly basic PPF is the Hartley architecture where two RC filters are used at the I & Q paths followed by an adder to reject the image frequency. Another approach which is less sensitive to the process variations is to use the poly-phase filter to generate a 90 degree shift instead of using two LPF filters. The real signal model of the complex filter is shown in Fig. 22.

The complex filter can be implemented in the analog domain [23] or in the digital domain [24]. The analog complex filter is mostly used in standards where the power specification is the main concern, but the image rejection requirements is somehow relaxed compared to high performance standards where the image rejection ration is more stringent.
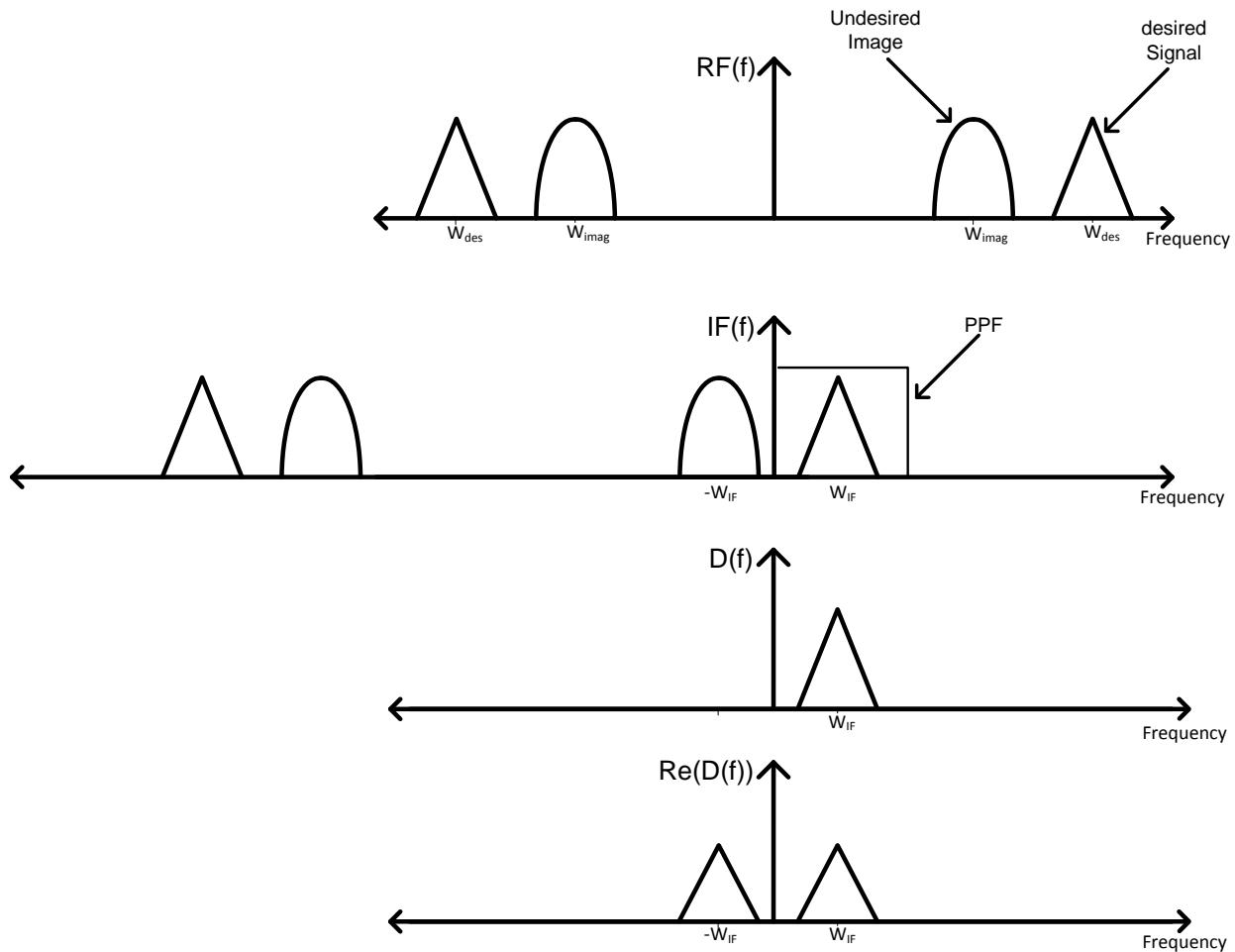
Fig. 21: Complex Frequency Spectrum For the Quadrature Mixing & Image Signal Filtration
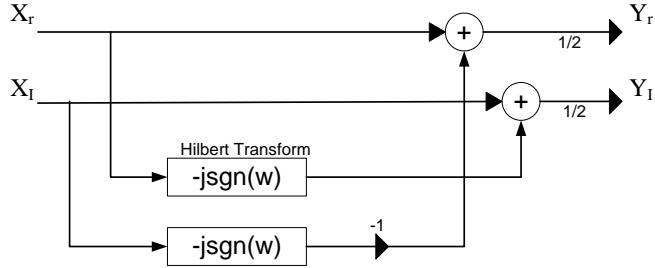
Fig. 22: Real Signal Model For the Complex Filter

The rejection achieved by the complex filter depends on the filter order even at ideal conditions, were the filter is centered at a definite IF frequency with a certain resolution for the filter tuning, this adds a limitation into the range of the IF frequency that can be covered, unlike the image reject mixer which normally covers wider bandwidths achieving ideal IRR of infinity, another limitation is that designing a BPF at high IF frequency is not easy as well, that is why when complex filters are used more constrains occur on the choice of the IF frequency unlike the image reject mixers which adds no constrains on the choice of the IF frequency value.

Increasing the order of the filter will increase its rejection ratio, but unfortunately the component mismatches will increase as well, due to the extra filter stages, degrading the SNDR once again, so there is an optimum order for the filter beyond which the SNDR will not be enhanced [25].

After discussing the advantages and disadvantages of the basic image reject receiver architectures, this work will focus on the secondary double quadrature mixer receiver (Modified Weaver architecture) being a potential solution for multi standard single chip solutions. The mathematical model will be derived using real and complex signaling considering the IQ mismatch in the model.

2.4. Secondary Quadrature Mixer Receiver Mathematical Model With IQI

As discussed in section 2.3.3, the secondary quadrature mixing generates the desired signal using two cascaded mixing stages followed by an addition process, in the same way the image signal can be generated using two more adders as sown in Fig. 23, generating the image signal with such a little overhead is an important advantage for this topology. The mathematical derivation for the modified Weaver architecture generating the desired and the image signal assuming frequency independent IQI will be derived in this section using the complex signaling approach [9, 10]:

28
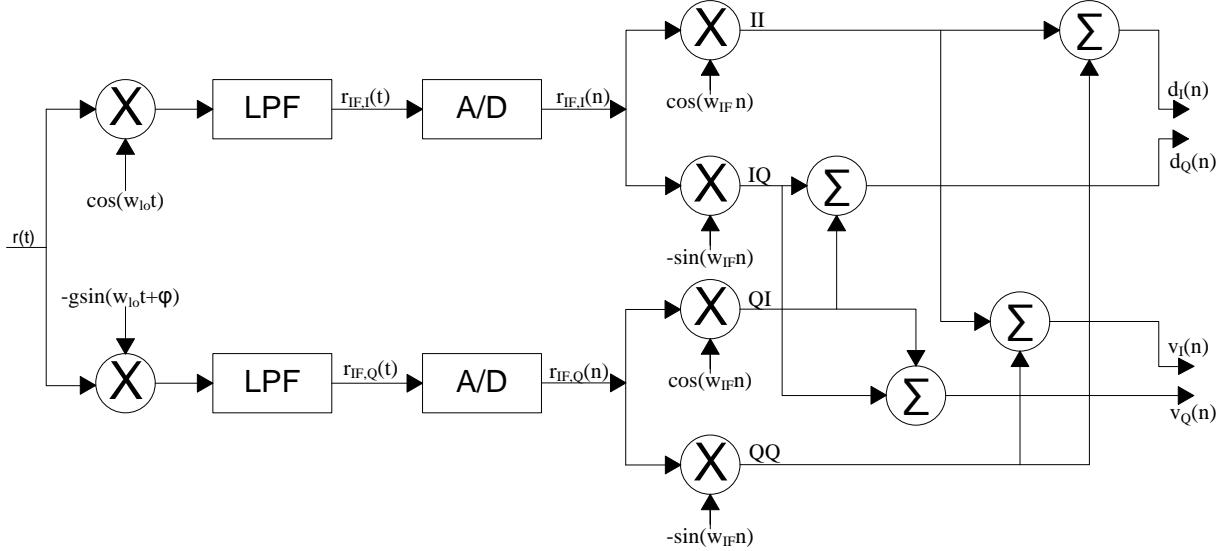
Fig. 23: Modified Weaver Architecture Model Including IQ Mismatches

2.4.1. Secondary Quadrature Mixing Receiver Mathematical model

The secondary quadrature mixing receiver shown in Fig. 23 can be expressed in the complex domain as shown in Fig. 24 [9, 10], for the sake of intuition at each step a clarification will be given for each signal being real or complex.
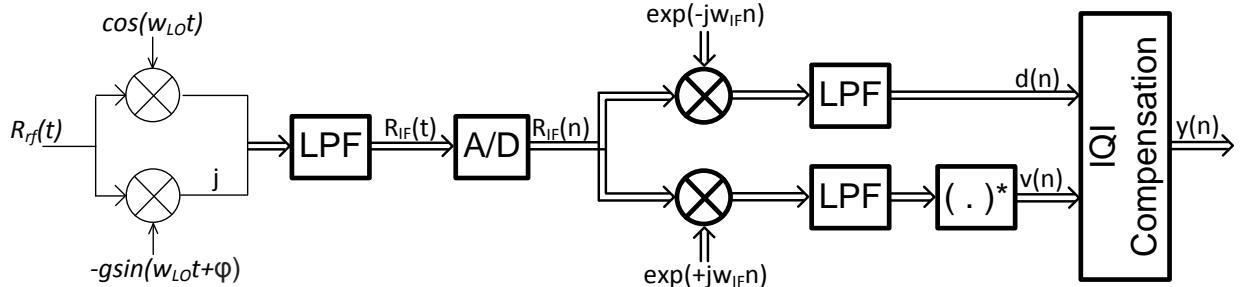
Fig. 24: Modified Weaver Architecture in Complex Domain

The non ideal LO signal in the complex representation can be modeled as:

$$x_{lo}(t) = \cos(w_{lo}t) - jg\sin(w_{lo}t + \Phi) \tag{2.9}$$

Converting the sinusoidal of (2.9) to the exponential form and doing some mathematical simplifications it can be rewritten as:

$$x_{lo}(t) = K_1 e^{-jw_{lo}t} + K_2 e^{jw_{lo}t} \tag{2.10}$$

where K1 and K2 are two complex quantities defined as:

$$K_1 = \frac{1 + ge^{-j\Phi}}{2} \tag{2.11}$$

$$K_2 = \frac{1 - ge^{j\Phi}}{2} \tag{2.12}$$

where at ideal conditions g=1 and $\Phi = 0$, so K₁=1 & K₂=0.

A very important relation between K_1 and K_2 is obtained using (2.11) and (2.12) to be:

$$K_1 = 1 - K_2^* \tag{2.13}$$

A simple way to model the *r(t)* is to define its baseband equivalent signal *z(t)* for the RF signal consisting of the desired signal *s(t)* and image signal *i(t)* , as shown in Fig. 25 given that *s(t)* and *i(t)* are real physically existing signals with a symmetric frequency response while *z(t)* is a complex signal so it is frequency response might not be symmetric across the Y-Axis.
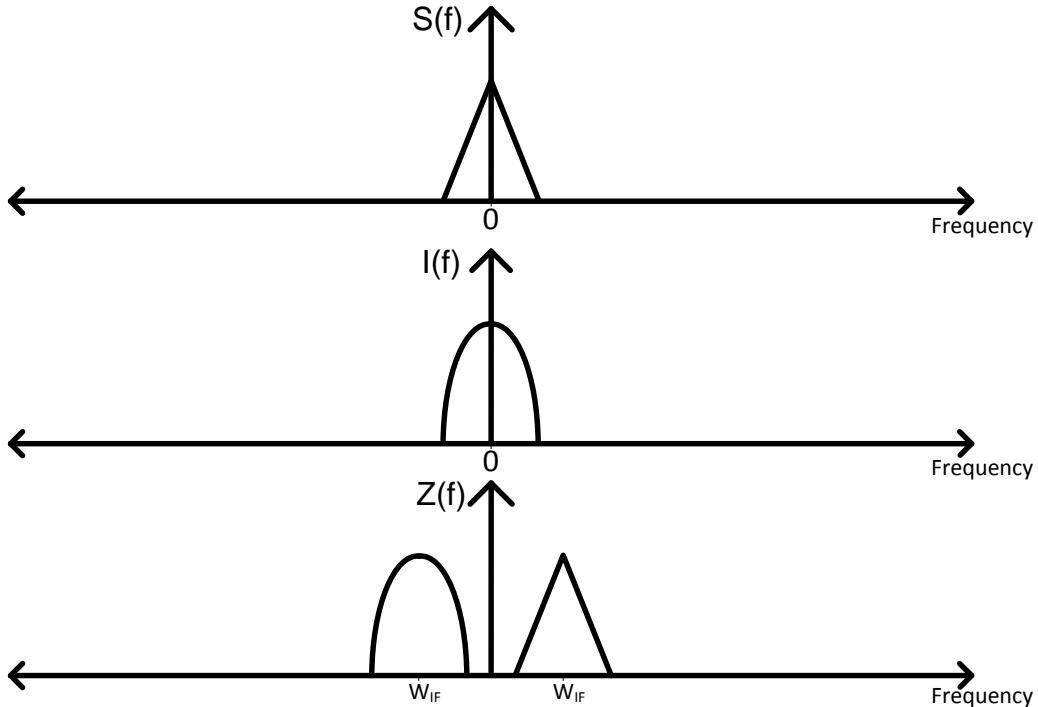
Fig. 25: Frequency response of the base band desired Signal, base band image signal, Non Symmetric Low Pass Equivalent signal for the RF signal

So the RF input signal r(t) shown in Fig. 26 can be defined as:

$$r_{rf}(t) = 2Re\{z(t)e^{jw_{lo}t}\} = z(t)e^{jw_{lo}t} + z^*(t)e^{-jw_{lo}t} \tag{2.14}$$

Noting that conjugating a signal in the time domain is equivalent to mirroring it in the frequency domain across the y-axis. Where $R_{rf}(f)$ is symmetric across the Y-Axis because it is a real physically existing signal.
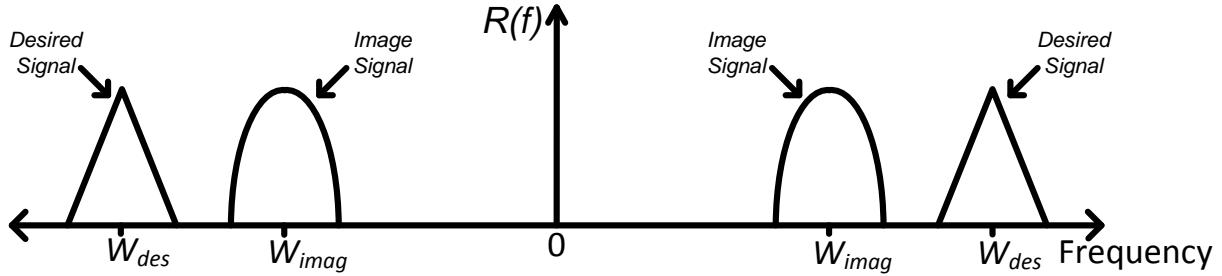
Fig. 26: Frequency Response of the RF signal r(t)

Multiplying (2.14) by (2.10) and low pass filtering to remove the higher order frequencies results in the IF signal $r_{IF}(t)$ in terms of the desired and the image signals, as follows and shown in Fig. 27:

$$r_{IF}(t) = K_1 z(t) + K_2 z^*(t) \tag{2.15}$$
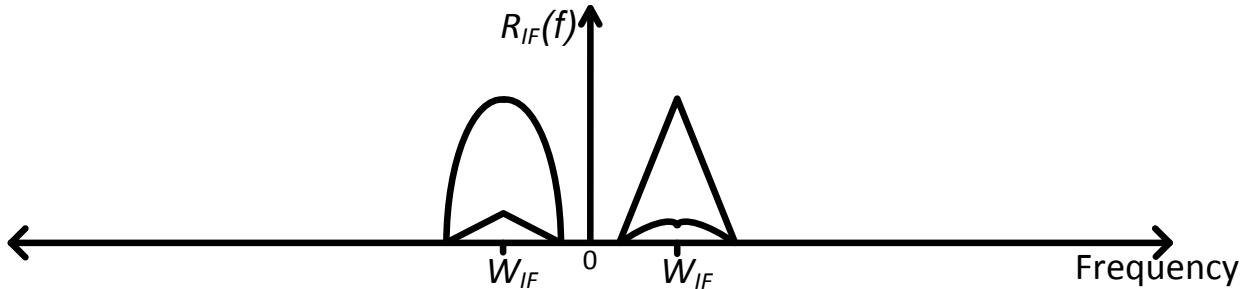
Fig. 27: Frequency Response of the IF Signal With IQI

Again $r_{IF}(t)$ is a not a real signal because it is combining the I and the Q paths, so it is a complex signal with non symmetric frequency response. When $K_2=0$, at no gain or phase imbalances, the IF signal $r_{IF}(t)$ becomes interference free.

Note that the term "interference free" does not mean that the IF signal does not contain the image signal, it only means the image signal is separable from the desired signal and did not leak on the desired signal yet.

Digitizing the analog signal $r_{IF}(t)$ using the ADC, so we can now represent all the signals in n-samples domain, doing the second frequency conversion to the baseband having the contaminated desired signal defined as:

$$d(n) = K_1 s(n) + K_2 i^*(n) \tag{2.16}$$

Where the first term is the scaled desired signal, while the second is the image interference as shown in Fig. 28, and similarly the image signal is corrupted by the leaked desired signal as:

$$v(n) = K_2^* s(n) + K_1^* i^*(n) \tag{2.17}$$

And so the IRR is defined as shown in (2.18) which is the same as (1.1):

$$IRR = \frac{|K_1|^2}{|K_2|^2} \tag{2.18}$$

31
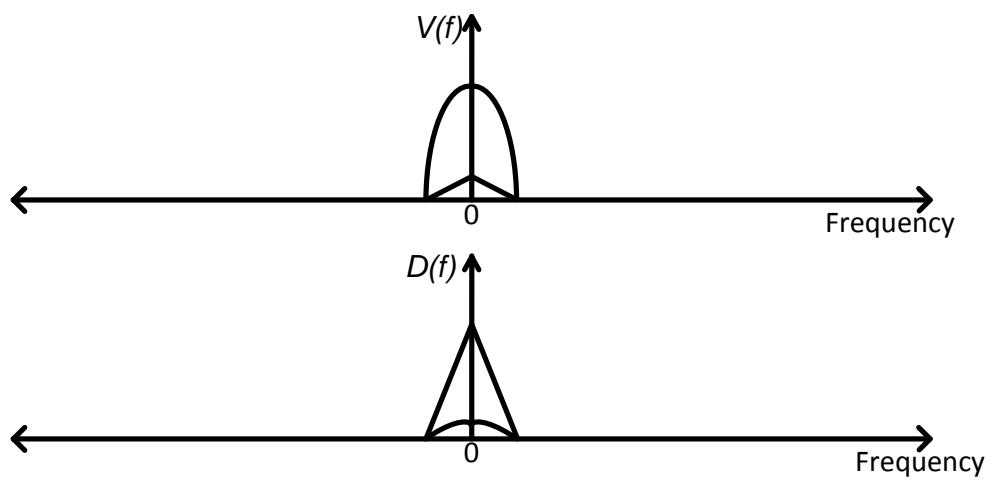
Fig. 28: a) The Image signal corrupted by the desired signal b) The desired signal corrupted by the image signal

After going through the mathematical representation of the secondary quadrature mixing including the IQI, in the next chapter we will review the most common IQI calibration and compensation techniques using the complex domain representation for its simplicity and intuition.

3. IQI Compensation Techniques

Historically layout techniques had been used to reduce the IQI such as increasing the transistor sizes and using specific aspect ratios for the resistors and the capacitors, these techniques add extra constrains on the circuit designs leading to non-optimum designs in terms of system specifications. On the other hand the IRR values that can be reached using such layout techniques become not sufficient for advanced communications standard, it is common to have 1-5% gain mismatch and 1-5degree phase mismatch resulting in an IRR of 25-40 dB. In Low-IF down converters higher image to signal ratios are experienced by the receiver where the image signal might be an adjacent channel, that is why new methods have been proposed to cancel out or compensate for the IQI reaching much better IRR.

IQI calibration and compensation techniques can be classified in different ways. Based on the literature we will classify the IQI compensation methods to two major groups: IQI Calibration & IQI Compensation methods as shown in Fig. 29. More details for the different categories will be introduced next.
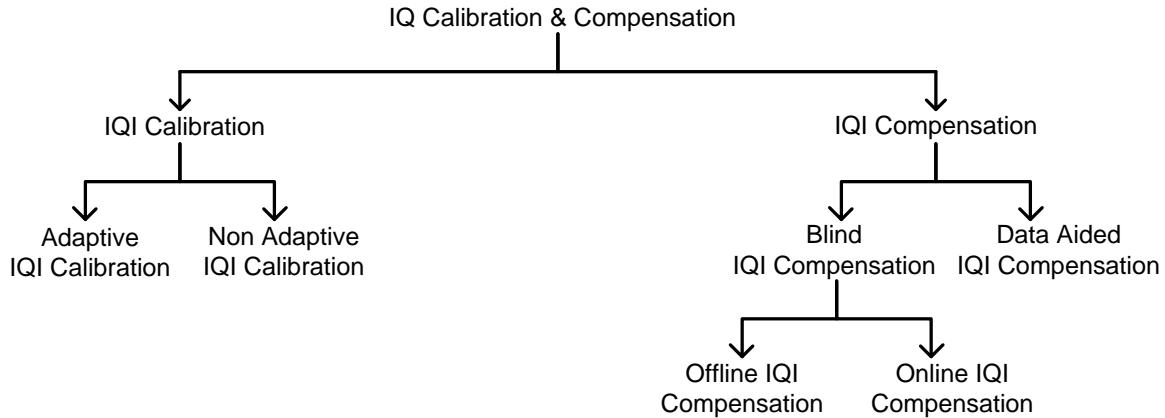
Fig. 29: IQI Calibration and Compensation Classification

3.1. IQI Calibration

IQI calibration is the process of adjusting the gain and the phase of the analog front end mixer and local oscillator (LO) [26] either by using an external or an internal test signal at the image frequency. In the non adaptive IQI calibration a factory or a lab calibration is performed where a test tone at the image frequency is used as an input for the receiver, initially an analog tuning approach were followed where an auxiliary path were used to generate the feedback signal that will be used to update the gain and phase adjusting blocks as shown in Fig. 30 [27], although it is a simple approach it required two more mixers adding area and cost. Then a digital tuning approach where proposed in [11] where no auxiliary paths are required instead the output of the receiver is used directly as the error signal for an LMS algorithm as shown in Fig. 31, in ideal conditions there will be no output from the receiver when the input is the image signal, but practically due to the existence of the IQI leaked image appears at the output of the down converter. The LMS_algorithm updates the gain and phase knobs in the RF mixer & the local

oscillator to reduce the IQI. So after settling the error signal (output signal) will converge to a certain mean square error (MSE) value depending on the algorithm accuracy.
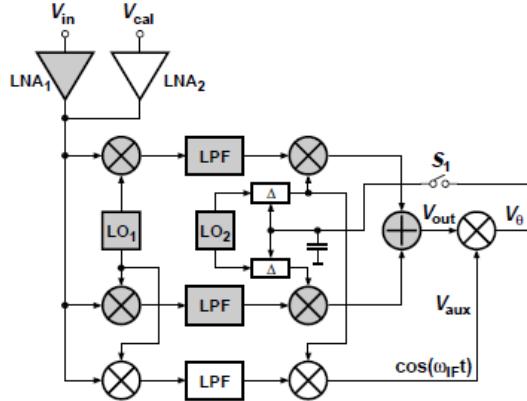
Fig. 30: Image reject receiver with phase calibration loop using auxiliary path
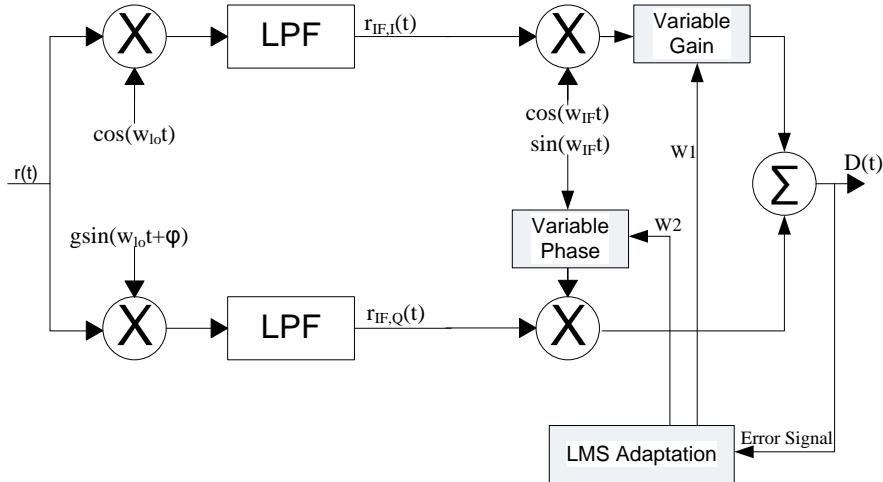
Fig. 31: Image reject receiver with IQI Calibration loops using LMS adaptation and an external test tone at the image frequency

To allow the IQI calibration to be adaptive and avoid lab or factory calibration, trials have been made to generate the image signal on-chip as shown in Fig. 32 [9, 28] instead of using a test signal, having a digital tuning algorithm to adjust the gain and phase in the analog domain. This approach allowed the calibration to be done whenever needed instead of being a one-time lab calibration, that is why it is an adaptive technique, but still it is an offline technique because it is not done during signal reception and it required an extra hardware to generate the image signal increasing the chip area and so the overall cost. Also these IQI calibration approaches might be suitable for narrow band solutions but not as a wide band solution because the calibration is done using a single test tone and so the calibration is done at a single frequency.
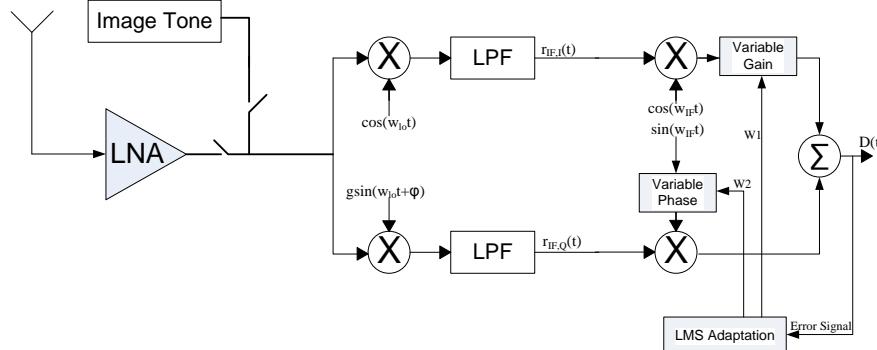
Fig. 32: Generating the image signal on chip to allow adaptive calibration

IQI calibration techniques reviewed above are simple and straight forward consuming low power as calibration is done only once, being independent of the type of modulation, signal statistics, receiver architecture or the IF frequency, though, lab calibrations increase the production costs and testing time [28], and being not adaptive leads to performance sensitivity to temperature, aging and operating conditions variations such as the RF power level. Also using a single test tone in the calibration process is only suitable for narrow frequency bands standards where the mismatches can be assumed flat across the frequency band, so it is not suitable for multi standard designs or wide bandwidth standards. To avoid those issues IQI compensation approaches had been proposed as will be discussed next.

3.2. IQI Compensation

In the IQI compensation techniques the gain and phase mismatches are not adjusted instead their effect are compensated for or cancelled, this can be done either offline during idle modes of the receiver or online during normal signal reception.

3.2.1. Offline IQI Compensation

To avoid the phase adjusting knobs which might be an issue in some frequency bands an approach was used in [23] where a test signal is used at the image frequency and a complex filter is used to do image rejection as shown in Fig. 33, so the output of the complex filter is used as the error signal to the LMS algorithm. But instead of adjusting the gain and phase knobs in the analog front end the LMS algorithm is used to tune a compensating block "C" shown in Fig. 34 that is inserted in the signal path. To avoid any extra IQI from the complex filter or from the compensating block "C" and make use of the technology scaling, the complex filter and the compensating block "C" were implemented in the digital domain in [29]. Although this approach eliminated the need to have phase adjusting knobs, it still requires a test tone at the image frequency either generated internally or externally and so this method suffers from the same drawbacks of the IQI calibration.
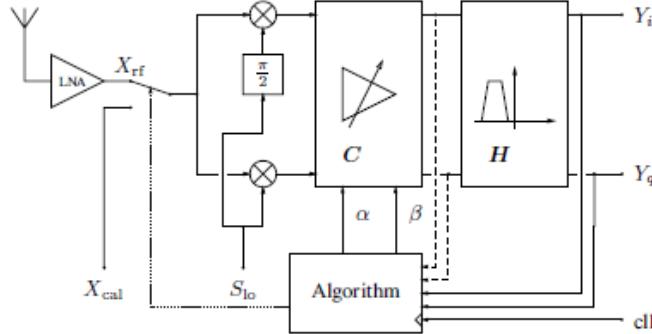
Fig. 33: Low IF Receiver with complex filter, Adjusting IQI using Adjusting Block "C" [17]
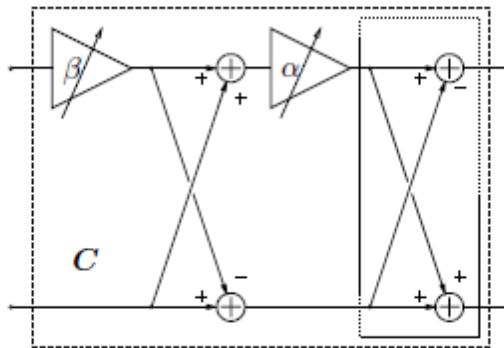
Fig. 34: Adaptive block for IQI Compensation in signal path [17]

In order not to use a test signal at the image frequency another approach was proposed in [29], which exploits the relation between the I&Q signals in the presence of IQI. As shown in Fig. 35, when the gain mismatch exists the power in the I path is no more equal to the power in the Q path but they stay uncorrelated so the difference in the powers of the I path and the Q path can be used as an estimation or an error signal for the gain mismatch, but when phase mismatch exists the I and Q signals become correlated so there correlation can be used as an estimation or an error signal for the phase mismatch.
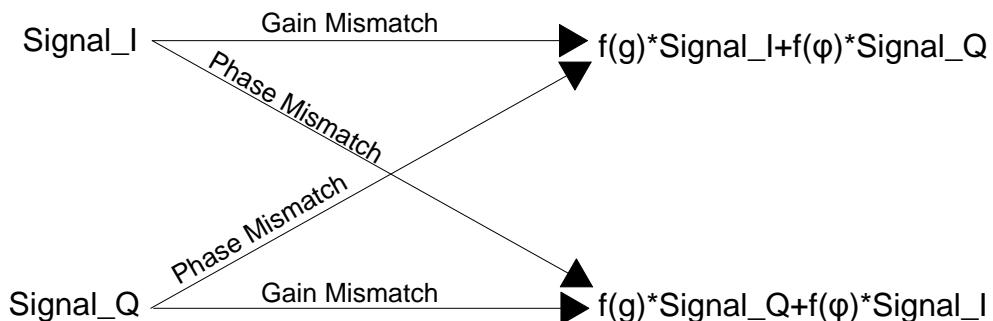
Fig. 35: Impact of the IQ mismatch on the Relation Between the I & Q Signals

This concept was used in [29, 30, 31] generating an estimation for the gain mismatch and another estimation for the phase mismatch as shown in Fig. 36, using these estimations to update a compensating block in the signal path which is represented in Fig. 37 .
Similar approach was used for wider bandwidth applications [32] where the relation between the desired signal and the image is used instead of using the relation between the I-signal and the Q-

36

signal. In such approach the image signal and the desired signal must be generated, where the correlation between them will be the error signal that will be used to compensate for the gain and phase mismatch, noting that the desired and image signal are two complex quantities and so the correlation between them will also be a complex quantity, and then the real part can be used to compensate for the gain imbalance and the imaginary part can be used to compensate for the phase imbalance. This approach were used in [33] as shown in Fig. 38 generating the image signal and the desired signal in the analog domain using two complex filters and using the LMS algorithm to update an analog compensating block in the signal path. Similar approach can be used the secondary quadrature receiver generating the image signal using two additional adders in modified weaver architectures.
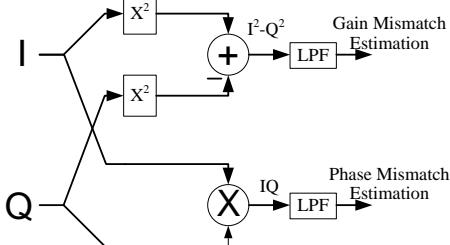
Fig. 36: The IQ Correlation Used as indication for phase mismatch, while the difference between the variances is used as indication for the gain mismatch [22]
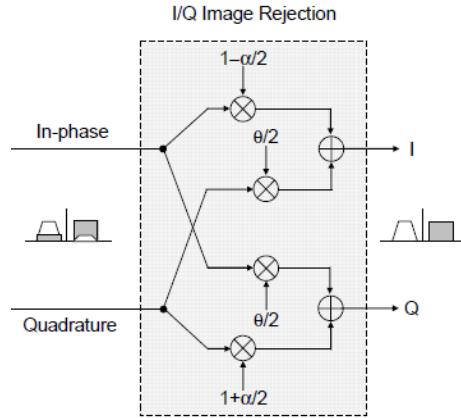
Fig. 37: Gain & Phase Mismatch Estimates are used as inputs for a Compensating block in the signal path
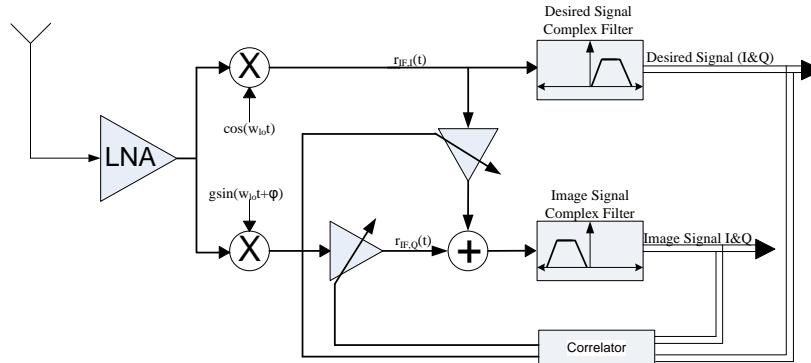
Fig. 38: IQ compensation generating the desired and image signal using two analog complex filters [25]

The compensation techniques introduced above eliminated the need to do lab calibration, reducing the production costs and allowed the calibration to be done when required. But it is not recommended to use such techniques on an online basis during continuous reception because the analog domain IQI compensating blocks introduced in the signal path might generate signal non linearity's on the received signal worsening the SNDR of the received signal, so this techniques will be suitable only for TDMA systems where the IQI compensation is executed at idle states

[30]. That is why online adaptive compensation techniques where introduced in the literature to be used on an online basis during signal reception as will be discussed in the next section.

3.2.2. Online IQI Compensation

In the online IQI compensation methods the leaked image is cancelled in the digital domain without adapting the gain and phase of the front end [8, 10, 34]. Different approaches were used to implement the online calibration process as will be explained next.

3.2.2.1. Single-Tap IQI Compensation Using LMS Algorithm (Interference Cancellation)

Interference cancellation is similar to the noise cancellation technique introduced in [12]. As shown in Fig. 39 The basic idea of the noise cancellation technique is to have a noise source "n_1" correlated to the noise corrupting the signal "n_0", and uncorrelated to the signal itself "s". So by subtracting a scaled version of n_1 from the corrupted signal we can get a noise free version of the signal "z".
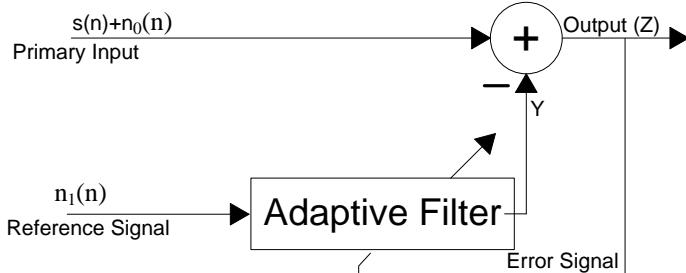
Fig. 39: Noise Cancellation Block Diagram

The Same technique is used in the single-tap IQI compensation technique using LMS proposed in [8], where a single-tap filter is used to cancel the image signal as shown in Fig. 40, assuming a frequency independent IQI without losing generality, the corrupted desired signal $d(n)$ is the input signal to the algorithm. At low signal to interference ratio the reference signal $v(n)$ is correlated to the image signal and uncorrelated to the desired signal. Note that this method depends on the statistical characteristics of the input and the reference signals, so it is a statistically based compensation (cancellation) method, that is why the choice of the IF frequency in such architectures is important because the IF frequency is preferred to be chosen so that the image signal is an adjacent channel to assure that it is totally uncorrelated from the desired signal.
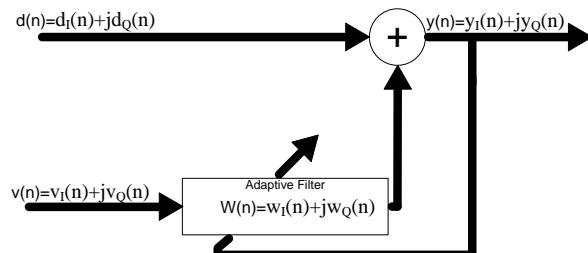
Fig. 40: Single-tap IQI Compensation using LMS Block Diagram

38

Based on Fig. 40 the output equation for the interference cancellation system is:

$$y(n) = d(n) - W^*(n) \cdot v(n) \tag{3.1}$$

where d(n) and v(n) where derived from the modified weaver architecture in chapter 2 as [10]:

$$d(n) = K_1 s(n) + K_2 i^*(n) \tag{3.2}$$
$$v(n) = K_2^* s(n) + K_1^* i^*(n) \tag{3.3}$$

where K_1 and K_2 were defined in (2.8) and (2.9).

Using (2.8) & (2.9) in (3.1) we get:

$$y(n) = (K_1 - W^* K_2^*)s(n) + (K_2 - W^* K_1^*)i^*(n) \tag{3.4}$$

From (3.4) we can derive the output SIR (SIR_{out}) as:

$$SIR_{1Tap} = \frac{E(|K_1 - w^* K_2^*|^2)P_s}{E(|K_2 - w^* K_1^*|^2)P_I} \tag{3.5}$$

Note that the output SIR is the difference (in dB) between the output signal after compensation and the output image (interferer). while the IRR is the ratio between the image signal gain to the desired signal gain, so the IRR is defined as:

$$IRR_{1Tap} = \frac{E(|K_1 - w^* K_2^*|^2)}{E(|K_2 - w^* K_1^*|^2)} \text{ --> Not function in SIR}_{IN} \tag{3.6}$$

So the relation between SIR_{out}, SIR_{in} and IRR can be defined as [10, 36]:

$$SIR_{out}(dB) = SIR_{IN}(dB) + IRR(dB) \tag{3.7}$$

Using zero forcing criteria to maximize SIR_{1Tap}, the optimum solution for "W" will be:

$$W_{1Tap}^{ZF} = \frac{K_2^*}{K_1} = \frac{(1 - ge^{-j\varphi})}{(1 + ge^{-j\varphi})} \tag{3.8}$$

Note that the optimum filter coefficient was derived using the zero forcing criteria achieving an infinite IRR without worrying about noise enhancement because the mismatch exist after the noise addition in the LNA.

Practically the IQI values are not known in order to derive the value of W_{1Tap}^{ZF}. So the MMSE criteria were used in [8] to estimate the filter coefficient, this approach is optimal if the image power is much higher than the desired that updates the adaptive filter coefficient equation. In chapter 4 mathematical details for the MMSE approach using the iterative LMS algorithm introduced in [8] will be represented and it is performance will be compared to a new proposed non-feedback based approach that depends on the method of moments to estimate the filter coefficient.

The IC compensation technique is simple and easy to be implemented, but the output SIR degrades as the input SIR increases due to the signal leakage problem. So other approaches were

proposed where a better reference signal is generated to update the adaptive filter coefficient [37, 8]. and to avoid the signal leakage problem as explained next.

3.2.2.2. Symmetric Adaptive De-Correlation IQI Compensation

To avoid the signal leakage problem suffered by the IC method (also called adaptive de correlation) at moderate and high input SIR values, a solution proposed in [16, 32, 35, 38, 39] was to have a symmetric adaptive filter (2 filters) instead of the single filter used in the IC technique, using this symmetric adaptive filter to generate the image signal free from any desired signal as shown in Fig. 41. Then the optimum filter coefficients will be the filter coefficients that de-correlate the two outputs from each other. This technique is called SAD (adaptive de-correlation) because it is based on separating the desired and the image signal instead of cancelling the image signal from the desired signal as was done in the single-tap IQI compensation technique.
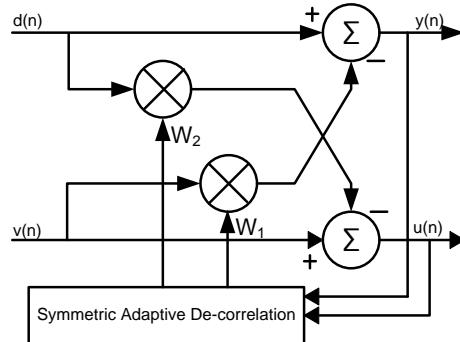
Fig. 41: Symmetric Adaptive De-correlation (SAD) Block Diagram[24]

Where again the symmetric filter might be single tap to compensate for frequency independent mismatches [10, 32, 40, 41] or multi tap to compensate for frequency dependent mismatches [16].

For the frequency independent IQ mismatches the output signal equations will be as follows:

$$y(n) = d(n) - v(n)W_1(n) \tag{3.9}$$
$$u(n) = v(n) - d(n)W_2(n) \tag{3.10}$$

Where the update equation for the filter coefficients will be as follows:

$$W_1(n + 1) = W_1(n) + 2\mu_1 y(n)u^*(n) \tag{3.11}$$
$$W_2(n + 1) = W_2(n) + 2\mu_2 u(n)y^*(n) \tag{3.12}$$

From (3.11) & (3.12), we can observe that after settling y(n) will be a scaled version of the desired signal free from the image signal while u(n) will be a scaled version of the image signal free from the desired signal. And the cross correlation between y(n) and u(n) will be equal to zero unlike the single-tap IQI compensation using LMS technique where the cross correlation between the output signal and the reference signal is not equal to zero at steady state due to the signal leakage problem.

To compensate for the scaling factor of the desired signal a solution were proposed in [28] to do post processing filtering for the output signal estimating the filter coefficient based on the W_1 and W_2 .

So the IC method will be suitable for low SIR_{in}, while SAD will be suitable for moderate and high SIR_{in} [10] trading off extra complexity. So an efficient solution would be to switch between the IC technique and the SAD technique based on the input SIR value.

The previously discussed methods, IC and SAD, where iterative (feedback based) solutions using LMS or RLS algorithms, iterative solutions are considered as a slowly converging techniques, that is why another approaches were proposed using the method of moments instead of using the iterative solutions as explained next.

3.2.2.3. Non-Feedback Based Blind IQI Compensation (Dual-Tap Method)

Another approach based on reconstructing the desired signal from the observation signals *d(n)* and *v(n)* was introduced in [42, 43]. Using (3.2) and (3.3) the desired signal is expressed as:

$$\begin{bmatrix} s(n) \\ i^*(n) \end{bmatrix} = \frac{1}{(|K_1|^2 - |K_2|^2)} \begin{bmatrix} K_1^* & -K_2 \\ -K_2^* & K_1 \end{bmatrix} \begin{bmatrix} d(n) \\ v(n) \end{bmatrix} \tag{3.13}$$

And so s(n) can be reconstructed using dual-tap filter as shown in Fig. 42 to weight *d(n)* and *v(n)*. Where the optimum filter coefficients will be:

$$W_1^{opt} = \frac{-K_2}{(|K_1|^2 - |K_2|^2)} \tag{3.14a}$$

$$W_2^{opt} = \frac{K_1^*}{(|K_1|^2 - |K_2|^2)} \tag{3.14b}$$

The estimates of W_1 and W_2 were obtained using the cross & auto correlation of d(n) & v(n) as shown in Fig. 42, where two moments are measured:

$$E[d(n)v^*(n)] = K_1 K_2 (P_s + P_I) \tag{3.15a}$$

$$E[|d(n) + v(n)|^2] = E[|z(n)|^2] = P_s + P_I \tag{3.15b}$$

Where P_s and P_I are defined as the desired signal power and the image power, respectively. Then using (3.15) and (2.13), K_1 and K_2 are estimated and so the filter coefficients W_1 and W_2.
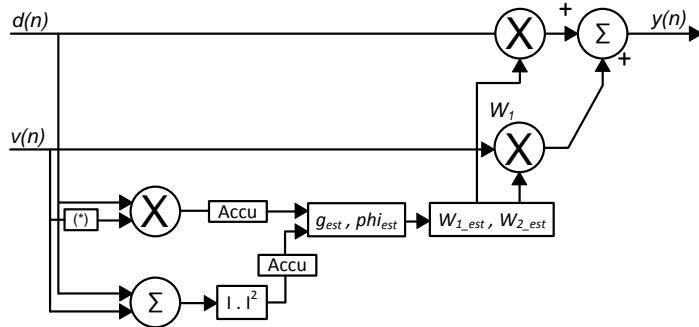
Fig. 42: IQI Compensation Using Signal & Image Separation using 2-Tap Filters

In [42] the estimated filter coefficients were obtained by estimating the IQI, in chapter 5 a simpler approach will be proposed estimating the filter coefficients in less mathematical steps, analyzing the mathematical derivation and the simulation results of this approach in more details, also a variation for this method will be introduced in which the input SIR will be estimated and used to optimize the number of symbols required to do the IQI compensation.

4. Single-tap IQI Compensation Method

In chapter 3 the interference cancellation method (single-tap IQI compensation method) using the LMS algorithm was reviewed briefly mentioning that this technique suffers from the signal leakage problem. In this chapter a new technique will be proposed to estimate the filter coefficient of the single-tap IQI compensation method using the method of moments instead of using the LMS algorithm, showing that the new proposed approach will enhance the settling time and achieves a constant convergence time across the input SIR range. Performance analysis will also be introduced to verify the simulation results.

At first the single-tap IQI compensation method using the LMS algorithm proposed in [10] will be reviewed in more details, then the proposed method will be introduced.

4.1. Single-tap IQI Compensation Method Using LMS Algorithm

In section 3.2.2 the optimum filter coefficient W_{1Tap}^{ZF} for the single-tap IQI Compensation method shown in Fig. 43 was obtained using the zero forcing criteria, for practical application the IQI values are unknown then the optimum filter coefficient cannot be directly estimated, so it was proposed in [10] to use the MMSE criteria using the output signal y(n) defined in (4.1) as the error signal, minimizing the cost function $E(|y(n)|^2)$ using steepest descend algorithms the Weiner filter solution is obtained as given by Eqn. (4.2).

$$y(n) = d(n) - W^*(n) \cdot v(n) \tag{4.1}$$

$$W_{1Tap}^{MMSE} = \frac{K_1^* K_2^* (P_s + P_I)}{|K_2|^2 P_s + |K_1|^2 P_I} \tag{4.2}$$

It can be observed that W_{1Tap}^{MMSE} reaches the optimum solution W_{1Tap}^{ZF} when $P_I/P_s \gg 0$. But for $P_I/P_s \ll 0$, W_{1Tap}^{MMSE} deviates from optimality due to the non purity of the reference signal (as it is not fully uncorrelated from the desired signal), this is called the signal leakage problem.
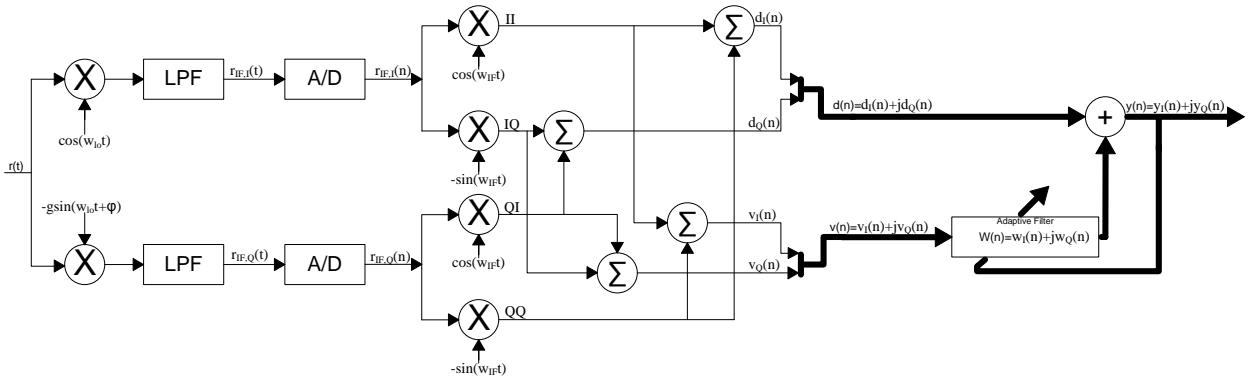
Fig. 43: Secondary Quadrature Mixing down converter with single-tap IQI Compensation Method

The metric used to evaluate the performance of the interference cancellation is the output signal to interference ratio (SIR_{out}), so to derive the SIR_{out} using W_{1Tap}^{MMSE}, substitute by (4.2) in (4.1) to get:

$$SIR_{1Tap}^{MMSE} = \frac{E\left(\left|K_1 - \frac{K_2^* K_2 K_1 (P_S + P_I)}{|K_2|^2 P_S + |K_1|^2 P_I}\right|^2\right) P_S}{E\left(\left|K_2 - \frac{K_1^* K_2 K_1 (P_S + P_I)}{|K_2|^2 P_S + |K_1|^2 P_I}\right|^2\right) P_I} \tag{4.3}$$

Doing the internal multiplications and taking common denominator we get:

$$SIR_{1Tap}^{MMSE} = \frac{E(|K_1|K_2|^2 P_S + K_1|K_1|^2 P_I - K_1|K_2|^2 (P_S + P_I)|^2) P_S}{E(|K_2|K_2|^2 P_S + K_2|K_1|^2 P_I - K_2|K_1|^2 (P_S + P_I)|^2) P_I}$$
$$= \frac{|K_1|^2 P_I}{|K_2|^2 P_S} \tag{4.4}$$

One of the mostly used methods to implement the steepest descend method is the LMS algorithm adding a new source of error which is the excess error added by the LMS iterative algorithm, LMS update equation is derived in Appendix A. The update the equation and the excess error are defined as:

$$W_{1Tap}^{LMS}(n+1) = W_{1Tap}^{LMS}(n) + \mu v(n) y^*(n) \tag{4.5}$$
$$e_{LMS}(n) = W_{1Tap}^{MMSE} - W_{1Tap}^{LMS}(n) \tag{4.6}$$
$$mse_{LMS}(n) = E[|e_{LMS}(n)|^2] \tag{4.7}$$

Now we will formulate the signal to interference ratio after using the LMS algorithm (SIR_{1Tap}^{LMS}), substituting by (4.6) in (4.1) to get:

$$y(n) = (K_1 - (W_{1Tap}^{MMSE})^* K_2^* - e_{LMS}^*(n) K_2^*) s(n) + (K_2 - (W_{1Tap}^{MMSE})^* K_1^* - e_{LMS}^*(n) K_1^*) i^*(n)$$
$$y(n) = \left(K_1 - K_2^*\left(\frac{K_1 K_2 (P_S + P_I)}{|K_2|^2 P_S + |K_1|^2 P_I}\right) - e_{LMS}^*(n) K_2^*\right) s(n) +$$
$$(K_2 - K_1^*(\frac{K_1 K_2 (P_S + P_I)}{|K_2|^2 P_S + |K_1|^2 P_I}) - e_{LMS}^*(n) K_1^*) i^*(n) \tag{4.8}$$

After taking common denominator (4.8) can be simplified to:

$$y(n) = (\frac{K_1 P_I (|K_1|^2 - |K_2|^2)}{|K_2|^2 P_S + |K_1|^2 P_I} - e_{LMS}^*(n) K_2^*) s(n) + (\frac{K_2 P_S (|K_2|^2 - |K_1|^2)}{|K_1|^2 P_I + |K_2|^2 P_S}$$
$$- e_{LMS}^*(n) K_1^*) i^*(n) \tag{4.9}$$

Defining:

$$G_1 = \frac{K_1 P_I (|K_1|^2 - |K_2|^2)}{|K_2|^2 P_S + |K_1|^2 P_I} \tag{4.10a}$$
$$G_2 = \frac{K_2 P_S (|K_2|^2 - |K_1|^2)}{|K_1|^2 P_I + |K_2|^2 P_S} \tag{4.10b}$$

Substituting by (4.10) in (4.9) we get the SIR_{1Tap}^{LMS} as shown below:

$$SIR_{1Tap}^{LMS} = \frac{((|G_1|^2 + mse_{LMS})|K_2|^2)P_S}{((|G_2|^2 + mse_{LMS})|K_1|^2)P_I} \tag{4.11}$$

Then from (4.11) we can define the IRR_{1Tap}^{LMS} as:

$$IRR_{1Tap}^{LMS} = \frac{((|G_1|^2 + mse_{LMS})|K_2|^2)}{((|G_2|^2 + mse_{LMS})|K_1|^2)} \tag{4.12}$$

In the next section a non feedback based approach (non iterative approach) will be proposed to estimate the adaptive filter coefficient, then the feedback based (LMS) and the non feedback based approaches will be compared in section 4.3.

4.2. Single-tap IQI Compensation Method Using Method of Moments

At low input SIR, we may approximate $v(n)$ in (3.3) as follows:

$$v(n) \simeq K_1^* i^*(n) \tag{4.13}$$

Where the ratio in (3.10) can be approximated, based on the method of moments, in terms of the statistics of $d(n)$ and $v(n)$ at low SIR_{in} using (4.13) as follows:

$$\frac{E[d(n)v^*(n)]}{E[|v(n)|^2]} \simeq \frac{K_1 K_2 P_I}{|K_1|^2 P_I} = \frac{K_2}{K_1^*} \tag{4.14}$$

Hence, we may estimate the LHS of (4.14) using sample variance and covariance, and consequently obtain the desired filter coefficient W^* as follows:

$$W_{1Tap\_MOM\_Acc}^*(n) = \frac{\sum_{l=1}^{N}(d(l)v^*(l))}{\sum_{l=1}^{N}(|v(l)|^2)} = \left(\widehat{\frac{K_2}{K_1^*}}\right) \tag{4.15}$$

Where N is the number of time samples used to estimate the filter coefficient. The above operations are described in Fig. 44. The proposed single-tap method is computationally less complex than the dual-tap method proposed in [42] as shown in Table 1 and results in the same output SIR at low input SIR region as we will see in the simulations section.

The exact expression of the ratio of expectations in (4.14) is given by:

$$\begin{aligned}\frac{E[d(n)v^*(n)]}{E[|v(n)|^2]} &= \frac{E[K_1 K_2 |s(n)|^2 + K_1 K_2 |i(n)|^2]}{E[|v(n)|^2]} \\ &= \frac{K_1 K_2 P_s + K_1 K_2 P_I}{|K_2|^2 P_s + |K_1|^2 P_I} \triangleq W^*_{1Tap\_MOM}\end{aligned} \tag{4.16}$$

In order to define the output SIR, we define the error in the estimated filter coefficient as:

$$e_{MoM}(n) = W_{1Tap\_MOM\_Acc}^*(n) - W^*_{1Tap\_MOM} \tag{4.17}$$

Then using (4.1) the output SIR is defined as:

$$E[SIR_{1Tap\_acc}(n)] = \frac{E[|(K_1 - W_{1Tap\_MOM\_Acc}^*(n)K_2^*)|^2]P_s}{E[|(K_2 - W_{1Tap\_MOM\_Acc}^*(n)K_1^*)|^2]P_i} \tag{4.18}$$

So by substituting from (4.17) into (4.18) as in [10], the output SIR can be expressed in terms of K_1, K_2, P_s P_I and the mean squared error expressed as, $mse_{MoM}(n) = E[|e_{MoM}(n)|^2$, as:

$$SIR_{1Tap\_acc}(n) = \frac{((|G_1|^2 + \text{mse}_{\text{MoM}}(n))|K_2|^2)P_S}{((|G_2|^2 + \text{mse}_{\text{MoM}}(n))|K_1|^2)P_I} \tag{4.19}$$

Equation (4.19) will be used to evaluate the performance of the proposed method, but in the next subsection a closed form expression for the output SIR will be derived and compared to the simulation results.
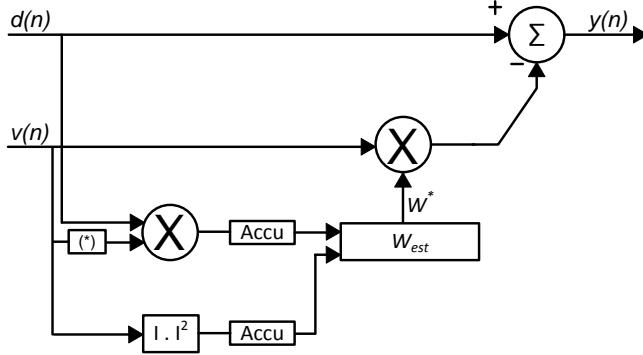
Fig. 44: Single-tap IQI Compensation Using Method of Moments

Table 1: Complexity Analysis Comparing single-tap IQI compensation and dual-tap IQI compensation proposed in [42]

Operation	Proposed single-tap method	[42]
sin^{-1},sine & cosine	--	3
Square root	--	1
Complex division	2	1
Real Division	--	1
Real Multipliers	12	16
Real Adders	9	11

4.2.1. Single-tap IQI Compensation Method Performance Analysis

We first substitute from (4.15) into (4.18) and do some simplifications without any approximations to get:

$$E[ISR_{1Tap\_acc}] = \frac{|K_1|^2}{|K_2|^2} \frac{E\left[\left|\frac{K_2}{K_1^*} - \left(\widehat{\frac{K_2}{K_1^*}}\right)\right|^2\right]}{E\left[\left|\frac{|K_1|^2 - |K_1|^2}{K_1^* K_2^*} + \frac{K_2}{K_1^*} - \left(\widehat{\frac{K_2}{K_1^*}}\right)\right|^2\right]} \frac{P_i}{P_s} \tag{4.20}$$

Then defining the absolute estimation error and the quantity "A" as:

$$\Delta = \frac{K_2}{K_1^*} - \frac{\sum_{l=1}^{N}(d(l)v^*(l))}{\sum_{l=1}^{N}(|v(l)|^2)} = \frac{K_2}{K_1^*} - \left(\widehat{\frac{K_2}{K_1^*}}\right) \tag{4.21a}$$

$$A = \frac{|K_1|^2 - |K_2|^2}{K_1^* K_2^*} \tag{4.21b}$$

Substituting by (4.21) into (4.20) the ISR_{1Tap_acc} is expressed as:

$$E[ISR_{1Tap\_acc}] = \frac{|K_1|^2}{|K_2|^2} \frac{E[|\Delta|^2]}{E[|A+\Delta|^2]} \frac{P_i}{P_s}$$
$$= \frac{|K_1|^2}{|K_2|^2} \frac{E[|\Delta|^2]}{(|A|^2 + E[|\Delta|^2] + AE[\Delta^*] + A^*E[\Delta])} \frac{P_i}{P_s}$$

(4.22)

So we need to get Δ in terms of K_1, K_2, P_s, P_i and N in order to get the closed form for the expectation of ISR_{1Tap_acc}. At first we define P_s, P_i and R_{si} as:

$$\widehat{P_s} = \frac{1}{N} \sum_{n=1}^{N} |s(n)|^2 \qquad\qquad \widehat{P_i} = \frac{1}{N} \sum_{n=1}^{N} |i(n)|^2$$

(4.23a)

$$\widehat{R_{si}} = \frac{1}{N} \sum_{n=1}^{N} s(n)i(n)$$

(4.23b)

Substituting by (4.23) and (4.15) into (4.21a) and simplifying the absolute error "Δ" can be expressed as :

$$\Delta = \frac{(|K_2|^2 - |K_1|^2)(K_2\widehat{P_s} + K_1\widehat{R_{si}})}{K_1^*(|K_2|^2\widehat{P_s} + |K_1|^2\widehat{P_i} + K_1K_2^*\widehat{R_{si}} + K_1^*K_2\widehat{R_{si}^*})}$$

(4.24)

Now two approximations will be used to simplify (4.24):

1- At sufficient "N" $E[\widehat{P_i}] = P_i$, $E[\widehat{P_s}] = P_s$

2- Knowing that $|K_1|^2 >> |K_2|$. Then Δ, $E[\Delta]$ and $E|\Delta|^2$ can be simplified to:

$$\Delta \approx \frac{(|K_2|^2 - |K_1|^2)(K_2P_s + K_1\widehat{R_{si}})}{K_1^*(|K_2|^2P_s + |K_1|^2P_I)}$$

(4.25a)

$$E[\Delta] \approx \frac{(|K_2|^2 - |K_1|^2)(K_2P_s)}{K_1^*(|K_2|^2P_s + |K_1|^2P_I)}$$

(4.25b)

$$E(|\Delta|^2) \approx \frac{(|K_2|^2 - |K_1|^2)^2(|K_2|^2P_s^2 + |K_1|^2E(|\widehat{R_{si}}|^2))}{|K_1|^2(|K_2|^2P_s + |K_1|^2P_I)^2}$$

(4.25c)

where the variance of $\widehat{R_{si}}$, assuming the usage of interleaver at the transmitter that breaks up any memory between the transmitted symbols, is given by [44] :

$$E(|\widehat{R_{si}}|^2) = \frac{P_sP_i}{N}$$

(4.26)

So using (4.25) and (4.26) back into (4.22) we get the expectation of ISR_{1Tap_acc} in terms of K_1, K_2, P_s, P_I and N. In the simulations section next the derived closed form for the output SIR defined by (4.22), will be compared to the actual simulation results defined by (4.19), proving the validity and accuracy of our analysis and simulations.

4.3. Simulation Results

Without lose of generality QPSK modulation scheme with symbol rate sampling is used, using 100 iterations to estimate the ensemble mean square error. The mismatches used in the simulations are (1-g=1.02, phi=2 degree's) & (2- g=1.1, phi=10 degree's). In general ADC de-sensitization will occur at low input SIR [30] due to the high image power compared to the desired signal power, but in our model we assume ideal sampling.

At first the response of the single-tap IQI compensation method using the LMS algorithm across time is shown in Fig. 45 & Fig. 46 , showing that the settling time is not constant across the input SIR range having longer settling time for lower input SIR values. By comparing that to the response of the proposed single-tap IQI compensation method using the method of moment across time shown in Fig. 47 & Fig. 48, it can be observed that the method of moment guarantee the same settling time for different input SIR values, and the settling is much less than the LMS algorithm as shown in Fig. 49.
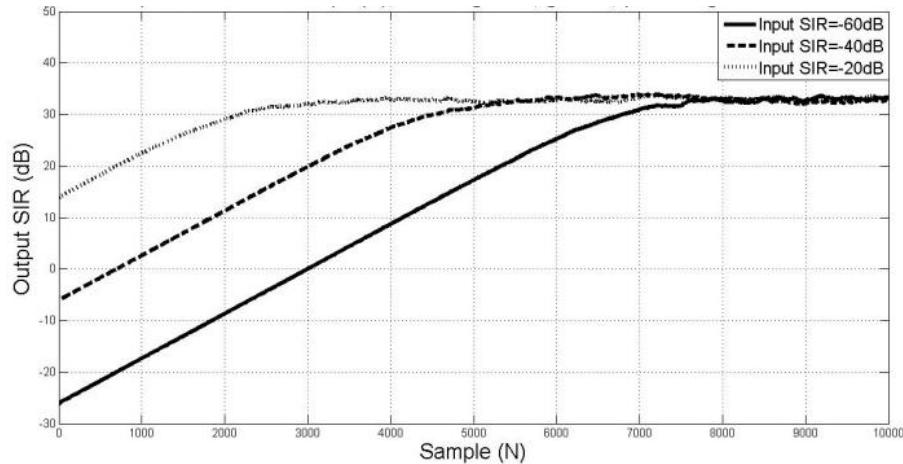
Fig. 45: single-tap IQI compensation method using LMS, Output SIR across Time, g=1.02, phi=2^0, SNR=35dB
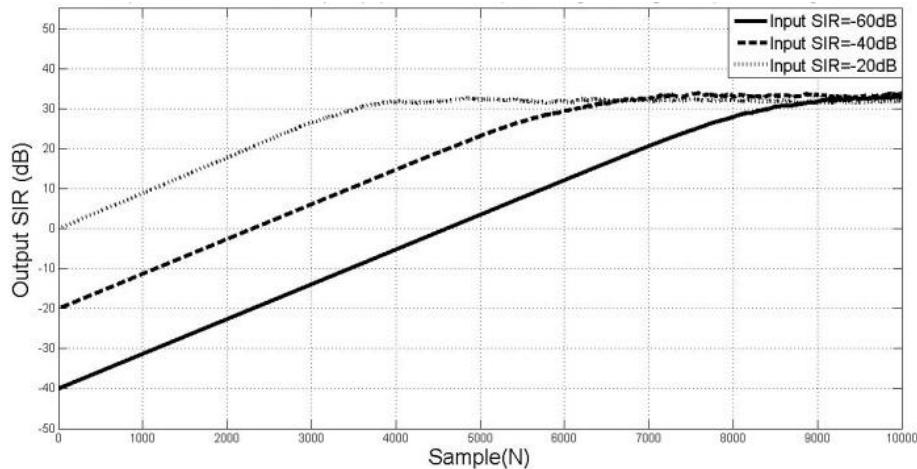
Fig. 46: single-tap IQI compensation method using LMS, Output SIR across Time, g=1.1, phi=10^0, SNR=35dB
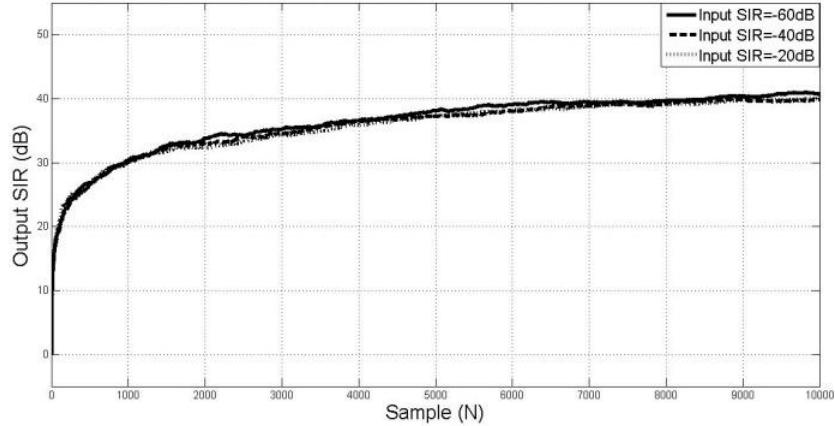
Fig. 47: single-tap IQI compensation method using Method of Moment, Output SIR across Time, g=1.02, phi=2^0, SNR=35dB
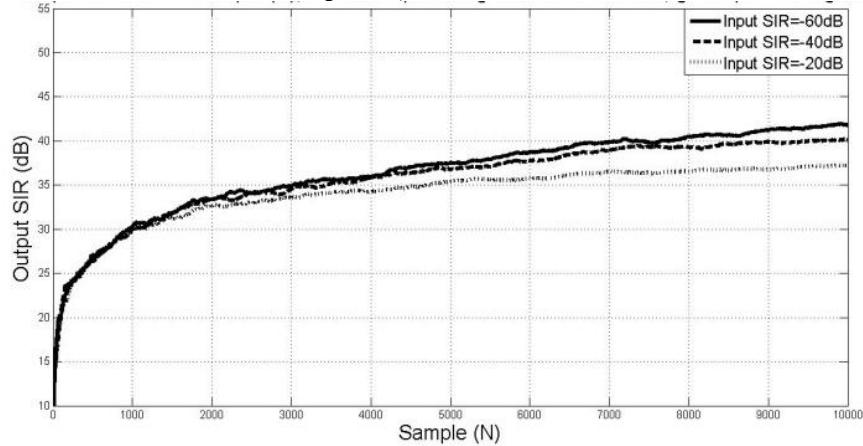
Fig. 48: single-tap IQI compensation method using Method of Moment, Output SIR across Time, g=1.1, phi=10^0, SNR=35dB
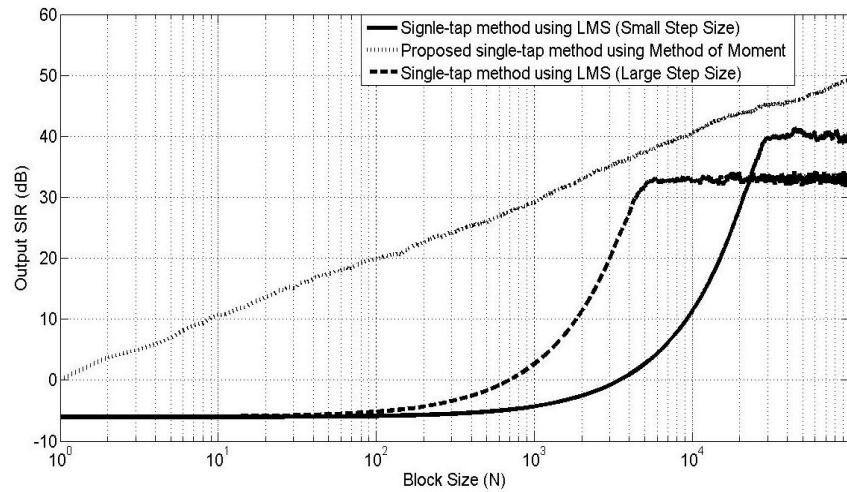
Fig. 49: SIR$_{out}$ across time (*n*) for the single-tap method using LMS and the proposed single-tap method using Method of Moments, SIR$_{in}$=-40dB, SNR=35dB, g=1.02 and phi=2^0

48

After comparing the settling time of the two methods, the steady state output SIR can be studied by plotting the output SIR across the input SIR at steady state for both methods as shown in Fig. 50, as can be observed the closed form solution expressed by (4.22) showed very good match to the simulation results verifying our model and hand analysis. It can be concluded from this comparison that the proposed single-tap IQI compensation using method of moments achieves higher output SIR and/or less settling time compared to the single-tap IQI compensation using the LMS algorithm. Where both are suffering from the signal leakage problem leading to degraded output SIR values at moderate and high input SIR range, and the degradation increases as the values of the IQI increase.
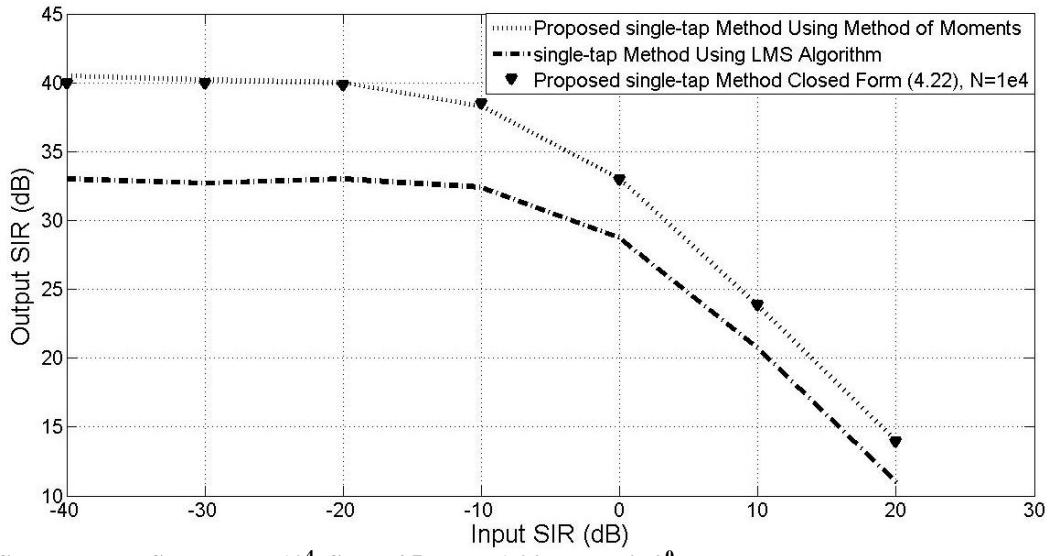
Fig. 50: SIR$_{out}$ across SIR$_{in}$ at N=10^4, SNR=35dB, g=1.02 and phi=2^0.

Although the single-tap IQI compensation using method of moments showed better performance in terms of steady state output SIR and/or less settling time, the LMS method tracks the time varying IQI in a better way as shown in Fig. 51 where the gain and phase mismatches were changed gradually from g=1.02 to g=1.03 and from phi=2^0 to phi=2.5^0 starting from N=5000 to N=6000. It can be observed that the LMS algorithm returned to the steady state output SIR faster than the method of moment approach because the method of moment is affected by the memory influence measuring the received signal statistical expectations or second order moments, unlike the LMS algorithm which is iterative and works on sample by sample basis. To enhance the response of the method of moment it is better to dump the filter coefficient and restart the computations if a change in the IQI were sensed. And the rate of change of the IQI can be determined by monitoring the rate of change of the filter coefficients, or alternatively the filter coefficient can be re-calculated at each reception mode to avoid the memory effect.

Finally the effect of the additive noise on the performance of the single-tap IQI compensation methods was tested as shown in Fig. 52 plotting the output SIR across SNR, it can be observed that at the region of interest for the input SIR both approaches are insensitive to the additive

49

noise and so the output SIR value stays approximately the same across the different SNR values, the reason for that is having the noise as a part of the desired signal without affecting the statistical characteristics of the desired signal. To quantize the benefit from the IQI compensation we can see in Fig. 53 how the BER is enhanced comparing the uncompensated situation (d(n)) to the compensated output signal (y(n)) where approximately constant BER can be observed because the output SIR is constant across SNR as was shown in Fig. 52, highlighting that the plotted BER include the errors during the settling of the algorithm (before reaching the targeted output SIR) and so it is considered as a pessimistic performance compared to the real performance that will be achieved after the targeted output SIR is reached.
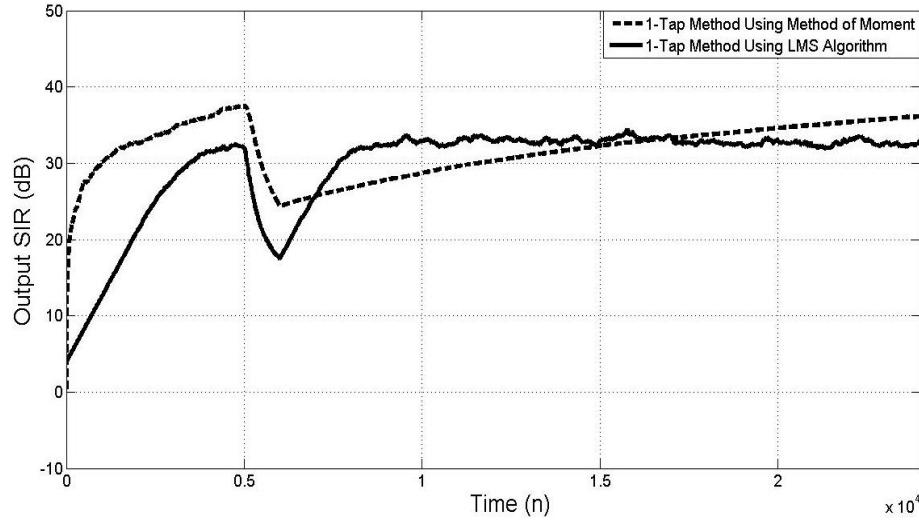
Fig. 51: Output SIR across Time(n) at input SIR=-30dB and SNR=35dB, varying gain mismatch linearly from g=1.02 to g=1.03 and phase mismatch from g=2^0 to g=2.5^0 starting at n=5000 till n=6000.
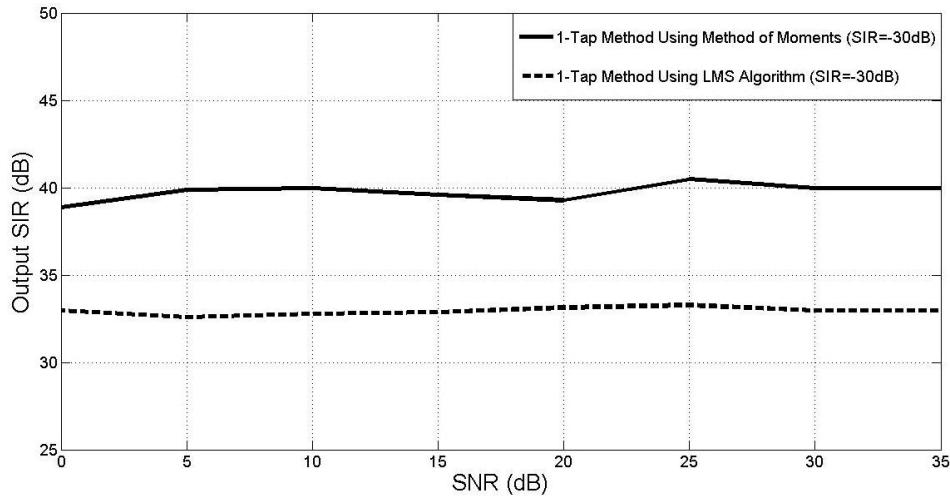
Fig. 52: Output SIR across SNR at different values of input SIR, g=1.02, phi=2^0
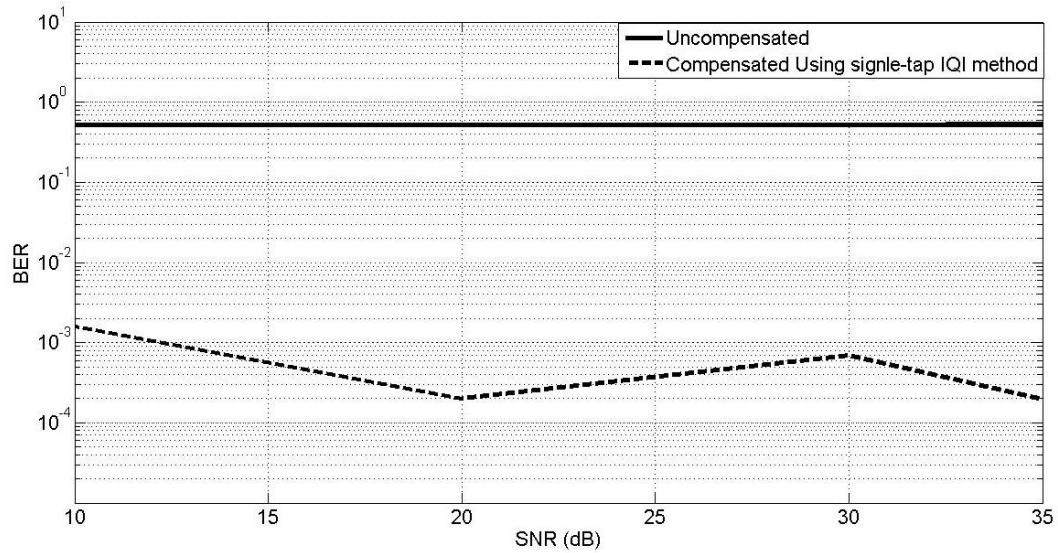
Fig. 53: BER across SNR for the single-tap IQI compensation technique, g=1.02, phi=2 degree's, input SIR=-40dB

The single-tap IQI compensation method proposed is suitable for the low range of the input SIR, at moderate and high input SIR the output SIR degrades due to the signal leakage problem and the effect of the signal leakage as the values of the IQI increases. That is why in the next chapter two methods will be proposed that suit the moderate and high input SIR regions using a dual-tap IQI compensation technique instead of the single-tap method used before without requiring the front end blocks to support any calibration knobs, also we will propose a methodology that can be used to switch between both techniques, i.e. single-tap and dual-tap, for the best compromise between performance and complexity.

5. Dual-Tap IQI Compensation Method

The single-tap IQI compensation described before was suitable for the low input SIR range, and it is performance degrades at moderate and high input SIR ranges due to desired signal leakage onto the reference signal, that is why some methods of compensation were proposed in the literature such as the non iterative source separation in [42] and the iterative symmetric adaptive de correlation in [16] achieving better performance at moderate and high input SIR regions using a dual-tap filter instead of a single-tap filter paying off an extra complexity. In this chapter a variant will be introduced to the method proposed in [42] in which an estimate for the input SIR will be obtained and used to optimize the number of symbols for the compensation achieving the same performance with less computational complexity, also another variant will be introduced for the method used in [16] in which an updating equation will be saved leading to less complex solution using an extra two taps to avoid the need for post processing filter.

5.1. Non Feedback Dual-Tap IQI Compensation Using Method of Moments

5.1.1. Mathematical Model

The baseband received signal for the secondary quadrature receiver architecture was given in (3.2) and (3.3) and repeated below for our reference as:

$$d(n) = K_1 s(n) + K_2 i^*(n) \tag{5.1}$$
$$v(n) = K_2^* s(n) + K_1^* i^*(n) \tag{5.2}$$

So the purpose of the compensation technique is to re generate the desired signal s(n) from d(n) and v(n). By Re-writing (5.1) and (5.2) in a matrix form and processing (5.3) to get the desired signal in terms of the observation signals d(n) and v(n) as given in (5.5), it's clear that two filter coefficients are needed to rescale the observation signals d(n) and v(n) as shown in Fig. 54 and so reconstruct the desired signal *s(n)*.

$$\begin{bmatrix} d(n) \\ v(n) \end{bmatrix} = \begin{bmatrix} K_1 & K_2 \\ K_2^* & K_1^* \end{bmatrix} \begin{bmatrix} s(n) \\ i^*(n) \end{bmatrix} \tag{5.3}$$

$$\begin{bmatrix} s(n) \\ i^*(n) \end{bmatrix} = \frac{1}{(|K_1|^2 - |K_2|^2)} \begin{bmatrix} K_1^* & -K_2 \\ -K_2^* & K_1 \end{bmatrix} \begin{bmatrix} d(n) \\ v(n) \end{bmatrix} \tag{5.4}$$

$$s(n) = \frac{1}{(|K_1|^2 - |K_2|^2)} [K_1^* d(n) - K_2 v(n)] \tag{5.5}$$

$$i^*(n) = \frac{1}{(|K_1|^2 - |K_2|^2)} [-K_2^* d(n) + K_1 v(n)] \tag{5.6}$$
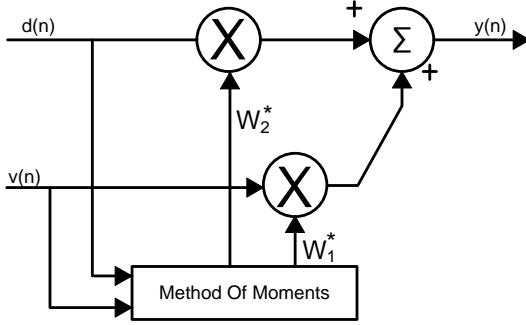
Fig. 54: Dual-Tap IQI Compensation Method

And so based on Fig. 54 the output equation for the proposed blind IQI compensation technique will be:

$$y(n) = W_2^* d(n) + W_1^* v(n) \tag{5.7}$$

Comparing (5.7) to (5.5) the optimum filters coefficients are:

$$W_1 = \frac{-K_2^*}{(|K_1|^2 - |K_2|^2)} \tag{5.8}$$

$$W_2 = \frac{K_1}{(|K_1|^2 - |K_2|^2)} \tag{5.9}$$

Knowing that K_1 & K_2 are related as:

$$K_1 = 1 - K_2^* \tag{5.10}$$

So it is enough to estimate K_1 and K_2 in order to estimate for W_1 and W_2. In our proposed method, the input SIR will be additionally estimated and used to optimize for the block size required to guarantee a minimum SIR_{out} across the whole range of the SIR_{in}. These three estimates will be obtained by measuring various second order moments about the observation signals $d(n)$ and $v(n)$, and solving the resulting non-linear simultaneous equations.

Two approaches will be introduced in this work. In the first, we measure the three moments in the LHS of the following equations and solve them together with (5.10) for the unknown quantities K_1, K_2, P_I, and P_s:

$$E[|d(n)|^2] = |K_1|^2 P_s + |K_2|^2 P_I \tag{5.11a}$$

$$E[|v(n)|^2] = |K_2|^2 P_s + |K_1|^2 P_I \tag{5.11b}$$

$$E[d(n)v^*(n)] = K_1 K_2 (P_s + P_I) \tag{5.11c}$$

After solving the set of equations (5.11) using (5.10) as shown in Appendix B, the estimates of K_1, K_2 can be written in closed form as:

$$Im(K_1) = \frac{Im(E[d(n)v^*(n)])}{Re(E[|d(n)|^2] + E[|v(n)|^2] + 2 * E[d(n)v^*(n)])} \tag{5.12a}$$

$$Re(K_1) = \frac{1 + \sqrt{1 - 2X}}{2} \tag{5.12b}$$

Where "X" is defined as:

$$X = 1 + 2Im(K_1)^2 - \frac{E[|d(n)|^2] + E[|v(n)|^2]}{Re(E[|d(n)|^2] + E[|v(n)|^2] + 2 * E[d(n)v^*(n)])} \tag{5.13}$$

And the input SIR can be obtained by substituting from (5.12) into (5.11a) and (5.11b) to get P_s and P_I as follows:

$$P_I = \frac{|K_1|^2 E[|v(n)|^2] - |K_2|^2 E[|d(n)|^2]}{(|K_1|^2)^2 - (|K_2|^2)^2} \tag{5.14a}$$

$$P_s = \frac{E[|d(n)|^2] - |K_2|^2 P_I}{|K_1|^2} \tag{5.14b}$$

The second approach requires an extra moment, which is used in [31]:

$$E[|d(n) + v(n)|^2] = E[|z(n)|^2] = P_s + P_I \tag{5.15}$$

This approach allows us to decouple the equations and solve first for K_1 and K_2 using (5.15) and (5.11c), then substitute back in (25.a) and (25.b) to obtain P_s and P_I. In [42] the IQI mismatches (g and φ) were estimated first then the filter coefficients were estimated, here we derive for K_1 and K_2 directly without estimating g and φ and so saving an unnecessary computational overhead, by solving (5.15) with (5.11c) we get:

$$K_1 K_2 = \frac{E[d(n)v^*(n)]}{E[|z(n)|^2]} \tag{5.16}$$

Equating the imaginary parts of (5.16) and using (5.10) we get the imaginary part of K_1 as:

$$Imag(K_1) = Imag(\frac{E[d(n)v^*(n)]}{E[|z(n)|^2]}) \tag{5.17}$$

Doing the same for the real parts we get the real part of K_1 as:

$$Real(K_1) = \frac{1 + \sqrt{1 - 4(Imag(K_1)^2 + Real\left(\frac{E[d(n)v^*(n)]}{E[|z(n)|^2]}\right))}}{2} \tag{5.18}$$

For both approaches the running accumulators were used as shown in Fig. 55 and Fig. 56 to estimate the required moments, so the accuracy of the estimated filter coefficients W_{1_est} and W_{2_est} is a function of the block size "N" used in the running accumulators to compute those expectations, the performance analysis of the dual-tap IQI compensation were introduced in [44], and here we introduce an equivalent way to express the output SIR in terms of the mean square error of the estimated filter coefficients. The mean square error as the difference between the estimated filter coefficient and the optimum filter coefficient can be defined as:

$$e_1(n) = W_{1_{est}}(n) - W_1 = W_{1_{est}}(n) - \frac{-K_2^*}{(|K_1|^2 - |K_2|^2)}, \; mse_1(N) = E[|e_1|^2] \tag{5.19a}$$

$$e_2(n) = W_{2_{est}}(n) - W_2 = W_{2_{est}}(n) - \frac{K_1}{(|K_1|^2 - |K_2|^2)}, \; mse_2(N) = E[|e_2|^2] \tag{5.19b}$$

In order to quantify the performance of the proposed blind compensation technique an expression for the output SIR in terms of K_1, K_2, P_s, P_I & the mean square errors for the filter coefficients is derived. Substituting by d(n) and v(n) from Eqn. (5.3) into Eqn. (5.7) we get:

$$y(n) = W_{2\_est}^*\big(K_1 s(n) + K_2 i^*(n)\big) + W_{1\_est}^*\big(K_2^* s(n) + K_1^* i^*(n)\big)$$
$$= \big(W_{2\_est}^* K_1 + W_{1\_est}^* K_2^*\big)s(n) + \big(W_{1\_est}^* K_1^* + W_{2\_est}^* K_2\big)i^*(n) \tag{5.20}$$

Substituting by (5.19) into (5.20) we get:

$$y(n) = \big(1 + K_1 e_2^*(n) + K_2^* e_1^*(n)\big)s(n) + \big(K_1^* e_1^*(n) + K_2 e_2^*(n)\big)i^*(n) \tag{5.21}$$

So the output SIR can be defined from (5.21) as:

$$E[SIR_{Compensation}] = \frac{E[|1 + K_1 e_2^*(n) + K_2^* e_1^*(n)|^2]P_S}{E[|K_1^* e_1^*(n) + K_2 e_2^*(n)|^2]P_I}$$
$$= \frac{(1 + |K_1|^2 mse_2 + |K_2^*|^2 mse_1)P_S}{(|K_1^*|^2 mse_1 + |K_2|^2 mse_2)P_I} \tag{5.22}$$

Which will be used in the next section to evaluate the performance of the proposed method, as expected at ideal conditions where $mse_1 = mse_2 = 0$, the $E[SIR_{out}]$ will be infinite.
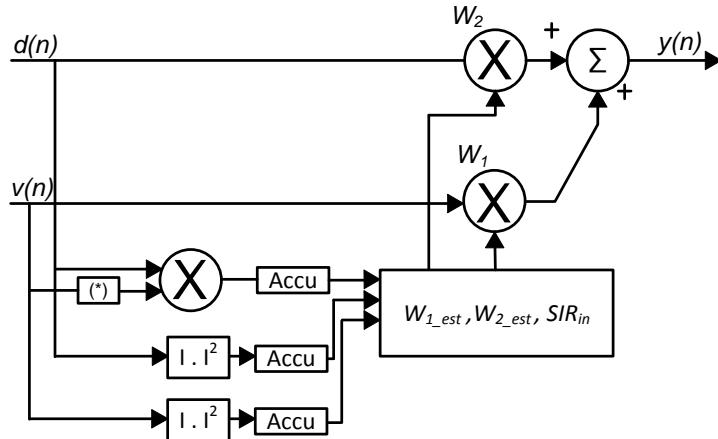
Fig. 55: Dual-Tap IQI Compensation using method of moments, first approach measuring three moments
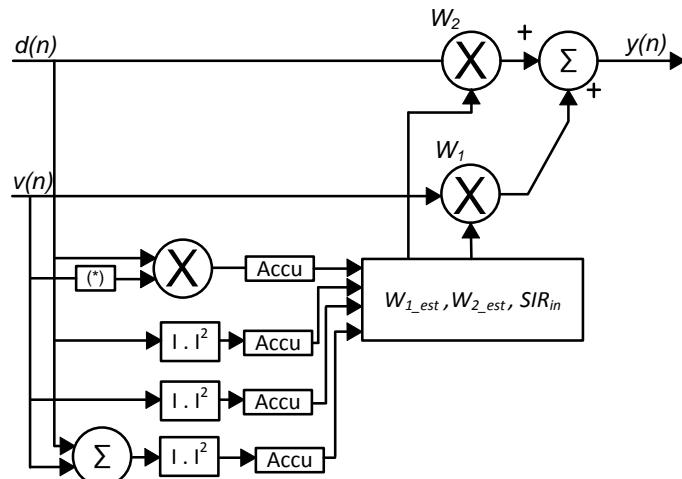
Fig. 56: Dual-Tap IQI Compensation using method of moments, second approach measuring four moments

5.1.2. Simulation Results

The simulation conditions used in this section is similar to the simulation conditions used in section4.3. At first the steady state performance where examined by plotting the output SIR against the input SIR (at N=1e4) in Fig. 57 & Fig. 58 showing that a minimum output SIR is guaranteed across the input SIR range, and unlike the single-tap IQI compensation method the output SIR is enhanced at high input SIR as expected. Then the output SIR is plotted against the block size "N" as shown in Fig. 59 showing that settling time is less than the single-Tap IQI compensation method using the LMS algorithm, and that the output SIR is enhanced as long as "N" increases. In practical scenarios, a minimum output SIR is required beyond which insignificant sensitivity improvement is gained. Hence, if the input SIR is estimated, the block size can be optimized to satisfy the output SIR requirement. In Fig. 60, the input SIR was estimated using (5.14) showing that a pretty good estimate is achieved using only 10 samples for various input SIR values. Using this estimate for the input SIR, the optimum block size is plotted in Fig. 61 against the input SIR to achieve an output SIR of 40 dB. This shows that a huge gain can be obtained by decreasing the block size from $N=10^4$ by up to two orders of magnitude according to the estimate of the input SIR.

In order to monitor the effect of the additive noise on the dual-tap IQI compensation using method of moments, the steady state output SIR is plotted against the SNR in Fig. 62, showing that the additive noise starts to affect the performance at SNR approximately below SNR of 15 dB. That is why when plotting the BER across the SNR in Fig. 63 a nearly constant value is observed across the SNR till SNR of 15 dB then it started to degrade because of the degraded output SIR, again these BER curves include the samples during settling before reaching the targeted output SIR that is why it is considered pessimistic, while the constellation of the QPSK is plotted in Fig. 64 showing that the compensated signal enhances the output SNR of the signal compared to the uncompensated signal.
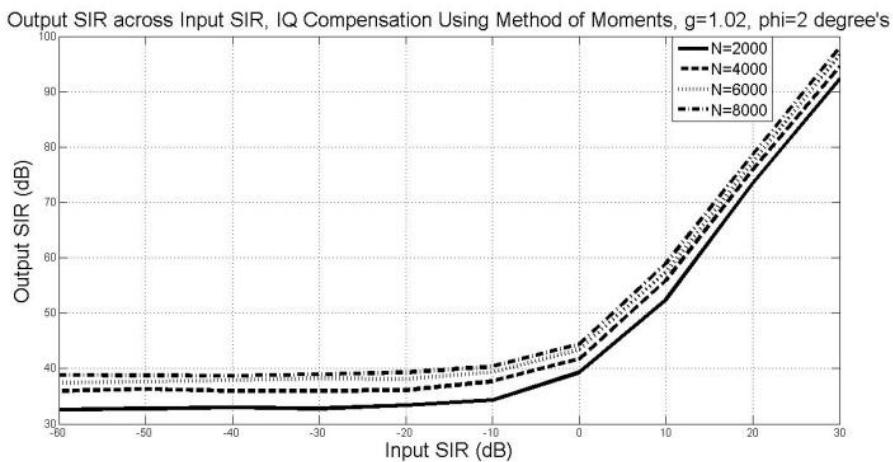
Fig. 57: 2-Tap Method Using Method of Moment, Output SIR across input SIR, g=1.02, phi=2^0, SNR=35dB
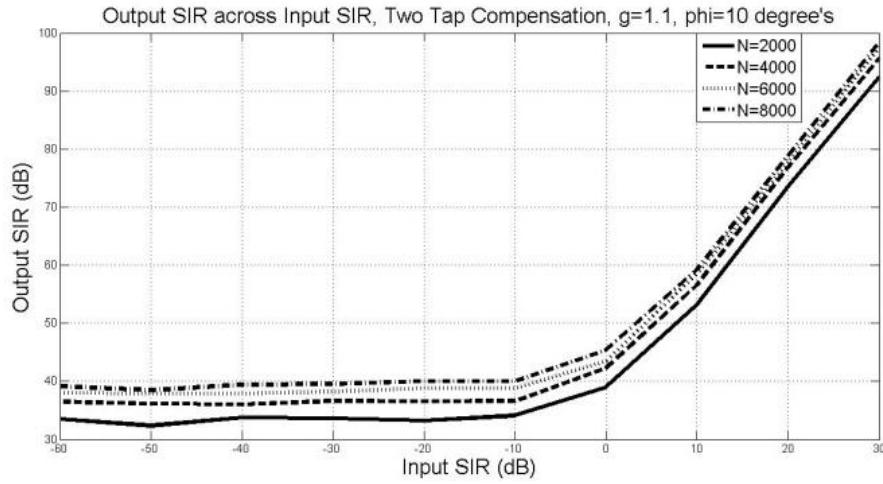
Fig. 58: 2-Tap Method Using Method of Moment, Output SIR across input SIR, g=1.1, phi=10^0, SNR=35dB
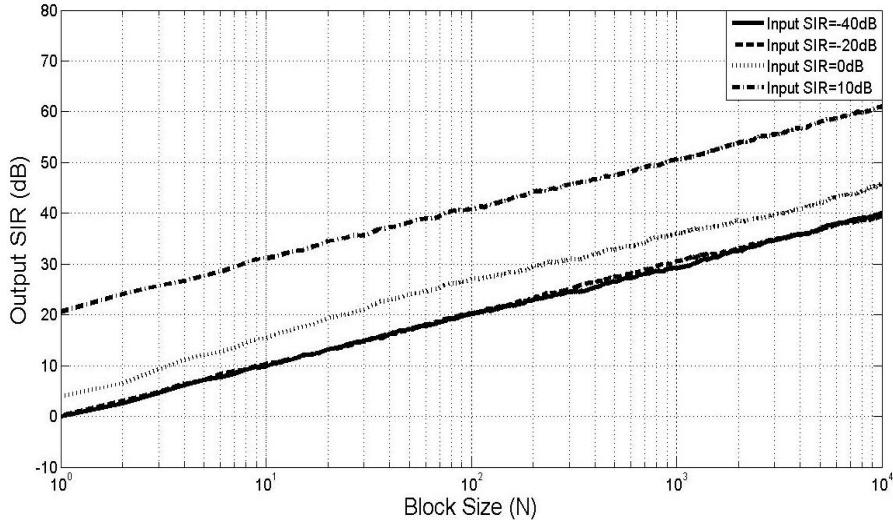
Fig. 59: Dual-tap IQI compensation using method of moments, Output SIR across Time Iterations (N), g=1.02, phi=2^0, SNR=35dB
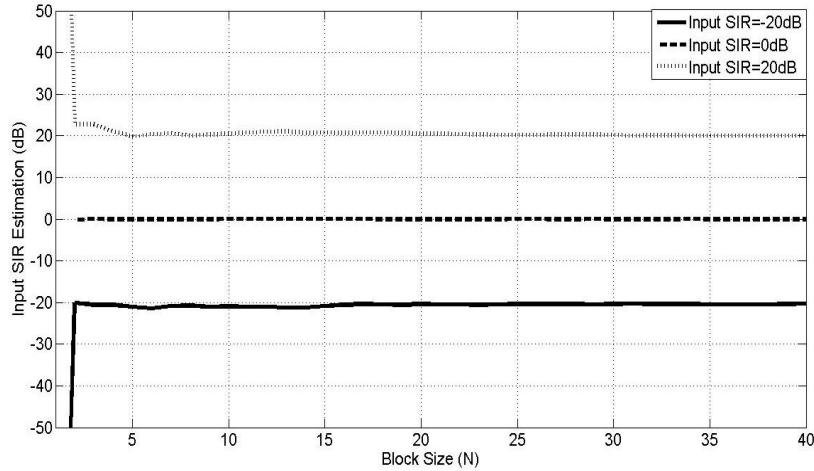
Fig. 60: SIR$_{in}$ estimation against the block size (*N*) at SNR=35dB using a single realization, g=1.02 and phi=2^0
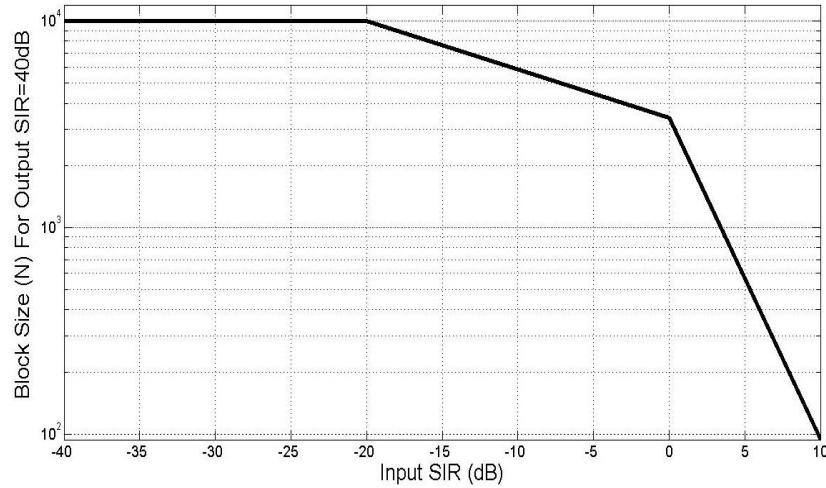
Fig. 61: The Block Size (*N*) required to reach SIR$_{out}$=40dB across SIR$_{in}$ for the proposed dual-tap IQI Compensation Using Method of Moments.
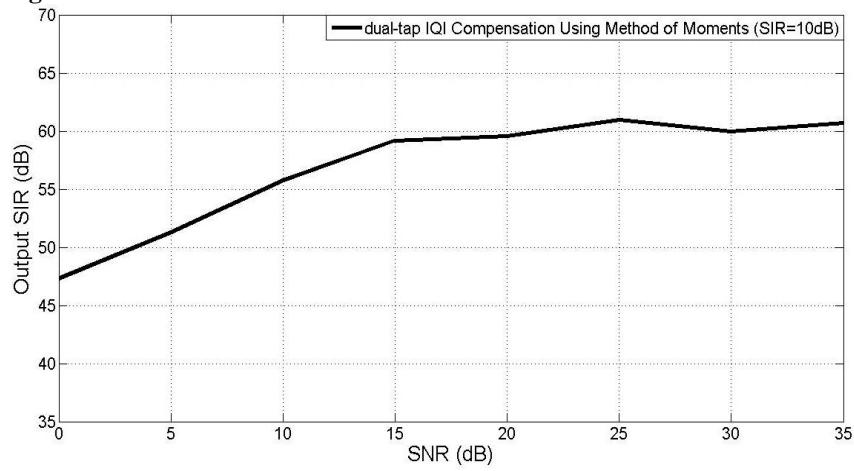
Fig. 62: Output SIR across SNR for the dual-tap IQI compensation using method of moments
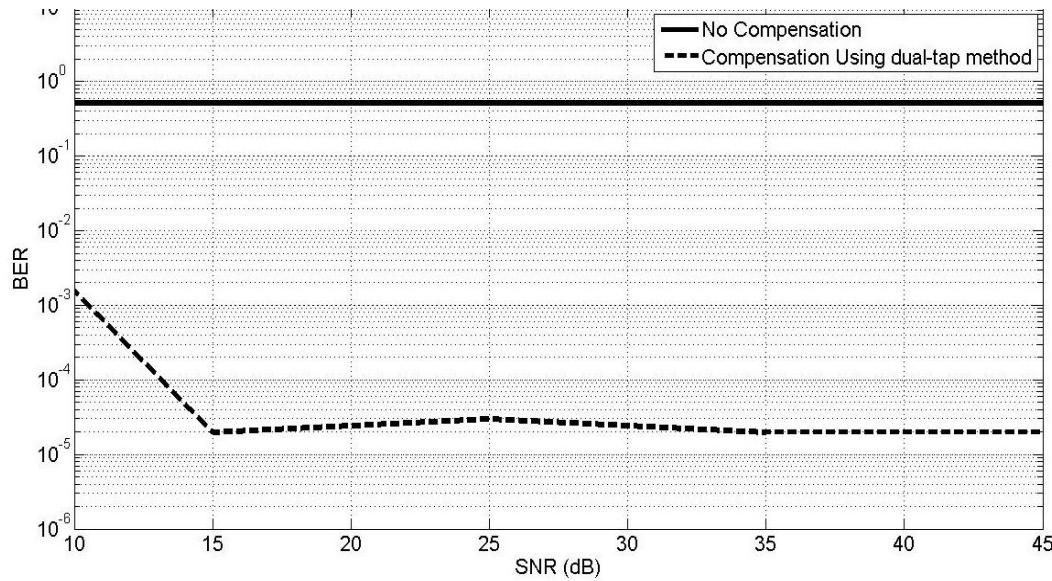
Fig. 63: BER across SNR for the dual-tap IQI compensation technique, g=1.02, phi=2 degree's, input SIR=-40dB
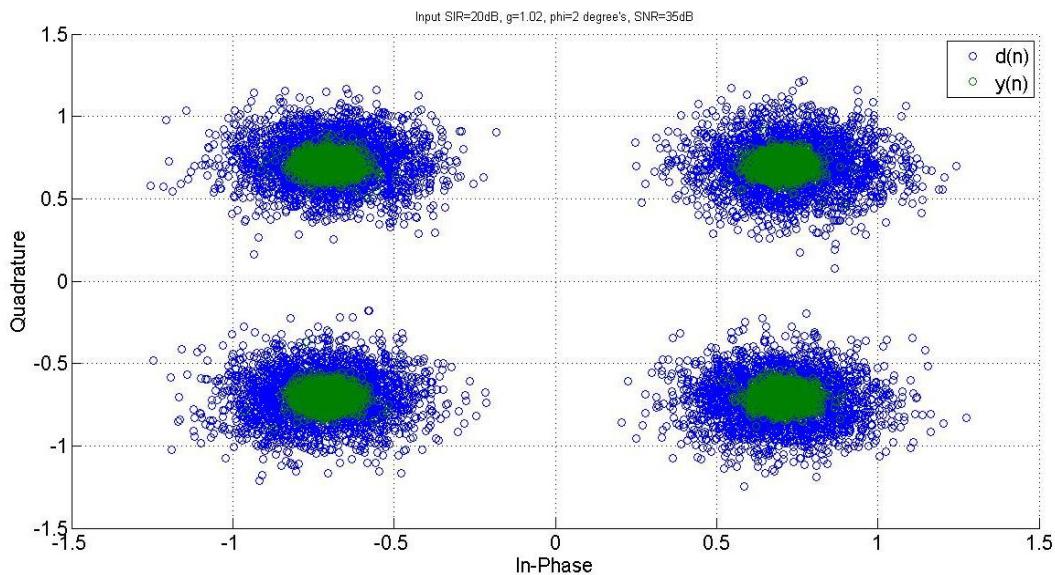
Fig. 64: Signal constellation for the compensated signal y(n) and the uncompensated signal d(n), g=1.02, phi=2 degree's, input SIR=-20dB

5.2. Feedback Based Dual-Tap IQI Compensation Using LMS Algorithm

5.2.1. Mathematical Model

The symmetric adaptive de-correlation (SAD) introduced in [16] and [45] is based on generating a clean reference signal u(n) free from any desired signal using another filter W_2 as shown in Fig. 65, where the output equations and the updating equations for such SAD method are as follows [16]:

$$y(n) = d(n) - W_1 v(n) \tag{5.23a}$$
$$u(n) = v(n) - W_2 d(n) \tag{5.23b}$$
$$W_1(n+1) = W_1(n) + 2\mu_1 y(n) u^*(n) \tag{5.24a}$$
$$W_2(n+1) = W_2(n) + 2\mu_2 u(n) y^*(n) \tag{5.24b}$$
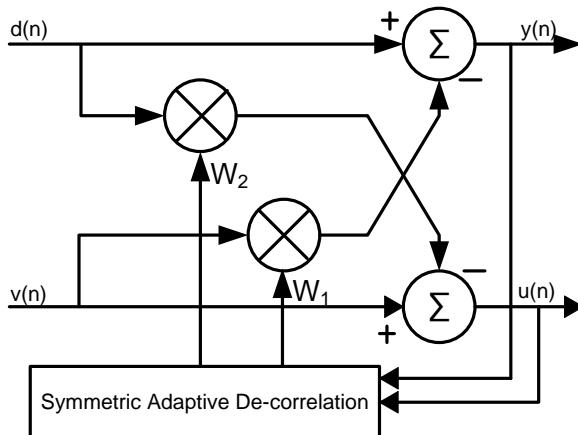
Fig. 65: Symmetric Adaptive De-correlation

Comparing (5.24a) to (5.24b) we can observe two main differences:

1- The updating factors μ_1 and μ_2 are different

2- The cross correlations in (3) and (4) are related as : $y(n)u^*(n) = conj(u(n)y^*(n))$

This means that if we assumed that $\mu_1 = \mu_2 = \mu$ and that $W_1(1) = W_2(1) = 0$, then the two updating equations can be simplified into one updating equation, estimating the other filter coefficient as:

$$W_1(n+1) = W_1(n) + 2\mu y(n) u^*(n) \tag{5.25a}$$
$$W_2(n+1) = W_1^*(n+1) \tag{5.25b}$$

Also the steady state output of the symmetric adaptive de-correlation technique proposed in [45] is a scaled version of the desired signal s(n), that is why in [28] and [45] an equalization filter was proposed as shown in Fig. 66, where the W_{equ} were defined as:

$$W_{equ} = \frac{1}{1 - W_1 W_2} \tag{5.26}$$
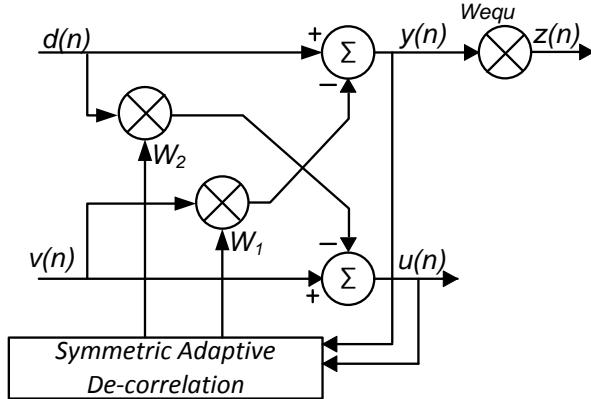
Fig. 66: Symmetric Adaptive De-correlation With Equalizing Filter

A discussion about the equalizing filter being realizable had been introduced in [45] highlighting that for this filter to be realizable a necessary and sufficient condition is to have $W_1(n).W_2(n)$ not to be equal to 1 in every iterations step in order to guarantee that the equalizing filter is realizable, to avoid this limitation we propose the usage of two additional multipliers as shown in Fig. 67 to weight the observation signals $d(n)$ and $v(n)$ and so reconstruct the desired signal without the need to do post processing. Knowing that the filter coefficients are related from(5.4):

$$W_2 = W_1^*, W_3 = 1 - W_1^*, W_4 = 1 - W_1 \tag{5.27}$$
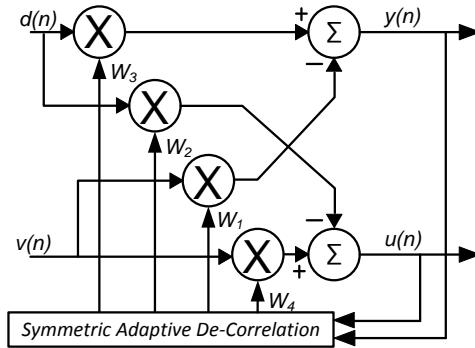
Fig. 67: Proposed dual-tap IQI compensation with output signal rescaling

So we will need only one updating equation to re construct the signal without using any post processing, and the output and updating equations will be as follows:

$$y(n) = W_3 d(n) - W_1 v(n) \tag{5.28a}$$
$$u(n) = W_4 v(n) - W_2 d(n) \tag{5.28b}$$
$$W_1(n+1) = W_1(n) + 2\mu y(n)u^*(n) \tag{5.28a}$$

Using (11) to get the rest of the filter coefficients as follows:

$$W_2(n+1) = W_1^*(n+1) \tag{5.29a}$$
$$W_3(n+1) = 1 - W_1^*(n+1) \tag{5.29b}$$
$$W_4(n+1) = 1 - W_1(n+1) \tag{5.29a}$$

5.2.2. Simulation Results

To evaluate the performance analysis of the proposed dual-tap IQI compensation using the LMS algorithm the steady state output SIR is plotted against the input SIR in Fig. 68 and compared to the performance of [16], showing that approximately the same output SIR is achieved saving an updating equation and the equalization filter, and as expected the output SIR is enhanced at moderate and high input SIR avoiding the signal leakage problem. Then the output SIR is plotted against the time iterations "n" in Fig. 69. Again the same conclusion can be reached here when comparing the iterative dual-tap IQI compensation using LMS and the dual-tap IQI compensation using method of moments, as shown in Fig. 70 the method of moment converges faster to higher output SIR values, but it responds slower than the LMS iterative method toward time varying IQI.

So the choice of the used IQI compensation technique depends on the application and on the communication standard, if the IQI is time varying unexpectedly then the iterative solutions will be more adequate, but if it is slowly varying or constant or it is time varying but in a way that can be expected, e.g. at different gain settings or reception mode, then the non iterative method of moments solutions will guarantee better steady state performance and convergence times.

The techniques proposed above were blind techniques but in some communication standards signal pilots (training sequence) are available which allows the usage of data aided (non-blind) techniques to compensate for the IQI, in the next chapter a new method will be proposed which exploit signal pilots inherited within the desired signal to estimate the filter coefficients of the dual-Tap filter method and so compensate for the IQI.
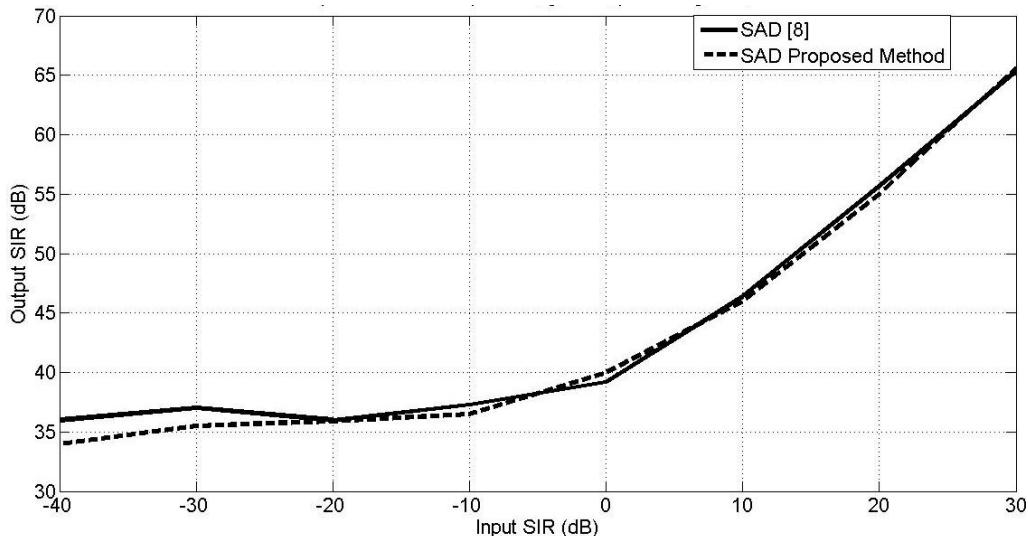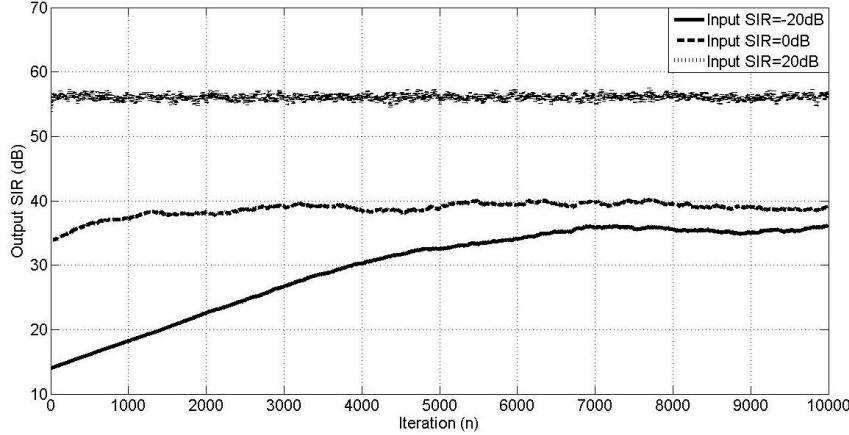
Fig. 68: Output SIR across Input SIR for the SAD in [11] and the its variant proposed in this work, g=1.02, phi=2 degree's, N=1e4

Fig. 69: Proposed dual-tap IQI compensation Using LMS Algorithm, Output SIR across Time Iterations (n), g=1.02, phi=2^0, SNR=35dB
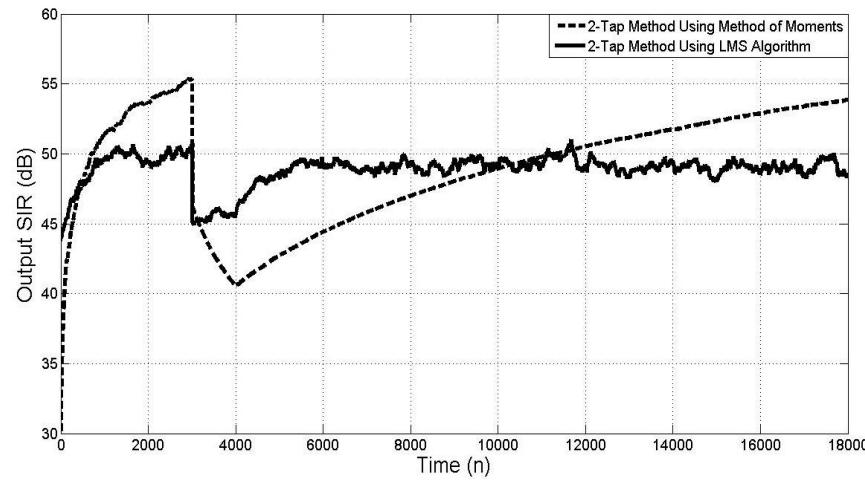
Fig. 70: Output SIR across Time(n) at input SIR=10dB, varying the gain mismatch at n=3000 from g=1.02 to g=1.05 then linearly from g=1.05 to g=1.1 till n=4000, and increasing phase mismatch linearly from g=2^0 to 3^0 starting at n=3000 till n=4000.
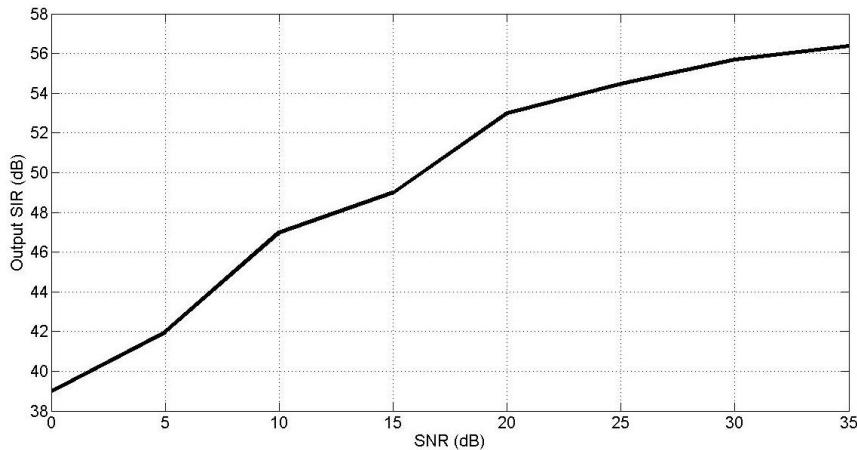
Fig. 71: Output SIR across SNR at different values of input SIR, g=1.02, phi=2^0

6. Data Aided IQI Compensation

Instead of the blind (non data aided) compensation methods introduced before, data aided compensation methods can be used if the communication standard allows the usage of a preamble sequences or pilot training sequence, but in the low-IF receivers no information about the timing or the data of the image signal pilot signals are available, that is why in this section we propose a data aided compensation algorithm that exploits known preamble sequence or pilot signals within the desired signal not within the image signal to estimate and compensate for the IQI. Three approaches will be introduced here, in the first approach AWGN of slow fading channel is assumed exploiting a known sequence (preamble) to generate an orthogonal nulling vector or an orthogonal nulling matrix to this known sequence using this vector or matrix to estimate and compensate for the IQI. In the second and third proposed methods fading channels are considered, in the second method a pilot signal consisting of two symbols is used to solve for the IQI and for the channel fading. While in the third approach the firth approach is extended to be suitable for fading channels as well compensating for the IQI achieving better performance compared to the second approach because of the noise averaging inherited in the least squares estimate method.

6.1. Data Aided IQI Compensation Using Preamble Sequence

In this section a known sequence of the desired signal s(n) is used to estimate and compensate for the IQI.

6.1.1. Vector-Nulling IQI Compensation Method

6.1.1.1. Mathematical Model

Assuming that the transmitter is sending a training signal s(n) of length (L) which is already known to the receiver. Representing the baseband signal d(n) and v(n) which are the outputs from the digital mixers as follows:

$$\underbrace{\begin{bmatrix} d(1) & \dots & d(L) \\ v^*(1) & \dots & v^*(L) \end{bmatrix}}_{\equiv \mathbf{Y}} = \begin{bmatrix} K_1 & K_2 \\ K_2^* & K_1^* \end{bmatrix} \begin{bmatrix} \alpha\, s(1) + n_1 & \dots & \alpha\, s(L) + n_L \\ i^*(1) & \dots & i^*(L) \end{bmatrix} \tag{6.1}$$

where "α" is the complex fading coefficient and $LT_s < T_c$ where T_s and T_c denote the sampling time and channel coherence time, respectively. Now, taking the transpose of $\mathbf{Y}$ as follows:

$$\mathbf{Y}^T = [\alpha\, \mathbf{s}_L + \mathbf{n_L} \quad \mathbf{i}_L] \begin{bmatrix} K_1 & K_2^* \\ K_2 & K_1^* \end{bmatrix} \tag{6.2}$$

Where $\mathbf{s}_L = [s(1)\, s(2)\, \dots\dots\, s(L)]^T$ and $\mathbf{i}_L = [i^*(1)\, i^*(2)\, \dots\dots\, i^*(L)]^T$, then multiplying the matrix $\mathbf{Y}^T$ by the vector $\mathbf{e}^H$ where $\mathbf{e}$ is chosen to be orthogonal to $\mathbf{s}_L$, i.e. $\mathbf{e}^H \mathbf{s}_L = 0$. Hence,

$$\mathbf{w}^T = \mathbf{e}^H \mathbf{Y}^T = [\alpha\, \mathbf{e}^H \mathbf{s}_L + \mathbf{e}^H \mathbf{n_L} \quad \mathbf{e}^H \mathbf{i}_L] \begin{bmatrix} K_1 & K_2^* \\ K_2 & K_1^* \end{bmatrix}$$
$$= [\mathbf{e}^H \mathbf{n_L} \quad \mathbf{e}^H \mathbf{i}_L] \begin{bmatrix} K_1 & K_2^* \\ K_2 & K_1^* \end{bmatrix} \tag{6.3}$$

A possible candidate for $\mathbf{e}^H$ that will be used in the proposed model is:

$$\mathbf{e}^H = [1 \quad 0 \quad \dots \quad 0] - \frac{s(1)\mathbf{s}_L^H}{\mathbf{s}_L^H \mathbf{s}_L} \tag{6.4}$$

At ideal conditions (no additive noise) (6.3) can simplified to:

$$\mathbf{w}^T = \mathbf{e}^H \mathbf{Y}^T = \mathbf{e}^H \mathbf{i}_L [K_2 \quad K_1^*] = [W_1 \quad W_2] \tag{6.5}$$

And so K_2/K_1^* can be estimated as follows:

$$A = \left(\frac{\widetilde{K_2}}{\widetilde{K_1^*}} \right) = \frac{w_1}{w_2} \tag{6.6}$$

Knowing that $K_1 = 1 - K_2^*$ and substituting by it in (6.6) we get estimates for K_1 & K_2 as follows:

$$K_1 = 1 - \left(\frac{A}{1+A} \right)^2, \quad K_2 = \frac{A}{1+A} \tag{6.7}$$

So using (6.7) to estimate K_1 and K_2 the filter coefficients for the dual-Tap method W_1 & W_2 can be estimated and used to do the IQI compensation.

6.1.1.2. Simulation Results

The performance of the vector-nulling method is monitored by plotting the output SIR across the known sequence length (L) as shown in Fig. 72, showing that the achieved output SIR saturates after a definite known sequence "L". The reason for this behavior is that whatever the length "L" only one equation is used in (6.6) to estimate for the IQI and so no noise averaging is performed. So in the next section a modification for this method will be performed that generate (L-1) equation and solve for them using the least squares estimate performing noise averaging and so benefiting from increasing the length of the known sequence.
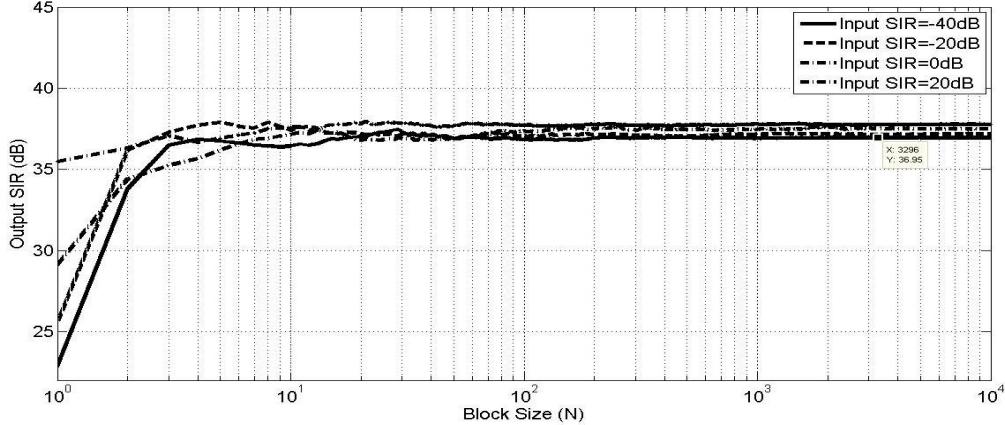
Fig. 72: Output SIR across the known sequence length "L", at SNR=35dB, g=1.02, phi=2 degree's

6.1.2. Matrix-Nulling IQI Compensation Method

To make use of the longer sequence length, a modification is introduced in this section to the vector-nulling method, in which an orthogonal matrix is generated from the known sequence instead of the orthogonal vector and so the least squared estimates can be used, we introduced the noise terms in the analysis of the vector-nulling method to highlight the effect of the additive noise, this effect will stay the same in the rest of the methods and so the noise terms will be omitted for clarity without losing or generality.

6.1.2.1. Mathematical Model

Assuming that we have the same known sequence as the vector-nulling method, since s_L is a vector of dimension "L" then "L-1" vector can be generated which are linearly independent from s_L, these vectors will be generated and used to construct the matrix $\boldsymbol{P}$, the left null projection matrix of s_L, and so multiplying the matrix $\boldsymbol{Y}^T$ by the $\boldsymbol{P}$ matrix of size (L-1,L) will satisfy the following condition i.e. $\boldsymbol{P}_{(L-1)XL}\boldsymbol{s}_{LX1} = 0_{(L-1)X1}$. Hence,

$$
\begin{aligned}
\mathbf{W}^{\mathbf{T}}_{(\mathbf{L-1X2})} = \boldsymbol{P}\mathbf{Y}^T &= [0 \quad \boldsymbol{Pi}_{L_{L-1X1}}]\begin{bmatrix} K_1 & K_2^* \\ K_2 & K_1^* \end{bmatrix} = [0 \quad \boldsymbol{Pi}_L]\begin{bmatrix} K_1 & K_2^* \\ K_2 & K_1^* \end{bmatrix} \\
&= \boldsymbol{Pi}_L[K_2 \quad K_1^*] = K_1^*\boldsymbol{Pi}_L\begin{bmatrix} \dfrac{K_2}{K_1^*} & 1 \end{bmatrix} = \begin{bmatrix} \underbrace{\mathbf{W}_1}_{(L-1)X1} & \underbrace{\mathbf{W}_2}_{(L-1)X1} \end{bmatrix}
\end{aligned}
\tag{6.8}
$$

And so using (6.8) using the ratio of expectations the estimate of $\left[\dfrac{\widetilde{K_2}}{K_1^*}\right]$ can be obtained as:

$$
A = \left(\widehat{\dfrac{K_2}{K_1^*}}\right) = \dfrac{\sum_{j=1}^{j=L-1} W_{1j}W_{2j}^*}{\sum_{j=1}^{j=L-1}\left|W_{2j}\right|^2}
\tag{6.9}
$$

Knowing that $K_1 = 1 - K_2^*$ and substituting by it in (6.9) we get estimates for K_1 & K_2 as follows:

$$K_1 = 1 - \left(\frac{A}{1+A}\right)^2, K_2 = \frac{A}{1+A}$$

<div align="right">(6.10)</div>

Where the null projection matrix "P" is generated as:

$$P = I - \frac{S * S^H}{S^H * S}$$

<div align="right">(6.11)</div>

Although (6.10) generate an (LXL) matrix, only (L-1) raw can be used as linearly independent vector for the vector "s".

So using (6.10) to estimate K_1 & K_2 the filter coefficients for the dual-tap method, W_1 & W_2, can be estimated based on (5.8) & (5.9).

6.1.2.2. Simulation Results

The performance of the proposed method is examined by plotting the output SIR across the pilot length "L" for different input SIR values. As shown in Fig. 73, as the length of the pilot vector increases the output SIR is enhanced proportionally, achieving higher output SIR values compared to the blind method using dual-tap IQI compensation using method of moments proposed before. The output SIR at N=100 is plotted against the input SIR in Fig. 74 showing that the proposed IQI compensation method guarantee a constant output SIR across the whole range of the input SIR. Then the effect of the additive noise is plotted in Fig. 75 by plotting the output SIR across the SNR for N=100, showing that the output SIR is decreasing approximately linearly with the decreasing SNR. Comparing the constellation diagram of the compensated signal y(n) to the uncompensated signal d(n) we can see the huge enhancement in Fig. 76. In order to realize the advantage of using the data aided method if the appropriate pilots or known sequence were available Fig. 77 shows a comparison between the data aided method and the blind method at input SIR of -40dB showing that the data aided method outperform the blond method by approximately 35 dB, so this proves that at high SNR the data aided method will perform much better than the blind methods.

In the vector-nulling method and the matrix-nulling method slow fading conditions were assumed, in the next two sections we will propose two methods that are suitable to fast fading conditions as well.
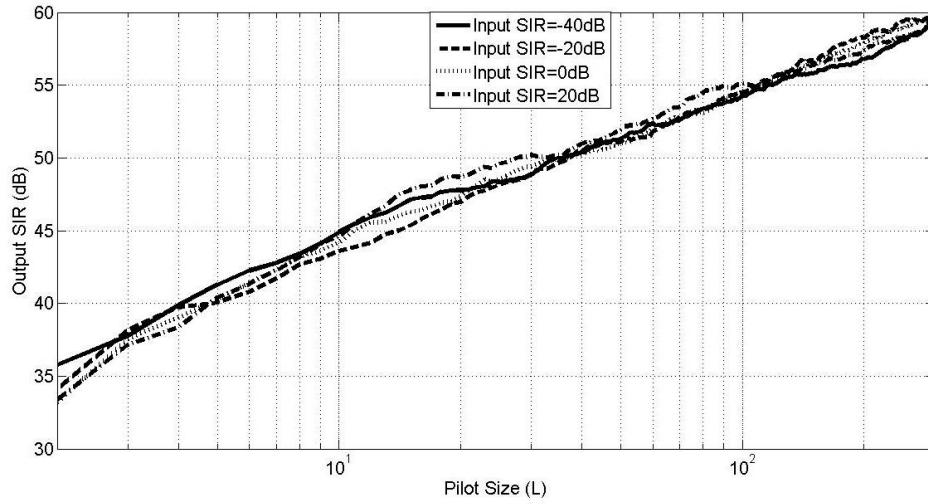
Fig. 73: Output SIR across pilot length (L), SNR=35dB, g=1.02, phi=2 degree's
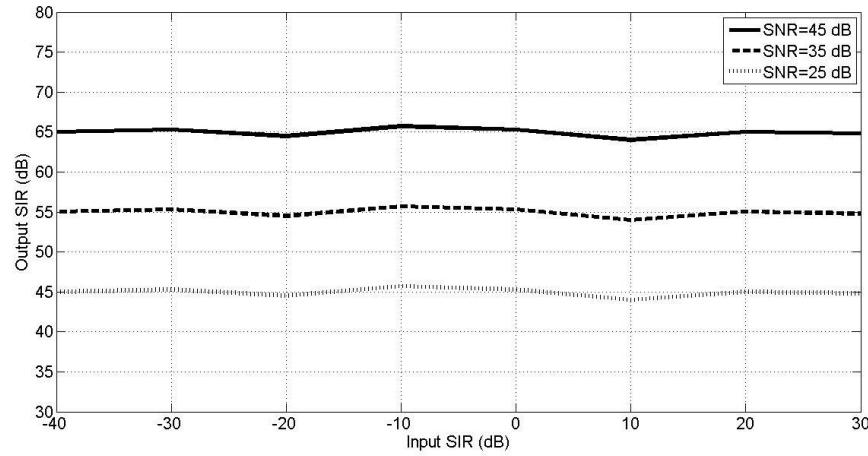
Fig. 74: Output SIR across Input SIR for different SNR values, g=1.02, phi=2 degree's
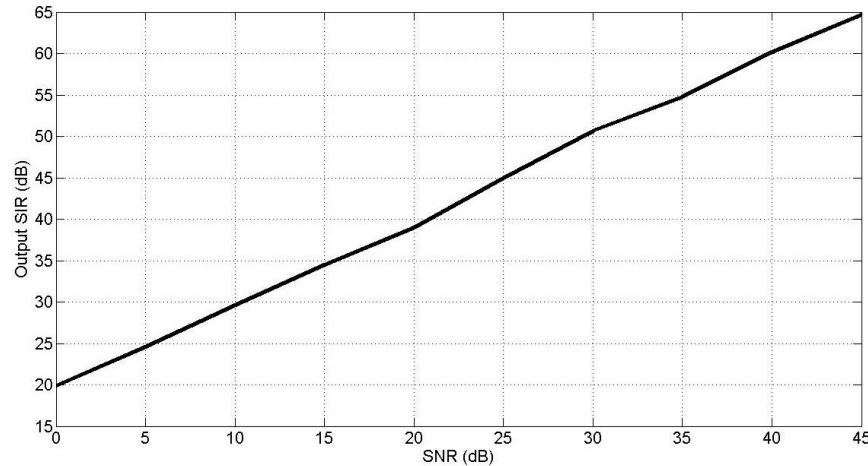
Fig. 75: Output SIR across the SNR for input SIR=-20dB, g=1.02, phi=2 degree's

68
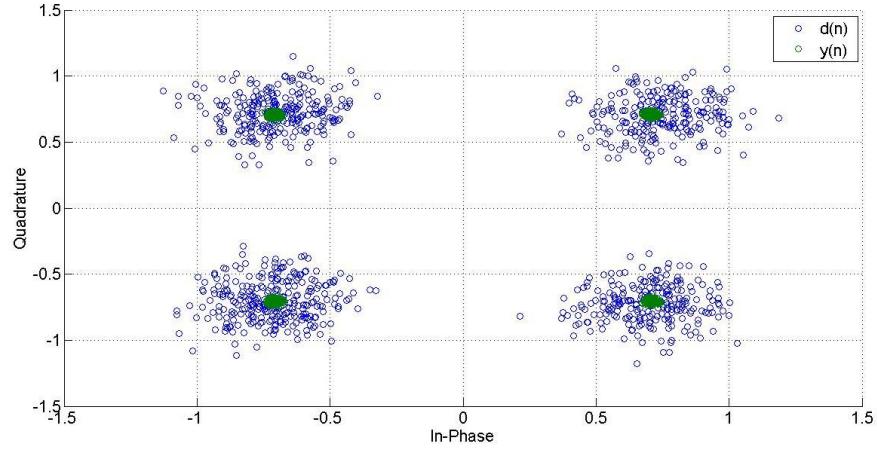
Fig. 76: Signal constellation for the compensated signal y(n) and the uncompensated signal d(n), g=1.02, phi=2 degree's, input SIR=-20dB, SNR=35dB
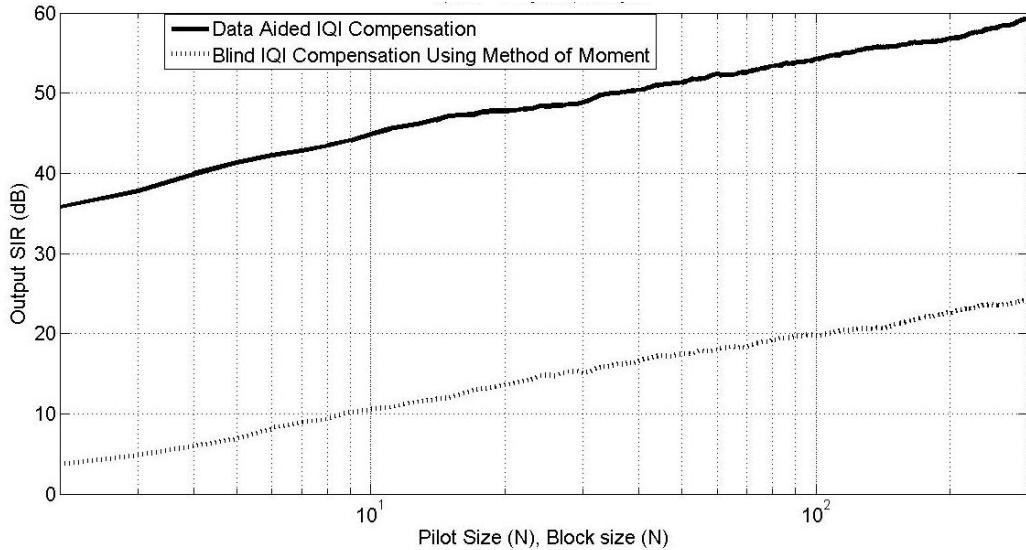
Fig. 77: Output SIR across the block size "N" for the blind IQI compensation using method of moments, and across the pilot size "N" for the data aided matrix-nulling method

6.2. Data Aided IQI Compensation Using Pilot Symbols

6.2.1. IQI Compensation Using Pairs of Symbols as Pilot Signals

6.2.1.1. Mathematical Model

In this approach we assume that we have a pilot signal consisting of two known symbols, including channel fading which is for practical cases will be the same for the two adjacent symbols, considering this situation we will have the observation signals d(n) and v(n) as follows:

$$d(1) = K_1 \propto_1 s(1) + K_2 i^*(1) \tag{6.12a}$$
$$v(1) = K_2^* \propto_1 s(1) + K_1^* i^*(1) \tag{6.12b}$$
$$d(2) = K_1 \propto_1 s(2) + K_2 i^*(2) \tag{6.13a}$$

$$v(2) = K_2^* \propto_1 s(2) + K_1^* i^*(2) \tag{6.13b}$$
$$K_2 = 1 - K_1^* \tag{6.14}$$

So we have 5 complex equations in 5 complex unknowns: K_1, K_2, $i(1)$, $i(2)$ & α_1. Theoretically these sets of equations are solvable, but practically in order to get an analytical solution for this set of equations an assumption was made that the pilot symbols are identical, i.e. $s(1) = s(2)$ detailed solution is presented in Appendix C.

So after some mathematical steps, removed here for clarity, K_1 and α was solved to be:

$$K_1^* = \frac{1}{1 + \left[\dfrac{d(1) - d(2)}{v(1) - v(2)}\right]} \tag{6.13a}$$

$$\propto_1 = \frac{v(2) - \dfrac{K_1^* d(2)}{1 - K_1^*}}{s(2)\left[(1 - K_1) - \dfrac{K_1 K_1^*}{1 - K_1^*}\right]} \tag{6.13b}$$

So as given by (6.13a) the filter coefficients are estimated by solving using the observation signals $d(n)$ and $v(n)$ for two consecutive symbols. In order to reduce the effect of the additive noise and so enhance the estimated output SIR, this operation is repeated over "N" number of pilots and then the estimated K_1 are obtained by averaging the N outcomes:

$$K_{1\_est}^*(N) = \sum_{l=1}^{l=N} \frac{1}{1 + \left[\dfrac{d_l(1) - d_l(2)}{v_l(1) - v_l(2)}\right]} \tag{6.14}$$

6.2.1.2. Simulation Results

At first the performance of the proposed method is examined with slow fading conditions, plotting the output SIR across the number of pilots "N", as shown in Fig. 78 as the number of pilots increase the output SIR is enhanced proportionally. Then a Rayleigh fading channel is used assuming a sampling frequency of 400 KHz with different maximum Doppler frequencies and the output SIR is plotted against the number of pilots in Fig. 79 and Fig. 80 showing that the Rayleigh fading channel has minimal effect on the proposed IQI compensation method. Finally the effect of the additive noise is examined in Fig. 81 by plotting the steady state output SIR across the SNR at N=100, showing that the output SIR is decreasing approximately linearly with the decreasing SNR.

Solving the equations simultaneously and solving for K_1 might not be the best solution in terms of noise averaging, that is why in the next section another approach is proposed in which a matrix is generated based on the preamble sequence or the pilot signals and used to null the desired signal pilot signal and then using the ratio of expectations K_1 and K_2 are estimated reaching better performance due to the inherit noise cancellation.
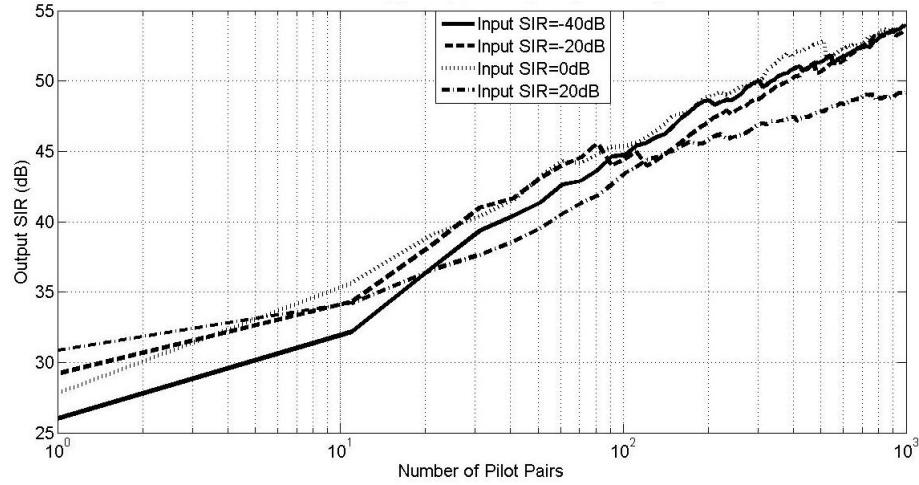
Fig. 78: Output SIR across number of Pilots "N" , g=1.02, phi=2 degree's, SNR=35dB with slow fading conditions
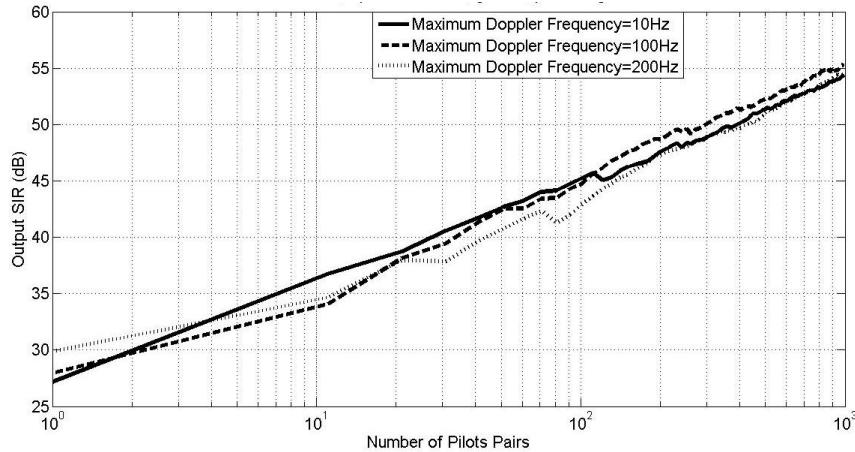
Fig. 79: Output SIR across number of Pilots "N" , g=1.02, phi=2 degree's, input SIR=-40dB, SNR=35dB with Rayleigh Fading
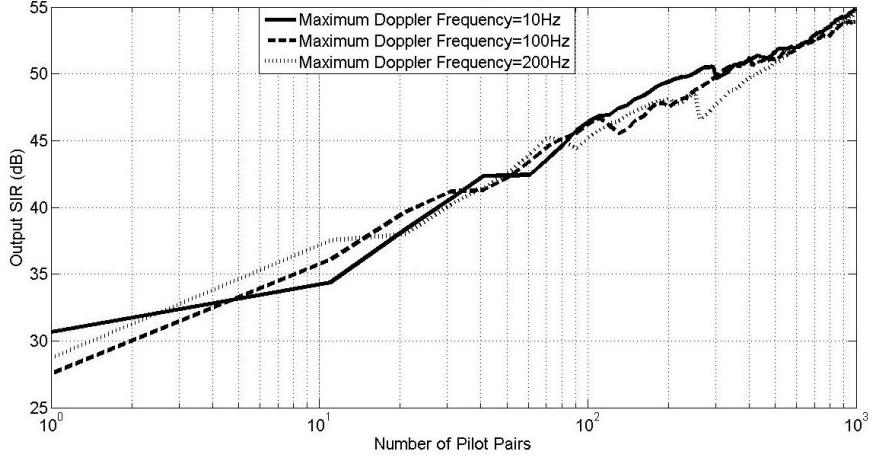
Fig. 80: Output SIR across number of Pilots "N" , g=1.02, phi=2 degree's, input SIR=-20dB, SNR=35dB with Rayleigh Fading
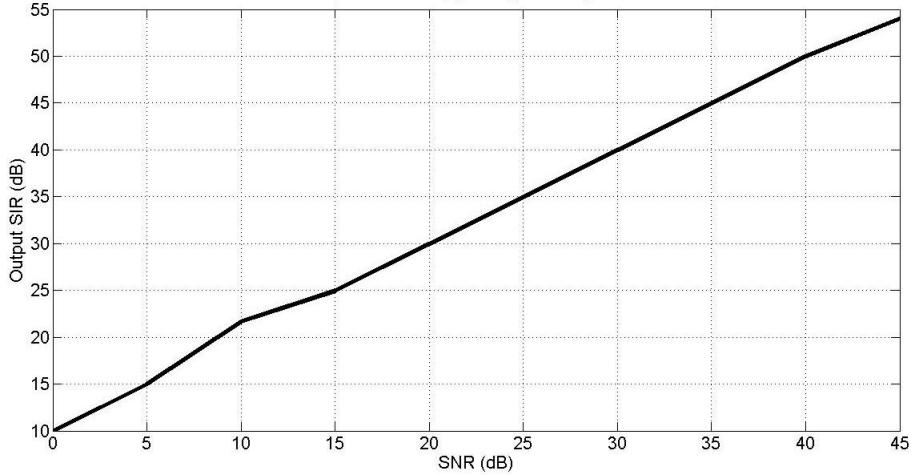
Fig. 81: Output SIR across SNR , g=1.02, phi=2 degree's, input SIR=-20dB and N=100

6.2.2. Data Aided IQI Compensation Using Full Pilot Design

6.2.2.1. Mathematical Model

In this approach we assume that we have (N/L) pilot signals each one is of length (L), where the channel fading is assumed to be constant along the L symbols, but not the same across the different pilot signals. Using these (N/L) pilot signals a matrix orthogonal to the desired signal s(n) is generated and used to estimate the IQI as explained in more details next.

$$Y = \begin{bmatrix} d(1) & ... & d(N) \\ v^*(1) & ... & v^*(N) \end{bmatrix}_{2XN} = \begin{bmatrix} K_1 & K_2 \\ K_2^* & K_1^* \end{bmatrix}_{2X2} \begin{bmatrix} \alpha_1 \, s_{l_1} & ... & \alpha_{N/L} s_{l_{N/L}} \\ i^*{}_{l_1} & ... & i^*{}_{l_{N/L}} \end{bmatrix}_{2XN} \tag{6.15}$$

Where s_{l_1} and $i^*{}_{l_1}$ are of length L, then an N/L matrix will be generated each of length L such that each one is chosen to be orthogonal to $\mathbf{s}_{L_j}$ satisfying the condition:

72

$$\mathbf{e_j}^T \mathbf{s}_{L_j} = 0. \tag{6.16}$$

A possible candidate for e^H that will be used in the proposed model is:

$$\mathbf{e}^T = [1 \quad 0 \quad ... \quad 0] - \frac{s(1)\mathbf{s}_L^H}{\mathbf{s}_L^H \mathbf{s}_L} \tag{6.17}$$

Then these N/L array are used to generate the diagonal matrix E as follows:

$$[E]_{\frac{N}{L}XN} = \begin{bmatrix} \mathbf{e_1}^T & 0 & 0 \\ 0 & \mathbf{e_2}^T & 0 \\ 0 & 0 & \mathbf{e_{N/L}}^T \end{bmatrix}_{\frac{N}{L}XN} \tag{6.18}$$

Then by multiplying (6.15) and (6.18) we get:

$$[E]_{\frac{N}{L}XN}[Y^T]_{NX2} = \begin{bmatrix} \mathbf{e_1}^T & 0 & 0 \\ 0 & \mathbf{e_2}^T & 0 \\ 0 & 0 & \mathbf{e_{N/L}}^T \end{bmatrix}_{\frac{N}{L}XN} \begin{bmatrix} \alpha_1 s_{l_1} & i^*{}_{l_1} \\ \vdots & \vdots \\ \alpha_{N/L}s_{l_{N/L}} & i^*{}_{l_{N/L}} \end{bmatrix}_{NX2} \begin{bmatrix} K_1 & K_2^* \\ K_2 & K_1^* \end{bmatrix}_{2X2} \tag{6.19}$$

From (6.19) and after doing the first multiplication for the RHS we get:

$$[E]_{\frac{N}{L}XN}[Y^T]_{NX2} = \begin{bmatrix} 0 & \mathbf{e_1}^T i^*{}_{l_1} \\ \vdots & \vdots \\ 0 & \mathbf{e_{N/L}}^T i^*{}_{l_{N/L}} \end{bmatrix}_{\frac{N}{L}X2} \begin{bmatrix} K_1 & K_2^* \\ K_2 & K_1^* \end{bmatrix}_{2X2} = \begin{bmatrix} \mathbf{e_1}^T i^*{}_{l_1} \\ \vdots \\ \mathbf{e_{N/L}}^T i^*{}_{l_{N/L}} \end{bmatrix} [K_2 \quad K_1^*] \tag{6.20}$$

Defining the matrix "X" as:

$$X = \begin{bmatrix} K_1^* \mathbf{e_1}^T i^*{}_{l_1} \\ \vdots \\ K_1^* \mathbf{e_{N/L}}^T i^*{}_{l_{N/L}} \end{bmatrix} \tag{6.21}$$

we can reformulate (6.21) to be:

$$[E]_{\frac{N}{L}XN}[Y^T]_{NX2} = \begin{bmatrix} K_1^* \mathbf{e_1}^T i^*{}_{l_1} \\ \vdots \\ K_1^* \mathbf{e_{N/L}}^T i^*{}_{l_{N/L}} \end{bmatrix} \begin{bmatrix} \frac{K_2}{K_1^*} & 1 \end{bmatrix} = \begin{bmatrix} \frac{K_2}{K_1^*} X & X \end{bmatrix}_{\frac{N}{L}X2} = [W_1 \quad W_2]_{\frac{N}{L}X2} \tag{6.22}$$

And similar to the vector-nulling method from (6.22) the estimate of $\begin{bmatrix} \widetilde{K_2} \\ K_1^* \end{bmatrix}$ can be obtained as:

$$A = \left(\widehat{\frac{K_2}{K_1^*}}\right) = \frac{\sum_{j=1}^{j=N/L} W_{1j}W_{2j}^*}{\sum_{j=1}^{j=N/L} |W_{2j}|^2} \tag{6.23}$$

Using the known relation between K_1 and K_2 with (6.23) we get estimates for K_1 and K_2 and so the estimate for the dual-tap IQI compensation filter coefficients, as:

$$\widehat{K_1} = 1 - \left(\frac{A}{1+A}\right)^2, \widehat{K_2} = \frac{A}{1+A} \tag{6.19}$$

An enhancement can be done of this extended method in which (L-1) orthogonal vector are generated for the each pilot signal and used to estimate K_1 and K_2 instead of the single

orthogonal vector generated in our proposed model (e^T). For L=2 the proposed method and the proposed enhancement will be the same because (L-1=1).

It is worth mentioning that the data aided method depends on the pilot signals, and so it is assumed that the location of the pilot signals is acquired, i.e. synchronization had occurred. In practical situations to perform synchronization moderate output SIR is required (0dB-20dB). Hence to overcome this problem blind IQI compensation or non data aided IQI calibration may be conducted first to obtain satisfactory output SIR for synchronization. Then the proposed data aided IQI compensation method can be used to enhance the output SIR based on the targeted value. Alternatively, joint IQI compensation and carrier frequency offset (CFO) synchronization tevhniques may be applied that use the pilot signals to jointly track CFO and IQI [46].

Although the data aided method had been driven and implemented for a single transmitter and receiver, it can be extended to higher number of transmitters and receivers (frequency selective channels), which will be left as a future work.

6.2.2.2. Simulation Results

The performance of the proposed method is examined with Rayleigh fading channel conditions using a sampling frequency of 400 KHz with different maximum Doppler frequencies, the output SIR is plotted against the number of pilots in Fig. 82 and Fig. 83 showing that the Rayleigh fading channel has minimal effect on the proposed IQI compensation method, and that as the number of the pilots "N/L" increases the output SIR increases proportionally as well because of the noise averaging achieved in (6.18) using ratio of expectations, reaching better performance compared to the dual-tap IQI compensation using method of moments. Also the output SIR across the input SIR in Fig. 84 showing that similar to the vector-nulling method a constant output SIR is satisfied across the input SIR range. Finally the effect of the additive noise is examined in Fig. 85 by plotting the steady state output SIR across the SNR at N=100, showing that the output SIR is decreasing approximately linearly with the decreasing SNR.

Fig. 82: Output SIR across number of Pilots "N/L" , g=1.02, phi=2 degree's, input SIR=-20dB, SNR=35dB with Rayleigh Fading, L=2
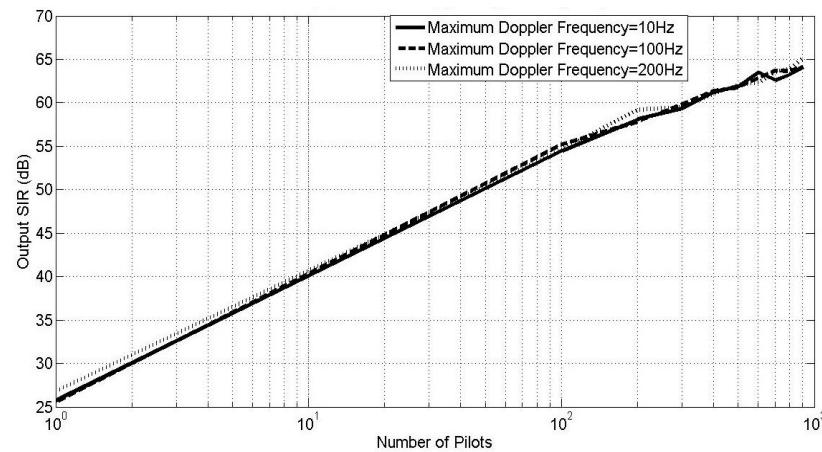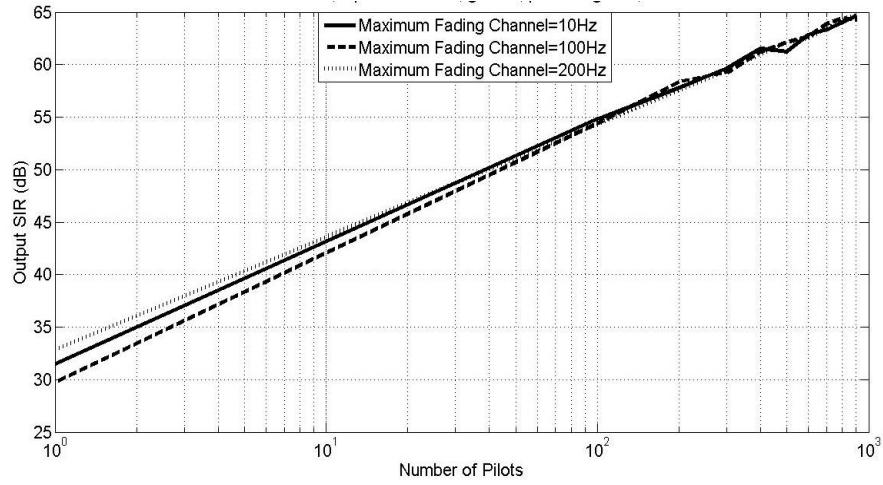
Fig. 83: Output SIR across number of Pilots "N/L" , g=1.02, phi=2 degree's, input SIR=20dB, SNR=35dB with Rayleigh Fading, L=2
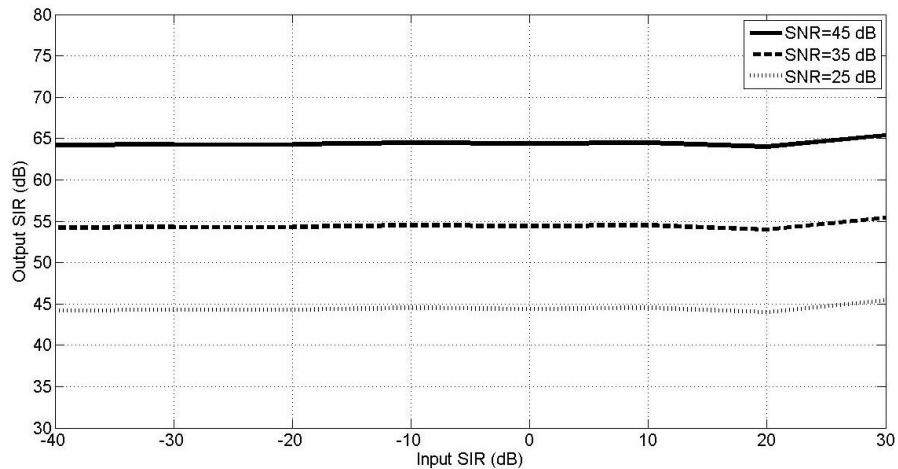

Fig. 84: Output SIR across input SIR for different SNR values, g=1.02, phi=2 degree's
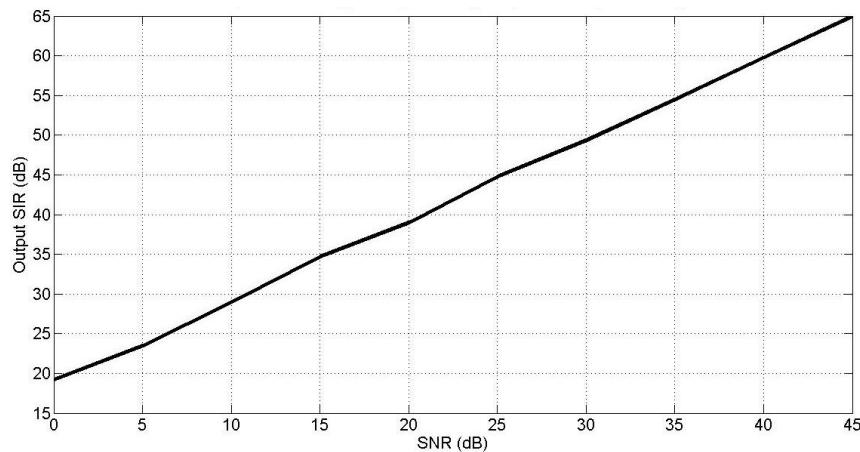

Fig. 85: Output SIR across SNR , g=1.02, phi=2 degree's, input SIR=-20dB and N=100

7. Conclusion

This work represented a review for the basic receiver architectures followed by a summary for the mostly used image reject receivers, explaining the IQ mismatch problem and its effect on the image rejection ratio, then a more detailed review where introduced for the IQ mismatch calibration and compensation techniques. After doing a comparison between the different IQ imbalance compensation techniques a mathematical formulations was performed for the single-tap IQI compensation method using LMS algorithm introduced in the literature and a new implementation was proposed for the single-tap IQI compensation using the non feedback based method of moments approach and compared to the LMS approach introduced in the literature, showing that the proposed approach achieves better output SIR and/or better convergence time while the LMS algorithm implementation responds better to the time varying IQI. The signal leakage problem suffered by the single-tap IQI compensation was discussed and another approach was proposed to compensate for the IQI using dual-tap filter in order to avoid the signal leakage problem enhancing the output SIR at moderate and high input SIR values. At first a dual-tap IQI compensation technique was proposed using the method of moments, in this method the input SIR is estimated and used to optimize for the number of samples required to perform the IQI compensation showing a huge saving across the input SIR range, another use for this estimated input SIR is to select between the single-tap and the dual-tap IQI compensation methods based on the input SIR and so optimizing between performance and complexity. After that a dual-tap IQI compensation method is proposed using LMS algorithm proposing a simplification on the method already introduced in the literature, simulation results shows that the performance is not affected achieving a less complex solution. The two dual-tap IQI compensation methods were compared showing that the non feedback based (non iterative) approach achieves higher output SIR and/or better convergence time but the iterative approach responds faster to the time varying IQI values.

After proposing those new methods for blind IQI compensation, a new data aided technique was proposed exploiting pilot training sequence within the desired signal, the first approach is exploiting a preamble pilot signal being suitable for slow fading across the preamble size, while the second approach is more general exploiting pilot signals being suitable for fast fading as well, simulation results showed that the performance of the second approach was not affected by the Rayleigh fading model. At high SNR values the proposed data aided IQI compensation technique achieved output SIR that is higher than the dual-tap blind IQI compensation method and at much less convergence time.

Appendix A (Derivation of LMS Update Equation)

The least mean square algorithm is used to adjust the weights of an adaptive filter (W) minimizing the mean square of the error signal (y), where the error signal is simply the difference between the input signal (d) and the reference signal (v) multiplied by the filter coefficient (W) that need to be adapted as was shown in Fig. 40, so the error can be expressed as:

$$y(n) = d(n) - v(n)W^* \tag{A.1}$$

In the LMS algorithm an approximation is done, compared to the minimum mean square error (MMSE), is to minimize the instantaneous squared y(n) signal instead of the mean squared y(n) signal, this is done because practically it is hard to implement the MMSE, so there is a compromise between the simplicity of the algorithm and the performance, in most of the cases the performance of the LMS algorithm is satisfactory and that is why it is the mostly used algorithm in the adaptive techniques.

Applying that to (A.1):

$$\frac{dE[|y(n)|^2]}{dW} = -2\,v\,(n)d^*(n) + 2W(n)v(n)v^*(n) \tag{A.2}$$

So the filter coefficient will be updated based on this gradient coefficient (A.2) using the steepest descend algorithm as follows:

$$W(n+1) = W(n) - \mu\left[\frac{\partial y^2(n)}{\partial W}\right] = W(n) - 2\mu v(n)[d^*(n) + W(n)v^*(n)] \tag{A.3}$$
$$= W(n) + 2\mu y^*(n)v(n)$$

Equation (A.3) shows that the filter coefficient is updated by multiplying the error signal by the input signal, that is why to use LMS the input signal y(n) and the error signal v(n) must be at the same frequency (dc or other frequency) that is why in [27] two extra mixers where added.

The previous analysis shows that the LMS is a suboptimal solution for the MSE steepest descend, and the excess error added due to the usage of the LMS algorithm depends on the update coefficient rate (μ) having a tradeoff between the achievable steady state excess error and the settling time.

Proving that $K_1 = 1 - K_2^*$ using equation (5.17) and (5.18) we can derive the relation between W_1 and W_2, at first K_1 & K_2 will be redefined as:

$$K_1 = \frac{1 + gcos(\varphi) - jgsin(\varphi)}{2} \tag{A.4}$$
$$K_2 = \frac{1 - gcos(\varphi) - jgsin(\varphi)}{2} \tag{A.5}$$

so $|K_1|^2$ and $|K_2|^2$ can be defined as:

$$|K_1|^2 = \frac{1 + 2g\cos(\varphi) + g^2\cos^2(\varphi) + g^2\sin^2(\varphi)}{4} = \frac{1 + 2g\cos(\varphi) + g^2}{4} \qquad (A.6)$$

$$|K_2|^2 = \frac{1 - 2g\cos(\varphi) + g^2\cos^2(\varphi) + g^2\sin^2(\varphi)}{4} = \frac{1 - 2g\cos(\varphi) + g^2}{4} \qquad (A.7)$$

So the denominator of (5.17) & (5.18) can be defined as:

$$|K_1|^2 - |K_2|^2 = g\cos(\varphi) \qquad (A.8)$$

So using equation(B.4), (B.5), (B.6) & (B.7) in equation (5.17) & (5.18) we get:

$$W_1 = W_{1r} + jW_{1I} = (\frac{1}{2g\cos(\varphi)} - \frac{1}{2}) + j\frac{\tan(\varphi)}{2} \qquad (A.9)$$

$$W_2 = W_{2r} + jW_{2I} = (\frac{1}{2g\cos(\varphi)} + \frac{1}{2}) + j\frac{\tan(\varphi)}{2} \qquad (A.10)$$

From (A.9) and (A.10) we can notice that the imaginary parts of W_1 & W_2 are equal, while there is a constant difference between the real parts equal to one, this can be summarized as:

$$W_{2r} = W_{1r} + 1 \ \& \ W_{2I} = W_{1I} \qquad (A.11)$$

So only W_1 need to be obtained iteratively and W_2 can be obtained using (A.11), and so the updating equation for this modified IC technique will be:

$$W_1(n + 1) = W_1(n) + \mu y^*(n)v(n) \qquad (A.12)$$

$$W_{2r}(n + 1) = 1 + W_{1r}(n + 1), W_{2I}(n + 1) = W_{1I}(n + 1), \qquad (A.13)$$

Appendix B (Solution of Non Linear Simultaneous Equations for Blind IQI Compensation)

K_1 and K_2 are two complex quantities while P_s and P_I are two real quantities so we have effectively 6 real unknowns, in the same time we have (5.11a) and (5.11b) as two real equations and we have (5.11c) and (2.13) as two complex equations, so effectively we have 6 real unknowns in 6 real equations and that is why they are solvable. To solve for K_1, K_2, P_s and P_I using (5.11) and (2.13) we start by using (2.13) to get the magnitude squared of K_2 as:

$$|K_2|^2 = 1 - 2Re(K_1) + |K_1|^2 \tag{B.1}$$

Substituting by (2.13) and (B.1) in (5.11) we get:

$$E[|d(n)|^2] = (P_s + P_I)(|K_1|^2) + P_I(1 - 2Re(K_1)) \tag{B.2}$$
$$E[|v(n)|^2] = (P_s + P_I)(|K_1|^2) + P_S(1 - 2Re(K_1)) \tag{B.3}$$
$$E[d(n)v^*(n)] = (K_1 - |K_1|^2)(P_s + P_I) \tag{B.4}$$

Adding (B.2) to (B.4) and (B.3) to (B.4):

$$A = (B.2) + (B.4) = P_I(1 - 2Re(K_1)) + K_1(P_s + P_I) \tag{B.5}$$
$$B = (B.3) + (B.4) = P_S(1 - 2Re(K_1)) + K_1(P_s + P_I) \tag{B.6}$$

In order to decouple K_1 from (P_s+P_I) we first solve for (P_s+P_I) as:

$$Re(A) + Re(B) = (P_s + P_I) \tag{B.7}$$

Then K_1 can be solved using (B.5) and (B.7):

$$Imag(K_1) = \frac{Imag(A)}{Re(A) + Re(B)} \tag{B.8}$$

Using (B.8) into (B.2) and (B.3) to get the real part of K_1 as:

$$\begin{aligned} E[|d(n)|^2] + E[|v(n)|^2] \\ = (P_s + P_I)(2Re(K_1)^2 - 2Re(K_1) + 1 + 2Imag(K_1)^2) \end{aligned} \tag{B.9}$$

By solving quadratic equation (B.9) the real part of K_1 is solved as:

$$Re(K_1) = \frac{1 + \sqrt{1 - 2X}}{2} \tag{B.10}$$

where:

$$X = 1 + 2Imag(K_1)^2$$
$$- \frac{E[|d(n)|^2] + E[|v(n)|^2]}{Re(E[|d(n)|^2] + E[|v(n)|^2] + 2E[d(n)v^*(n)])} \tag{B.11}$$

So now we estimated K_1, P_s and P_I can be estimated by substituting from (B.8) and (B.10) into (B.2) and (B.3) as:

$$P_I = \frac{|K_1|^2 E[|v(n)|^2] - |K_2|^2 E[|d(n)|^2]}{(|K_1|^2)^2 - (|K_2|^2)^2} \tag{B.12}$$

$$P_s = \frac{E[|d(n)|^2] - |K_2|^2 P_I}{|K_1|^2} \tag{B.13}$$

Appendix C (Solution of Non Linear Simultaneous Equations for Data Aided IQI Compensation Using Pair of Pilot Signals)

In order to solve for the 5 complex unknowns using the 5 complex equations defined as (6.12), (6.13) and (6.14), we start by substituting from (6.14) into (6.12) and (6.13):

$$d(1) = K_1 \propto_1 s(1) + (1 - K_1^*)i^*(1) \tag{C.1a}$$
$$v(1) = (1 - K_1) \propto_1 s(1) + K_1^* i^*(1) \tag{C.1b}$$
$$d(2) = K_1 \propto_1 s(2) + (1 - K_1^*)i^*(2) \tag{C.2a}$$
$$v(2) = (1 - K_1) \propto_1 s(2) + K_1^* i^*(2) \tag{C.2b}$$

At first we will omit i(1) from (C.1a) and (C.1b) to get :

$$v(1) = (1 - K_1) \propto_1 s(1) + K_1^* \left[\frac{d(1) - K_1 \propto_1 s(1)}{1 - K_1^*} \right] \tag{C.3}$$

Similarly i(2) will be omitted from (C.2a) and (C.2b) to get:

$$v(2) = (1 - K_1) \propto_1 s(2) + K_1^* \left[\frac{d(2) - K_1 \propto_1 s(2)}{1 - K_1^*} \right] \tag{C.4}$$

And so (C.3) and (C.4) are two complex equations in two complex unknowns K_1 and $\propto_1$.

Solving these two equations analytically is very complicated, so in order to simplify it to reach a closed form solution an assumption will be made that the pilot signal s(1) and s(2) are equal, in that case (C.3) and (C.4) can be solved as:

$$(C.3) - (C.4) = v(1) - v(2) = \frac{K_1^*}{1 - K_1^*} [d(1) - d(2)] \tag{C.5}$$

Then (C.5) is used to solve for K_1 and so for K_2 using (6.14) as:

$$K_1^* = \frac{1}{1 + \left[\frac{d(1) - d(2)}{v(1) - v(2)} \right]} \tag{C.6}$$

So as K_1 is available now it can be used into (C.3) or (C.4) to obtain the channel fading coefficient as:

$$\propto_1 = \frac{v(2) - \frac{K_1^* d(2)}{1 - K_1^*}}{s(2) \left[(1 - K_1) - \frac{K_1 K_1^*}{1 - K_1^*} \right]} \tag{C.7}$$

References:

1. Cetin, Ediz, Izzet Kale, and Richard CS Morling. "Analysis and compensation of RF impairments for next generation multimode GNSS receivers." *Circuits and Systems, May, 2007. ISCAS 2007. IEEE International Symposium on*. IEEE, 2007.
2. Woo, Sanghyun, et al. "Effects of RF impairments in transmitter for the future Beyond-3G communications systems." *Circuits and Systems, 2006. ISCAS 2006. Proceedings. 2006 IEEE International Symposium on*. IEEE, May, 2006.
3. Syu, Jin-Siang, et al. "Large improvement in image rejection of double-quadrature dual-conversion low-IF architectures." *Microwave Theory and Techniques, IEEE Transactions on* 58.7, July, 2010.
4. Martin, Kenneth W. "Complex signal processing is not complex." *Circuits and Systems I: Regular Papers, IEEE Transactions on* 51.9 , September, 2004.
5. Crols, Jan, and Michel SJ Steyaert. "A single-chip 900 MHz CMOS receiver front-end with a high performance low-IF topology." *Solid-State Circuits, IEEE Journal of* 30.12, December, 1995.
6. Behbahani, Farbod, et al. "A 2.4-GHz low-IF receiver for wideband WLAN in 6-/spl mu/m CMOS-architecture and front-end." *Solid-State Circuits, IEEE Journal of* 35.12, December, 2000.
7. Çetin, Ediz, İzzet Kale, and Richard CS Morling. "Adaptive self-calibrating image rejection receiver." *Communications, 2004 IEEE International Conference on*. Vol. 5. IEEE, June, 2004.
8. Valkama, Mikko, Markku Renfors, and Visa Koivunen. "On the performance of interference canceller based I/Q imbalance compensation." *Acoustics, Speech, and Signal Processing, 2000. ICASSP'00. Proceedings. 2000 IEEE International Conference on*. Vol. 5. IEEE, June, 2000.
9. Sever, Isaac. *"Adaptive Calibration Methods for an Image-Reject Mixer"*. MS Diss. Department of Electrical Engineering and Computer Sciences, University of California, 2001.
10. Valkama, Mikko, Markku Renfors, and Visa Koivunen. "Advanced methods for I/Q imbalance compensation in communication receivers." *Signal Processing, IEEE Transactions on* 49.10 , October, 2001.
11. Der, Lawrence, and Behzad Razavi. "A 2-GHz CMOS image-reject receiver with LMS calibration." *Solid-State Circuits, IEEE Journal of* 38.2, February, 2003.
12. Widrow, Bernard, et al. "Adaptive noise cancelling: Principles and applications."*Proceedings of the IEEE* 63.12, December, 1975.
13. Razavi, Behzad. *RF microelectronics*. Vol. 1. New Jersey: Prentice Hall, 1998.
14. Pandit, Vivek Kumar, and Sanjeev Gupta. "System level design of Bluetooth front end using novel low IF topology." *Recent Advances in Microwave Theory and Applications, 2008. MICROWAVE 2008. International Conference on*. IEEE, November, 2008.
15. Jensen, B., et al. "Performance of novel low intermediate frequency coherent optical DPSK receiver using baseband detection." *IEE Proceedings J (Optoelectronics)* 138.6, December, 1991.
16. Pun, K. P., et al. "Correction of frequency-dependent I/Q mismatches in quadrature receivers." IET *Electronics Letters* 37.23 , November, 2001.

17. Lang, G. R. "Complex analogue filters." *Proc. European Conf. on Circuit Theory Design, The Hauge,* Netherlands, August, 1981.
18. Nguyen, T-K., S-K. Han, and S-G. Lee. "Ultra-low-power 2.4 GHz image-rejection low-noise amplifier." IET *Electronics Letters* 41.15, July, 2005.
19. Eissa, Mohamed, and Mohammed El-Shennawy. "A technique for robust division ratio switching in Multi Modulus Dividers with modulus extension."*Microelectronics (ICM), 2010 International Conference on*. IEEE, December, 2010.
20. Vidojkovic, Vojkan, et al. "A DECT/Bluetooth multi-standard front-end with adaptive image rejection in 0.18 μm CMOS." *Circuits and Systems, 2004. ISCAS'04. Proceedings of the 2004 International Symposium on*. Vol. 1. IEEE, May, 2004.
21. Wiklund, Magnus, et al. "A 2GHz image-reject receiver in a low IF architecture fabricated in a 0.1 μm CMOS technology." *Circuits and Systems, 2003. ISCAS'03. Proceedings of the 2003 International Symposium on*. Vol. 2. IEEE, May, 2003.
22. Meng, C-C., et al. "2.4/5.7-GHz CMOS dual-band low-IF architecture using Weaver–Hartley image-rejection techniques." *Microwave Theory and Techniques, IEEE Transactions on* 57.3, March, 2009.
23. Chabloz, Jérémie, and Christian Enz. "A novel I/Q mismatch compensation scheme for a low-IF receiver front-end." *Circuits and Systems, 2004. ISCAS'04. Proceedings of the 2004 International Symposium on*. Vol. 4. IEEE, May, 2004.
24. Gimeno-Martín, Alejandro, José Manuel Pardo-Martín, and Francisco Javier Ortega-González. "Adaptive algorithm for increasing image rejection ratio in low-IF receivers." *IET Electronics Letters* 44.6, March, 2008.
25. Mahattanakul, Jirayuth. "The effect of I/Q imbalance and complex filter component mismatch in low-IF receivers." *Circuits and Systems I: Regular Papers, IEEE Transactions on* 53.2, February, 2006.
26. Lin, Jia, Muthukumaraswarmy Annamalai Arasu, and Yuan Xiaojun. "CMOS LC quadrature oscillator with phase mismatch compensation circuit for UWB application." *Radio-Frequency Integration Technology, 2009. RFIT 2009. IEEE International Symposium on*. IEEE, December, 2009.
27. Montemayor, Raymond, and Behzad Razavi. "A self-calibrating 900-MHz CMOS image-reject receiver." *Solid-State Circuits Conference, 2000. ESSCIRC'00. Proceedings of the 26rd European*. IEEE, September, 2000.
28. Kirei, Botond Sandor, Marius Neag, and Marina Dana Topa. "Symmetric Adaptive Decorrelation for I/Q imbalance compensation in narrowband receivers." *Electronics and Telecommunications (ISETC), 2010 9th International Symposium on*. IEEE, November, 2010.
29. Lerstaveesin, Supisa, and Bang-Sup Song. "A complex image rejection circuit with sign detection only." *Solid-State Circuits, IEEE Journal of* 41.12, December, 2006.
30. Riedel, Ines, Marcus Windisch, and Gerhard Fettweis. "On the impact of analog-to-digital conversion on blind I/Q imbalance parameter estimation in low-IF receivers." *Wireless Networks, Communications and Mobile Computing, 2005 International Conference on*. Vol. 1. IEEE, June, 2005.
31. Glas, Jack PF. "Digital I/Q imbalance compensation in a low-IF receiver."*Global Telecommunications Conference, 1998. GLOBECOM 1998. The Bridge to Global Integration. IEEE*. Vol. 3. IEEE, November, 1998.

32. Elahi, Imtinan, Khurram Muhammad, and Poras T. Balsara. "I/Q mismatch compensation using adaptive decorrelation in a low-IF receiver in 90-nm CMOS process." *Solid-State Circuits, IEEE Journal of* 41.2, February, 2006.

33. Yuanjin, Zheng, and C. B. Terry. "Self tuned fully integrated high image rejection low IF receivers: architecture and performance." *Circuits and Systems, 2003. ISCAS'03. Proceedings of the 2003 International Symposium on*. Vol. 2. IEEE, May, 2003.

34. de Witt, Josias Jacobus, and G-J. van Rooyen. "A blind imbalance compensation technique for direct-conversion digital radio transceivers."*Vehicular Technology, IEEE Transactions on* 58.4, May, 2009.

35. Kirei, Botond Sandor, Irina Dornean, and Marina Topa. "Image rejection filter based on complex LMS filter for low-IF receivers." *ELMAR, 2008. 50th International Symposium*. Vol. 1. IEEE, September, 2008.

36. Vallant, G., et al. "Analog IQ impairments in Zero-IF radar receivers: Analysis, measurements and digital compensation." *Instrumentation and Measurement Technology Conference (I2MTC), 2012 IEEE International*. IEEE, May, 2012.

37. Windisch, Marcus, and Gerhard Fettweis. "Blind I/Q imbalance parameter estimation and compensation in low-IF receivers." *Control, Communications and Signal Processing, 2004. First International Symposium on*. IEEE, 2004.

38. Sun, Lei, Zhijun Li, and Miao Yang. "Compensation of IQ imbalance based on a simplified blind source separation method." *Wireless Communications, Networking and Mobile Computing, 2009. WiCom'09. 5th International Conference on*. IEEE, September, 2009.

39. Cetin, Ediz, Izzet Kale, and Richard Morling. "On the performance of a blind source separation based I/Q-corrector." *RAWCON 2002: 2002 IEEE Radio and Wireless Conference* August, 2002.

40. Wang, Yifan, et al. "System simulation of adaptive I/Q mismatch compensation method using SystemC-AMS." *Ph. D. Research in Microelectronics and Electronics (PRIME), 2010 Conference on*. IEEE, July, 2010.

41. Huettner, Joerg, Steffen Reinhardt, and Mario Huemer. "Low complex IQ-imbalance compensation for low-IF receivers." *Radio and Wireless Symposium, 2006 IEEE*. IEEE, January, 2006.

42. Kirei, B. S., et al. "Image rejection filter based on blind source separation for low-IF receivers."*Automation, Quality and Testing, Robotics, 2008. AQTR 2008. IEEE International Conference on*. Vol. 3. IEEE, May, 2008.

43. Gil, Gye-Tae, Young-Doo Kim, and Yong H. Lee. "Non-data-aided approach to I/Q mismatch compensation in low-IF receivers." *Signal Processing, IEEE Transactions on* 55.7, July, 2007.

44. Windisch, Marcus, and Gerhard Fettweis. "Performance analysis for blind I/Q imbalance compensation in low-IF receivers." *Control, Communications and Signal Processing, 2004. First International Symposium on*. IEEE, 2004.

45. Van Gerven, Stefaan, and Dirk Van Compernolle. "Signal separation by symmetric adaptive decorrelation: stability, convergence, and uniqueness."*Signal Processing, IEEE Transactions on* 43.7, July, 1995.

46. Horlin, François, et al. "Impact of frequency offsets and IQ imbalance on MC-CDMA reception based on channel tracking." *Selected Areas in Communications, IEEE Journal on* 24.6, June, 2006.